# Future of Earthquake Early Warning: Quantifying Uncertainty and Making Fast Automated Decisions for Applications

Thesis by

Stephen Wu

In Partial Fulfillment of the Requirements

for the Degree of

Doctor of Philosophy


California Institute of Technology

Pasadena, California

2014

(Defended May 12, 2014)

To my parents, WingShu Wu and Lui Tin, for their unconditional love and sacrifices.

# Acknowledgements

First and foremost, I would like to sincerely thank my advisor, Prof. James L. Beck, for his guidance and support during my PhD study in Caltech. Caltech is such a unique environment for innovative thinking and cutting edge research. It is easy to lose clear direction when surrounded by many great ideas and brilliant minds. Prof. Beck has always been there to catch my hand when I was lost. He shared with me all his experience and wisdom that nurtured me to grow as a responsible and dedicated researcher. I respect him wholeheartedly as a great scientist, as well as a lifetime mentor.

I would like to also thank my other mentor, Prof. Jerome P. Lynch, who was my undergraduate research advisor. Prof. Lynch continues to give me selfless advices on various aspects in life even after I graduated from the University of Michigan. Without his guidance, I would not have landed in Caltech and be able to appreciate the true beauty of academia. He has had his footsteps in many of my important decisions in life. It is my pleasure and fortune to meet such a wonderful mentor when I was still young and naive.

My thanks to Prof. Thomas H. Heaton and Prof. Masumi Yamada for their guidance on my Earthquake Early Warning (EEW) study. Prof. Heaton's passion in science encouraged me to pursue a route that may not be trivial. He has taught me to be brave enough to tackle problems that people may not even want to confront. On the other hand, Prof. Yamada is a great leader and teacher in research and a caring friend outside of work. My research visit in Japan has been very fruitful because of her amazing character.

Thank you for all the resources provided by the California Institute of Technology. Thank you for the support from my committee members, Prof. Heaton, Prof. Beck, Prof. Benjamin J. Gillen and Dr. Elizabeth S. Cochran. Thank you Prof. Hiroo Kanamori for his knowledge on EEW. Thank you Margaret Vinci for helping me to find people interested in EEW. Thank you the always helpful Caltech staff, especially Carolina Oseguera, Christine Silva and Cheryl Geer, for taking care

of my troublesome requests. Thank you my awesome Caltech friends for being with me all these years, especially Ming Hei (Michael) Cheng, Shiyan Song, Ramses Mourhatch, Hemanth Siriki and Vanessa Heckman. Also, I would like to acknowledge the funding from the George Housner Fellowship, the U.S. Geological Survey and Gordon and Betty Moore Foundation for this project.

There are also many people outside Caltech who have given me a lot of support during my PhD study. I would like to thank my collaborators: Prof. Konstantin Zuev at University of Liverpool, Dr. Yong Huang and Prof. Hui Li at Harbin Institute of Technology, Tamaribuchi Koji at Japan Meteorological Agency, Dr. Mahalia Miller and Prof. Jack W. Baker at Stanford University, and Prof. Ikusama Yoshida at Tokyo City University. It was my great pleasure to have collaborators all around the world, opening my eyes to many exciting high quality research. Also, thank you Prof. Kuo-Fong Ma at National Central University for being a warm host during my visit in Taiwan. Thank you Kate Long at California Governor's Office of Emergency Services for the connections to the industry people. Thank you my friends in the Los Angeles area, especially the brothers and sisters in my church CBMC, and thank you my friends in the Bay area, especially Danny Lau for providing me a comfortable place to stay every time I visit San Francisco. My life in California has been greatly enriched with you all.

After all, I would like to acknowledge my parents for the countless days and nights worrying about their never-grown-up son. They have walked through darkness and pain, experienced poverty and persecution, sacrificed enjoyment and health. They came from very traditional families, but became very liberal parents to me. They have spent their whole life to raise me to be a useful man to the world, and I shall never let them down. Thank you for being the best parents that I could ever ask for. Also, I would like to thank my grandparents in heaven who motivated me to study civil engineering in college, and thank you my grandmother and uncle in the Los Angeles area for supporting me in many ways in the past six years.

Finally, I would like to give my deepest gratitude to four special persons, who have been walking along with me during different stages in my life: TinTin, Youjeen, Ed and Mayako. They are more than supportive friends; they are my role models. They contribute to all my changes as a person from a little teenager in Hong Kong to a yet childish man graduating with a PhD in the United States. Words cannot express my feelings. Tears are never enough to convey my thankful heart. My sincere gratitude and love to my special ones. Thank you for being part of my life.

# Abstract

Earthquake early warning (EEW) systems have been rapidly developing over the past decade. Japan Meteorological Agency (JMA) has an EEW system that was operating during the 2011 M9 Tohoku earthquake in Japan, and this increased the awareness of EEW systems around the world. While longer-time earthquake prediction still faces many challenges to be practical, the availability of shorter-time EEW opens up a new door for earthquake loss mitigation. After an earthquake fault begins rupturing, an EEW system utilizes the first few seconds of recorded seismic waveform data to quickly predict the hypocenter location, magnitude, origin time and the expected shaking intensity level around the region. This early warning information is broadcast to different sites before the strong shaking arrives. The warning lead time of such a system is short, typically a few seconds to a minute or so, and the information is uncertain. These factors limit human intervention to activate mitigation actions and this must be addressed for engineering applications of EEW. This study applies a Bayesian probabilistic approach along with machine learning techniques and decision theories from economics to improve different aspects of EEW operation, including extending it to engineering applications.

Existing EEW systems are often based on a deterministic approach. Often, they assume that only a single event occurs within a short period of time, which led to many false alarms after the Tohoku earthquake in Japan. This study develops a probability-based EEW algorithm based on an existing deterministic model to extend the EEW system to the case of concurrent events, which are often observed during the aftershock sequence after a large earthquake.

To overcome the challenge of uncertain information and short lead time of EEW, this study also develops an earthquake probability-based automated decision-making (ePAD) framework to make robust decision for EEW mitigation applications. A cost-benefit model that can capture the uncertainties in EEW information and the decision process is used. This approach is called the Performance-Based Earthquake Early Warning, which is based on the PEER Performance-Based

Earthquake Engineering method. Use of surrogate models is suggested to improve computational efficiency. Also, new models are proposed to add the influence of lead time into the cost-benefit analysis. For example, a value of information model is used to quantify the potential value of delaying the activation of a mitigation action for a possible reduction of the uncertainty of EEW information in the next update. Two practical examples, evacuation alert and elevator control, are studied to illustrate the ePAD framework. Potential advanced EEW applications, such as the case of multiple-action decisions and the synergy of EEW and structural health monitoring systems, are also discussed.

# Contents

# List of Figures

# List of Tables

# Chapter 1

# Introduction

## 1.1 Motivation, research goal and thesis plan

Due to the large uncertainty about the stress and strength distributions within the tectonic plates on Earth, earthquakes are one of the most unpredictable natural hazards. Accurate prediction of when an earthquake will happen is still not possible, but the concept of earthquake early warning (EEW) can be achieved because of the rapid development of computing power and network communication (Heaton, 1985). After earthquake motions are detected by sensors near the source, an EEW system provides a few seconds to a minute or so early warning before the strong shaking arrives at a site. Because the EEW information is highly uncertain, a decision for activating a loss mitigating action is a complicated trade-off problem between the potential of a false warning and a missed warning. Furthermore, human intervention for loss mitigation would likely use up too much of the short lead time, preventing the mitigation from being activated in a timely manner. These challenges limit the applications of EEW in practice.

The complete scope of the EEW problem can be summarized by four steps (Figure 1.1):

1. Observation—Collect seismic waveform data from the seismic network. This part includes the design of a reliable seismic network under scarce resources and an effective mechanism for recording and transmitting seismic waveform data.

2. Earthquake model—Predict earthquake parameters (e.g., hypocenter location, magnitude, origin time and local shaking intensity) based on incomplete waveform data and seismic models. This part includes extracting useful features from waveform data and developing a corresponding model based on the selected features to predict earthquake parameters.

3. System property—Extracting information from the earthquake model to predict local site or structure quantities, for example, using a ground motion prediction model to predict peak ground acceleration and using a structural model to predict the amount of inter-story drifts, peak floor acceleration or probability of collapse.

4. Decision-making—Making a decision for activating a loss mitigating action based on system quantities predicted from EEW information. This part represents the actual value that EEW will provide to the users.

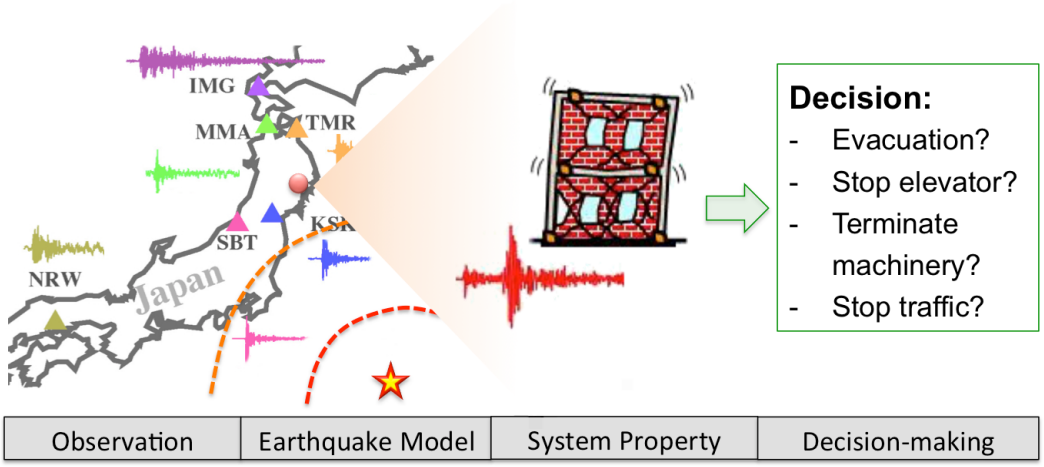


Figure 1.1: Summary of the complete problem in earthquake early warning.

In my thesis, I try to improve each part of the EEW problem based on a Bayesian probabilistic approach, and ultimately extend EEW to cover a broader range of applications by enhancing the quality of the decision-making process. The complete scope of EEW is a complex multi-disciplinary problem. Using Bayesian probability as the underlying framework, I combine techniques from machine learning and decision theories from economics to solve this problem. The main contributions of my thesis include:

1. Develop a probability-based EEW system based on an existing deterministic EEW system and solve the problem of concurrent earthquake event identification.

2. Develop a novel decision framework for EEW applications, called the earthquake probability-based automated decision-making (ePAD) framework, which includes EEW uncertainty and lead time into a cost-benefit model for decision-making.

3. Illustrate the ePAD framework with a practical example on elevator control using EEW information.

4. Suggest potential advanced applications of EEW (application with multiple mitigation actions and synergy of EEW and structural health monitoring system) and discuss their challenges

This thesis is outlined as follow: Chapter 1 gives the background on recent developments of EEW and its applications; Chapter 2 provides the basic knowledge on the theories and methodologies that are used in this thesis; Chapter 3 demonstrates a probability-based EEW system dedicated to accurately identify concurrent earthquakes with an example based on the earthquake sequence of the 2011 M9 Tohoku earthquake (foreshock, mainshock and aftershocks) in Japan; Chapter 4 illustrates the details of the earthquake probability-based automated decision-making (ePAD) framework, which is a novel framework for automated decision based on EEW information with a simple example on decision for releasing an evacuation alert; Chapter 5 shows a complete study on applying the ePAD framework to elevator control based on EEW information; Chapter 6 discusses some challenges on two potential advanced applications of EEW—decision-making for a multiple-action decisions case and synergy of EEW and structural health monitoring system; Chapter 7 concludes the thesis with some final remarks and suggestions on future research.

## 1.2 Fundamental concept of EEW

A major earthquake excites various kinds of waves, including P-waves, S-waves and surface waves. The P-wave is the fastest traveling wave with the least destructive power, while the S-wave and the surface waves are slower waves with much larger destructive power. EEW exploits two important speed differences to provide early warning before the destructive waves arrive at a site: 1) The speed difference between the P-waves and S-waves; 2) The speed difference between seismic waves and electronic signals (Satriano et al., 2011). Once a seismic network detects P-wave information generated from an earthquake source, the EEW system will perform fast prediction of the earthquake magnitude, hypocenter location and origin time. This information is then broadcast to users. It can also be used to predict local shaking intensity around the region of interest. In fact, a recently proposed method directly predicts local shaking intensity based on data from the seismic network, suggesting that skipping source inversion may potentially reduce overall uncertainty of

EEW predictions (Hoshiba, 2013). Figure 1.2 shows a cartoon of the basic concept of EEW.

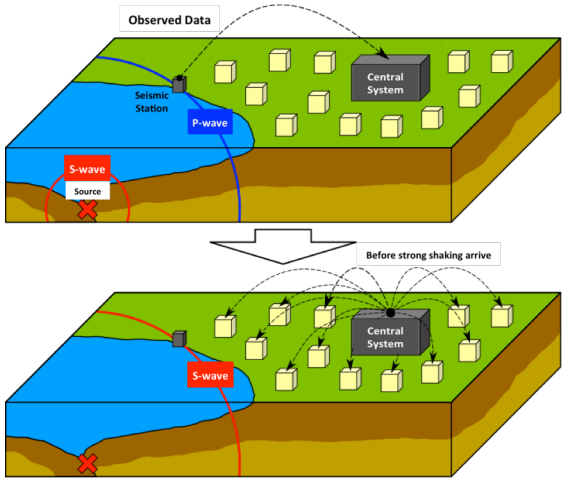


Figure 1.2: Visualization of EEW concept (Seismic station → Central system → Users) (Wikipedia, 2014).

In general, EEW system can be categorized into two types: an onsite or regional system. An onsite system provides warning mainly based on a single station (or sometimes a small group of two to three stations located next to each other). On the other hand, a regional system provides warning based on a large seismic network (usually covers the region with high probability of being the earthquake source). Compared with an onsite system, a regional system often uses a more complex algorithm for earthquake detection, but the warning is generally more reliable. Another way to categorize EEW systems is whether they are a single or multiple warning system. Some onsite systems may only provide one warning when the station is triggered by enough information from the recorded seismic waveform. Other onsite systems and regional systems may provide continual update of the warning. As the seismic waves propagate, the seismic network receives more data and, thus, improves the EEW predictions. Since the electronic signals travel much faster than seismic waves, the warning lead time provided by EEW system depends heavily on the distance between a site and the hypocenter. Generally, lead time is around a few seconds to a minute or so (e.g., lead times in California are expected to be around tens of seconds to a minute (Heaton, 1985; Wurman et al., 2007)). The short lead time becomes a big challenge for practical applications of EEW.

## 1.3 Worldwide EEW development

Rapid development of computing power and network communication allows the concept of earthquake early warning (EEW) to be achieved and developed quickly around the world (Figure 1.3). Many studies have been done on EEW in the past decade (Gasparini et al., 2007). EEW systems have been operating in several different regions. Japan has a long history of earthquake monitoring: Urgent Earthquake Detection and Alarm System (UrEDAS) of the Japan Railway Group, which was first implemented in 1988, is one of the earliest applications of EEW (Nakamura and Saita, 2007) and now most regions in Japan are covered by a public warning broadcast network operated by the Japan Meteorological Agency (JMA) (Allen et al., 2009b; Doi, 2000; Yamazaki et al., 1998). In Mexico, Taiwan, Istanbul, and Bucharest, warnings are released to one or more users outside the research community (Allen et al., 2009b). Especially after the Japan Tohoku earthquake in March 2011, EEW has been proven to be effective for many life-saving purposes, which enhances the awareness of its importance for seismically active regions (Hoshiba et al., 2011). Currently, an EEW system, called the California Integrated Seismic Network (CISN) ShakeAlert System, is in beta-testing in California, USA (Böse et al., 2014).

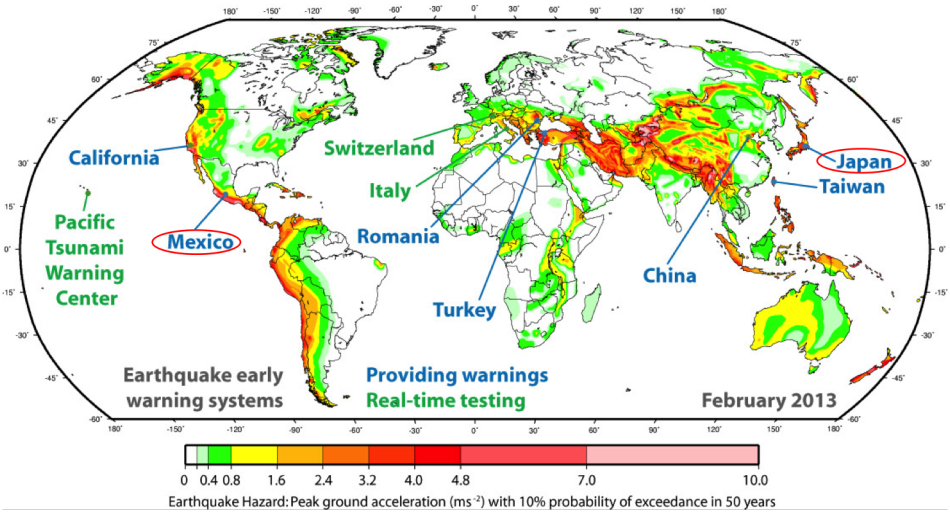


Figure 1.3: Development process of earthquake early warning around the world until February 2013 (Red circles indicate countries with official public notifications) (Allen et al., 2009b).

## 1.4 California EEW system

The California Integrated Seismic Network (CISN) research group has developed the CISN ShakeAlert System in California. It uses the combined outputs of three distinct early warning algorithms that are each based on a different theory: $\tau_c - P_d$ onsite algorithm, Earthquake Alarm Systems (ElarmS), and Virtual Seismologist (V-S) (see Figure 1.5). Figure 1.4 demonstrates a sample user interface of the CISN ShakeAlert System. Detailed information can be found in Böse et al. (2014). In addition, a smartphone version of the user interface is currently under development (Faulkner et al., 2011).

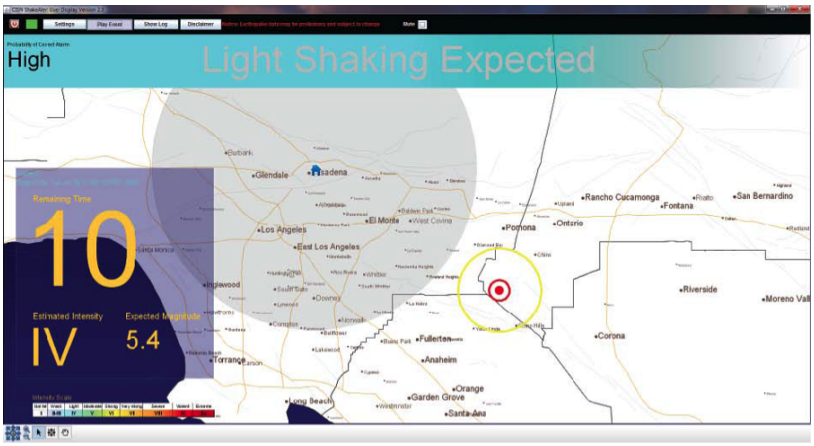


Figure 1.4: Sample of the CISN ShakeAlert user interface.

The $\tau_c - P_d$ onsite algorithm is based on observations from a single sensor with two key parameters: period parameter $\tau_c$ and high-pass filtered P-wave displacement amplitude $P_d$. These parameters are used to determine the size and expected shaking of an earthquake based on a study in Kanamori (2005). The vertical components of velocity and/or displacement data within the first 3 seconds window of P-waveforms are used to determine both parameters (Böse et al., 2009a,b). This algorithm has been modified to be a regional system in the latest update of the ShakeAlert system, which requires multiple stations to report information before warning is issued.

On the other hand, ElarmS and V-S are designed to be a regional network-based algorithm. For ElarmS, earthquake location estimation is mainly based on a grid search to minimize arrival time residuals when there are more than two sensors triggered in the network. Its magnitude estimation relies on the amplitude and frequency content of the detected P-wave. Acceleration, velocity, displacement, and predominant period (Allen and Kanamori, 2003) are continuously determined

from the vertical component of the P-waves from all stations (Allen et al., 2009a).

The V-S algorithm is based on a Bayesian method, which combines prior information with a likelihood function to narrow down the uncertainties. The V-S location estimation uses Voronoi Cells with a probabilistic approach. Its magnitude estimation relies on an attenuation model that is based on P- and S-wave envelopes (Cua and Heaton, 2007). The likelihood function is formulated in terms of the attenuation model, while prior information, such as network topology, station health status, regional hazard maps, earthquake forecasts, etc., may be utilized to construct the prior probability density function (PDF). The posterior PDF for the earthquake magnitude is then found by combining both likelihood function and prior PDF using Bayes Theorem (Cua et al., 2009). However, in the current version of the ShakeAlert system, this Bayesian approach has not been completely implemented yet.

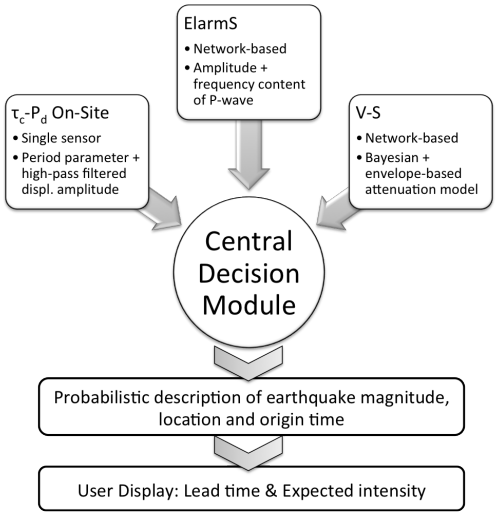


Figure 1.5: Flowchart of CISN ShakeAlert warning from three individual algorithms to the Centralized Decision Module.

All three algorithms receive data from the same CISN seismic network. Once a station is triggered within the network, each system runs its own algorithm to produce a PDF of earthquake magnitude, location and origin time based on the received data signals. Then, all results are integrated in a Centralized Decision Module (Figure 1.5), which produces a PDF for the desired earthquake information based on the PDFs from all three algorithms. Current version of the ShakeAlert system does not include uncertainty in the origin time estimation in any of the three algorithms. However, a rough estimate can be obtained based on a similar algorithm for location estimation

with inclusion of the average P- and S-wave speeds. Development of a more sophisticated method for earthquake origin time is still under consideration. Other ongoing efforts include improvements to existing algorithms and development of finite fault models (Yamada et al., 2007; Yamada and Heaton, 2008; Böse et al., 2012) and foreshock, main shock, and aftershock distinctions (Karakus and Heaton, 2012).

## 1.5 EEW applications

A few seconds to a minute of early warning can provide significant benefits to society. Some existing and potential applications of EEW categorized in terms of procedure complexity and potential action cost are given in Figure 1.6. For example, through broadcasting an early warning of an earthquake, evacuation from at-risk structures or hazardous locations may become possible in the near future. Also, automated actions can be taken to mitigate the impending earthquakes impact on society, such as pre-event elevator control to prevent people being trapped in the elevator during an earthquake (Kubo et al., 2011), inflating air-bearings to protect small structures (Fujita et al., 2011) or temporarily cutting off lifeline supplies. However, extreme care is needed for realtime lifeline control based on EEW because many other emergency responses may rely on the lifeline supplies. Other more sophisticated engineering applications include initiating active or semi-active control systems on civil structures to enhance their earthquake resistance (Maddaloni et al., 2011), fast structural response analyses to provide information for rapid emergency responses, automated train/automobiles control systems, and traffic control by stopping cars entering dangerous bridges.

There is a potential synergy between EEW and other existing monitoring systems, for instance, the use of EEW to provide a prior PDF in probability-based structural health monitoring (SHM) systems (Wu and Beck, 2012) is discussed in Chapter 6, and integration of EEW with regional shaking intensity maps or damage maps for early damage assessment is discussed in Hilbring et al. (2010). Research and development of EEW applications have not yet been emphasized in the earthquake engineering community, although rapid improvements of EEW are being observed in the seismology community. UrEDAS, the automated system for slowing and stopping Shinkansen bullet train in Japan (Nakamura et al., 2011) is one of the few sophisticated engineering applications of EEW that is successful and well known in the earthquake engineering community around the world. Besides the need of a flexible and robust information delivery system, I believe that

this slow development in engineering applications is partly because of the high uncertainty of EEW information and the significant cost corresponding to false alarms. Most of the engineering applications involve mitigation actions that have significant resulting costs, including downtime losses caused by interference with normal operations. The decision of whether to activate such a mitigation action is a complicated trade-off problem which, if time allowed, would best be done by human. However, due to the limited warning time and the uncertainty in the predictions from EEW, applications that involve human decision making are not practical. To achieve robust EEW applications, it is important to develop an automated decision-making system that can make rational decisions given uncertain predictions, as well as to make fast enough decisions to maximize available lead time for responding to the warning from the EEW. This motivated my research on a general framework for automated decision making that I call ePAD. As a result, the utility of EEW may be extended to cover a broader range of engineering applications. Hence, the impact of future large-scale earthquakes to society can be better mitigated.

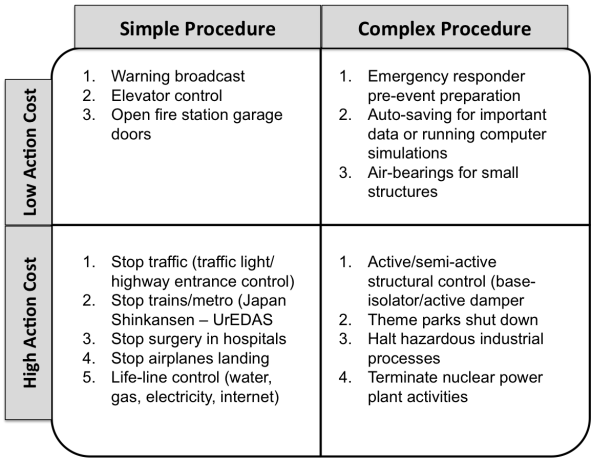


Figure 1.6: Examples of EEW applications categorized in terms of procedure complexity and potential action cost.

# Chapter 2

# Background and Theoretical Foundations

## 2.1 Notation

For consistency and the ease of reading, I adopt the following set of standard notations throughout this thesis:

- $p(x|y)$—conditional PDF of $x$ given $y$
- $P(x|y)$—conditional probability of $x$ given $y$
- $\phi(x) = \frac{1}{\sqrt{2\pi}}\exp\left(-\frac{1}{2}x^2\right)$—the standard Gaussian PDF
- $\Phi(x) = \frac{1}{\sqrt{2\pi}} \int_{-\infty}^{x} \exp\left(-\frac{1}{2}y^2\right)\, \mathrm{d}y$—the standard Gaussian cumulative density function (CDF)

## 2.2 Bayesian probability and model class selection

Bayesian probability is a way to understand or interpret the concept of probability. Different from the frequentist's point of view, which defines probability as a relative frequency of occurrence of an event in the long run, the Bayesian perspective looks at probability as a logical inference. Instead of being a property that exists in Nature, the probability distributions are description of incomplete human information about Nature (Jaynes, 1990). Therefore, uncertainty is a result of the lack of information about the subject one is studying. In this sense, there is really no "true probability model", but only better models that can make more accurate predictions because they may include a more relevant set of information. More detail in this subject can be found in Jaynes (2003). This

interpretation leads to a standard procedure for calculating probabilities using the Bayes' theorem ($A$ and $B$ denote any propositional statements):

$$p(A|B) = \frac{p(B|A)p(A)}{p(B)} \tag{2.1}$$

This equation is often used in Bayesian inference to find the posterior probability in many science or engineering problems. For example, in system identification, $A$ can be a set of model parameters $\boldsymbol{\theta}$ under a given model class $M_i$ and $B$ can be a set of data $\boldsymbol{D}$ obtained from empirical studies to improve the model. Equation 2.1 represents the process of Bayesian updating for the posterior PDF of model parameters based on the data (Beck, 2010):

$$p(\boldsymbol{\theta}|\boldsymbol{D}, M_i) = \frac{p(\boldsymbol{D}|\boldsymbol{\theta}, M_i)p(\boldsymbol{\theta}|M_i)}{p(\boldsymbol{D}|M_i)} \propto p(\boldsymbol{D}|\boldsymbol{\theta}, M_i)p(\boldsymbol{\theta}|M_i) \tag{2.2}$$

$p(\boldsymbol{\theta}|\boldsymbol{D}, M_i)$ is the posterior PDF of the model parameters after updating by the data; $p(\boldsymbol{D}|\boldsymbol{\theta}, M_i)$ is the likelihood function of the model parameters that represents the probability of the data given a specific set of $\boldsymbol{\theta}$ values; $p(\boldsymbol{\theta}|M_i)$ is the prior PDF of the model parameters before any data is collected; $p(\boldsymbol{D}|M_i)$ is the evidence (or sometimes called the marginal likelihood), which is a normalizing constant in the Bayesian inference problem and is often omitted during calculation.

If there exists more than one model class, e.g., $\mathcal{M} = \{M_i|i = 1, ..., N_M\}$, one can also use Bayes' Theorem to perform model class selection based on the data:

$$P(M_i|\boldsymbol{D}, \mathcal{M}) = \frac{p(\boldsymbol{D}|M_i)P(M_i|\mathcal{M})}{p(\boldsymbol{D}|\mathcal{M})} \propto p(\boldsymbol{D}|M_i)P(M_i|\mathcal{M}) \tag{2.3}$$

Note that $\mathcal{M}$ is omitted in the likelihood $p(\boldsymbol{D}|M_i)$ because the probability of data $\boldsymbol{D}$ is independent of the full set of model classes $\mathcal{M}$ once a specific model $M_i$ is given. In most cases, one may not want to introduce bias to any $M_i \in \mathcal{M}$ before any data is collected, and thus $P(M_i|\mathcal{M})$ is taken equal to the constant $1/N_M$. As a result, $P(M_i|\boldsymbol{D}, \mathcal{M})$ is proportional to $p(\boldsymbol{D}|M_i)$ (the evidence in equation 2.2) for any $i = 1, ..., N_M$. One may use the model class with the largest posterior probability $P(M_i|\boldsymbol{D}, \mathcal{M})$ for robust predictive analysis, or perform model class averaging where the final prediction is a weighted mean of the predictions from each model class with the weights equal to $P(M_i|\boldsymbol{D}, \mathcal{M})$ (Beck, 2010).

## 2.3 Variations of Monte Carlo Simulation

### 2.3.1 Monte Carlo Simulation

Although Bayesian theory is a powerful tool for plausible reasoning and problem solving, the actual application of the theory relies on numerical methods because of the lack of analytical solutions for the posterior PDF in most practical problems. The well-known numerical estimation method, Monte Carlo Simulation (MCS), approximates a PDF $p(x)$ where $x \in \mathbb{R}$ by $N_s$ samples drawn from that PDF and estimates an expected value of a function of $x$, $E_p[f(x)]$, by:

$$\begin{aligned} E_p[f(x)] &= \int f(x)p(x)\,\mathrm{d}x \approx \frac{1}{N_s}\sum_{j=1}^{N_s} f(\hat{x}_j) \\ &\text{where } \hat{x}_j \sim p(x) \end{aligned} \tag{2.4}$$

However, it is inefficient to use MCS when $f(x)$ is a complex function such as a computational model that requires significant computational effort, and sometimes it is difficult to directly draw samples from $p(x)$. These challenges lead to the development of various improved stochastic simulation methods (Liu, 2002; Tokdar and Kass, 2010; Neal, 1993).

### 2.3.2 Importance Sampling

In Bayesian analysis, it is often impossible to directly apply MCS because samples cannot be drawn from the posterior PDF, which one is trying to estimate due to the lack of an analytical solution. The Importance Sampling (IS) method is a simple solution to simulate samples from a target PDF that is known up to a constant of proportionality. The target PDF is approximated by $N_s$ samples $\hat{x}_j$ drawn from any proposal PDF $q(x)$ with weights $w_j$:

$$\begin{aligned} p(x) &\approx \sum_{j=1}^{N_s} w_j \delta(x - \hat{x}_j),\ \hat{x}_j \sim q(x) \\ &\text{where } w_j \propto \frac{p(\hat{x}_j)}{q(\hat{x}_j)},\ \sum_{j=1}^{N_s} w_j = 1 \end{aligned} \tag{2.5}$$

The closer the chosen $q(x)$ is to the target PDF $p(x)$, the less samples are needed for accurate estimation, and the better the efficiency of the method is. In Bayesian analysis, the posterior PDF

of a given model $M_i$ is proportional to the product of a likelihood function and a prior PDF, where both functions are specified by the model (Equation 2.2). Hence, it can be approximated using IS:

$$\begin{aligned} p(\boldsymbol{\theta}|\boldsymbol{D}, M_i) &\approx \sum_{j=1}^{N_s} w_j \delta(\boldsymbol{\theta} - \hat{\boldsymbol{\theta}}_j),\ \hat{\boldsymbol{\theta}}_j \sim q(\boldsymbol{\theta}) \\ \text{where } w_j &\propto \frac{p(\boldsymbol{D}|\hat{\boldsymbol{\theta}}_j, M_i) p(\hat{\boldsymbol{\theta}}_j|M_i)}{q(\hat{\boldsymbol{\theta}}_j)},\ \sum_{j=1}^{N_s} w_j = 1 \end{aligned} \tag{2.6}$$

A straightforward choice of $q(\hat{\boldsymbol{\theta}})$ is the prior $p(\hat{\boldsymbol{\theta}}_j|M_i)$, which leads to a simple weight calculation proportional to the likelihood function only, i.e., $w_j \propto p(\boldsymbol{D}|\hat{\boldsymbol{\theta}}_j, M_i)$. However, the posterior PDF is often very different from the prior PDF and so such a choice of the proposal PDF $q(\hat{\boldsymbol{\theta}})$ will lead to a large variance and significantly reduce the efficiency for accurately estimating the posterior distribution. Many methods have been proposed to improve IS in the past two decades (Tokdar and Kass, 2010).

### 2.3.3 Markov Chain Monte Carlo and Subset Simulation

Another widely used method for Bayesian analysis is the Markov Chain Monte Carlo methods. They are a class of sampling algorithms that generates a chain of correlated samples to estimate the target PDF, which reduces their statistical efficiency compared with independent and identically distributed sample generation. Another major drawback is that a burn-in period, where samples are discarded, is often needed before the chain of samples converges to the target PDF. The length of the burn-in period is difficult to determine, even empirically. Variations of MCMC techniques include Metropolis-Hastings algorithm, Gibbs sampling and Hybrid Monte Carlo (Neal, 1993). Recent development of MCMC algorithms includes the adaptive Metropolis-Hastings method (Beck and Au, 2002), Transitional Markov Chain Monte Carlo (TMCMC) (Ching and Chen, 2007) and Asymptotically Independent Markov Sampling (AIMS) (Beck and Zuev, 2013).

When estimating probabilities of rare events (often referred to as the tail of a PDF), even MCMC methods can be extremely inefficient because of the difficulty for the samples converging to the small probability region. A novel method, called Subset Simulation, has been proposed for solving this problem (Au and Beck, 2001). This method was originally developed to solve structural reliability problem, where the probability of failure of a structure $P_{\mathcal{F}}$ is estimated based on a pre-

determined definition of failure region $\mathcal{F}$ within a parameter space $\Theta$. Let $\theta \in \Theta$ be an uncertain state, $I_{\mathcal{F}}(\theta)$ be an indicator function such that $I_{\mathcal{F}}(\theta) = 1$ if $\theta \in \mathcal{F}$ and $I_{\mathcal{F}}(\theta) = 0$ otherwise, and $p(\theta)$ is a prior PDF of $\theta$:

$$P_{\mathcal{F}} = P(\theta \in \mathcal{F}) = \int I_{\mathcal{F}}(\theta) p(\theta) \, \mathrm{d}\theta \tag{2.7}$$

The basic idea of Subset Simulation is to represent $\mathcal{F}$ as a sequence of nested subsets: $\mathcal{F}_0 \supset \mathcal{F}_1 \supset ... \supset \mathcal{F}_{L-1} \supset \mathcal{F}_L = \mathcal{F}$. Then, $p_{\mathcal{F}}$ can be expressed by a product of conditional PDFs:

$$P_{\mathcal{F}} = P(\mathcal{F}_L) = P(\mathcal{F}_0) \prod_{i=1}^{L} P(\mathcal{F}_i | \mathcal{F}_{i-1}) \tag{2.8}$$

Each conditional PDF can be chosen to have a relatively large probability (e.g., 0.1) so that it can be efficiently estimated by an MCS or MCMC method. Figure 2.1 shows a visualization of the idea.

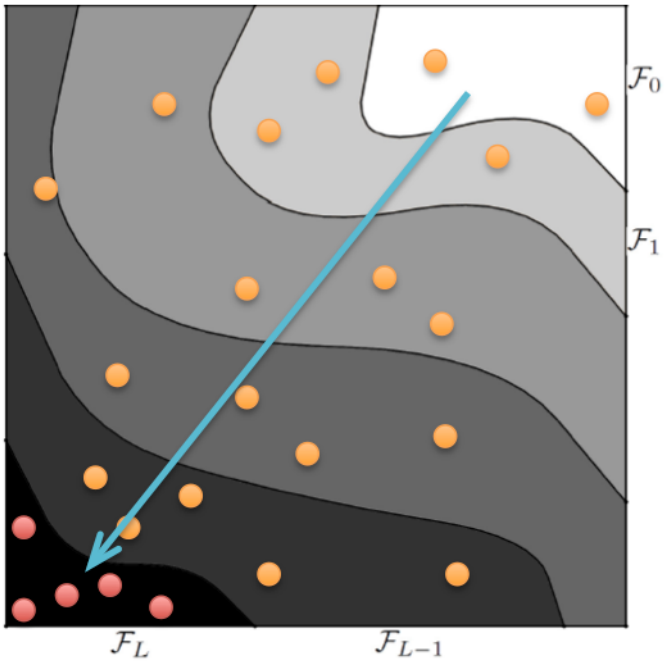


Figure 2.1: Visualization of the Subset Simulation idea. Orange dots are samples for estimating the intermediate conditional PDF and red dots are samples that lie in the actual failure region $\mathcal{F} = \mathcal{F}_L$, represented as a sequence of nested subsets: $\mathcal{F}_0 \supset \mathcal{F}_1 \supset ... \supset \mathcal{F}_{L-1} \supset \mathcal{F}_L$.

### 2.3.4 Sequential Monte Carlo methods

Many science or engineering problems involve dynamic processes that can be solved by a recursive method under the Bayesian probability framework. Consider a time dependent model parameter $\theta_t$ and data/measurement $D_t$ at each time step $t$ (denote a collection of data from time 1 to time $t$ to be $D_{1:t}$), the Bayesian inference problem can be divided into two stages:

1. Prediction stage: predict $\theta_t$ based on an evolution model $p(\theta_t|\theta_{t-1})$ for $\theta$ and the posterior PDF of $\theta$ from previous time step $t-1$.

$$p(\theta_t|D_{1:t-1}) = \int p(\theta_t|\theta_{t-1})p(\theta_{t-1}|D_{1:t-1})\,\mathrm{d}\theta_{t-1} \tag{2.9}$$

2. Updating stage: update $\theta_t$ with the new data $D_t$ collected at time $t$ based on a likelihood model and the PDF from the prediction stage.

$$p(\theta_t|D_{1:t}) = \frac{p(D_t|\theta_t)p(\theta_t|D_{1:t-1})}{p(D_t|D_{1:t-1})} \tag{2.10}$$

Many algorithms have been developed based on this method (Arulampalam et al., 2002). For example, the Kalman Filter is an analytical solution to this problem based on the assumptions that (1) the posterior PDF, the likelihood model and the evolution model follow a Gaussian model at every time step, and (2) the likelihood model and the evolution model are linear functions of the states $\theta_t$ and $\theta_{t-1}$. In many other cases, such as problems with a nonlinear model, numerical methods are developed based on the concept of MCS. One example is the particle filtering methods, where the posterior PDF at each time step is approximated by samples from the IS method and the weights are calculated by a recursive scheme. (A similar idea is used in Chapter 3).

## 2.4 Decision theory and cost-benefit analysis

Life is made up of decisions, and decisions are usually made under uncertainty because of incomplete information. An optimal decision is always desired, while its definition remains vague. In economics, rationality is a common assumption for making optimal decisions. It basically states that people have a natural preference for a more valuable choice. However, value is very subjective. It varies from person to person. One way to represent personal preference for what is valuable is to use a

*utility function*. A fundamental tenant of decision theory is to make a decision that maximizes the expected utility value (Von Neumann and Morgenstern, 1944; Raiffa and Schlaifer, 1961). Let $\Pi$ be a set of all possible decisions and $U(x)$ be a utility function controlled by variable $x$, then the optimal decision is:

$$\hat{\pi} = \text{argmax}_{\pi \in \Pi} E[U(x)|\pi] \tag{2.11}$$

Utility functions are generally categorized in three types (Figure 2.2):

1. Risk-taking (or risk-seeking): this represents a person who prefers a gamble with a known expected return rather than an investment with an equivalent certain return (a convex utility function of $x$).

2. Risk-averse: this represents a person who prefers an investment that guarantees a certain return rather than a gamble with an expected return of the equal amount (a concave utility function of $x$).

3. Risk-neutral: this represents a person that is neither of the above two cases (a linear utility function of $x$)

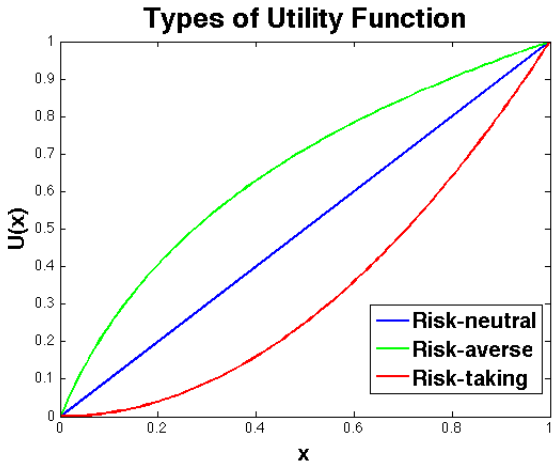


Figure 2.2: Example of the three types of utility functions given for positive $x$.

Cost-benefit analysis (sometimes called benefit-cost analysis) is a systematic way to evaluate different parts of a utility function and make decisions. In short, it separates the parts of the utility that results in a net increase (benefit) and a net loss (cost) and makes decisions by comparing the benefit and cost of each action. Although it provides a rigorous framework for applying the

theory of expected utility model, decision problems in reality usually involve too many factors and are often too complicated to perform a complete cost-benefit analysis. Assumptions are needed to constrain the problem within a tractable scope.

## 2.5 Surrogate model and relevance vector machine

Surrogate models, also known as meta-models or response surfaces, are often used to approximate a complex model in order to reduce computation time or to approximate some output that cannot be obtained directly from the model. For example, in seismic risk analysis for a structure, the reliability of the structure may be estimated numerically using MCMC techniques and this may involve many evaluations of a complex structural model, e.g., a sophisticated finite element model. Surrogate model based on a few simulation results from the complex model as training data can significantly reduce the computation time for the reliability analysis. They are also used in some design optimization problems and their development is a major topic in machine learning.

There are many methods developed for creating a surrogate model (Khuri and Mukhopadhyay, 2010). Here, I discuss a recently developed algorithm, called the relevance vector machine (RVM) (Tipping, 2001), which will be used in the later chapters of this thesis. It is a robust regression technique suitable for creating a sparse surrogate model using a kernel basis expansion. RVM is a machine learning technique that exploits the Bayesian probability framework to obtain an optimum regression model under a trade-off between the fit to the data and the information extracted from the data by the model (Tipping, 2004). It is sometimes referred to as the Bayesian version of the support vector machine (SVM) (Cortes and Vapnik, 1995), which makes predictions of $y$ as a function of variable $x$ based on a linear combination of kernel functions $K(x, x_i)$ with weights $w_i$ and data points $x_i$ for $i = 1, ..., N$:

$$y(x) = w_0 + \sum_{i=1}^{N} w_i K(x, x_i) \tag{2.12}$$

RVM applies the sparse Bayesian learning framework to find the posterior PDF of the weights and use it to perform robust predictions. The main reason that RVM can produce a sparse model is because of the use of the automatic relevance determination (ARD) prior (Mackay, 1994). This prior assigns an individual zero-mean Gaussian prior to each weight in the model with independent

variances. If the prior variance of a weight is zero, it means that the weight is equal to zero and the corresponding kernel can be dropped from the model. RVM uses a recursive algorithm to learn the values of the prior variances based on the collected data for the regression problem. The algorithm is developed based on the model evidence in calculating the posterior PDF of the weights. The original version of the RVM algorithm, referred to here as the Top-down algorithm (Huang et al., 2014), starts from the full kernel model and recursively drops out irrelevant terms based on the recursive algorithm. The algorithm involves matrix inversion, where the size of the matrix is equal to the number of data, and thus the number of kernels. When the number of data is large, Top-down RVM is extremely inefficient. A later version, referred to here as the Bottom-up algorithm (Huang et al., 2014), is developed to solve this problem at the expense of a possibly suboptimal result for the prior variances (Tipping and Faul, 2003). The Bottom-up algorithm starts from one kernel in the full model and recursively adds in relevant kernels until a convergence criterion is met.

There remains some challenges for using RVM in some specific cases. For example, the algorithm relies on the assumption that the model evidence used to derive the recursive algorithm is peaked around some optimal value, which implies that there is sufficient data to find a single optimal model. In compressive sensing problems, this assumption breaks down (Huang et al., 2014). Nevertheless, RVM is still a reliable algorithm for many engineering applications, when data is sufficient and sparse in some orthonormal basis.

## 2.6 Value of information

### 2.6.1 Basic theory: Flipping coin example

Value of information, also known as value of clairvoyance, is commonly defined as the expected value that a decision maker is willing to pay for information which may change a decision (Howard, 1966). It involves a comparison between the expected values of a decision policy without the information and if the information were to be obtained. It is usually based on the prior and posterior PDFs from Bayes' theorem but where the conditioning information is uncertain and so a probabilistic prediction of it must also be employed.

In general, let $G$ be a gain function, which is a function of a decision policy $\pi_I$ with information $I$ and a decision policy $\pi$ without information $I$. Then the value of information ($VoI$) can be

written as:

$$VoI = E[G(\pi_I)] - E[G(\pi)] = \int E[G(\pi_I)|I]p(I)\,\mathrm{d}I - E[G(\pi)] \tag{2.13}$$

The main step in Equation 2.13 is to find the expected value of $G$ based on $\pi_I$ by marginalizing the contribution of information $I$. To do so, some knowledge about the PDF of $I$ is essential. In other words, $VoI$ is a prediction of the influence of information $I$ on the final outcome of a decision (represented by the gain function $G$). The following simple example, a coin flipping gamble, demonstrates the concept.

Let there be a coin with unknown probability $x$ of getting a head in a flip. You are about to bet $c$ amount of money on getting a head in the next flip. If the next flip is indeed a head, you obtain a reward of $r \cdot c$; or else, you get nothing back. Based on a decision policy $\pi_0$ that one will always make a bet, the expected gain $G(\pi_0)$ in this game, given $x$, is:

$$E[G(\pi_0)|x] = r \cdot c \cdot x + 0 \cdot (1 - x) - c = c \cdot (r \cdot x - 1) \tag{2.14}$$

Without any prior information on $x$, we assume a uniform prior PDF for $x$ between 0 and 1. Hence, the prior expected gain is:

$$\begin{aligned} E[G(\pi_0)] &= \int E[G(\pi_0)|x]p(x)\,\mathrm{d}x \\ &= \int c \cdot (r \cdot x - 1) \cdot 1\,\mathrm{d}x = c\left(\frac{r}{2} - 1\right) \end{aligned} \tag{2.15}$$

Now, before you decide to make the bet or not, you are offered a chance to know the result of a previous flip. How much would you pay for this piece of information $I$? How would you make the decision of betting or not? By Bayes' theorem, the posterior PDF of $x$ given the previous flip was a head ($I = H$) is:

$$p(x|I = H) = \frac{P(I = H|x)p(x)}{P(I = H)} = \frac{x \cdot 1}{\int_0^1 x \cdot 1\,\mathrm{d}x} = 2x \tag{2.16}$$

Similarly, the posterior PDF of $x$ given the previous flip was a tail ($I = T$) is:

$$p(x|I = T) = \frac{P(I = T|x)p(x)}{P(I = T)} = \frac{(1 - x) \cdot 1}{\int_0^1 (1 - x) \cdot 1\,\mathrm{d}x} = 2(1 - x) \tag{2.17}$$

The prior probabilities of heads and tails, $P(I = H)$ and $P(I = T)$, in the denominator of Equation

2.16 and 2.17 are both equal to 1/2 based on the total probability theorem. The two probability functions are also known as the evidence functions for the posterior PDF of $x$ in the context of machine learning (these will be used when calculating $VoI$). The posterior of the expected gain $G(\pi_0)$ conditional on the possible information that you may get is:

$$\begin{aligned} E[G(\pi_0)|I=H] &= \int E[G(\pi_0)|x]p(x|I=H)\,\mathrm{d}x \\ &= \int c\cdot(r\cdot x-1)\cdot 2x\,\mathrm{d}x = c\left(\frac{2r}{3}-1\right) \qquad (2.18) \\ E[G(\pi_0)|I=T] &= \int E[G(\pi_0)|x]p(x|I=T)\,\mathrm{d}x \\ &= \int c\cdot(r\cdot x-1)\cdot 2(1-x)\,\mathrm{d}x = c\left(\frac{r}{3}-1\right) \qquad (2.19) \end{aligned}$$

At this stage, you do not know what information you will receive. Let us find the expected gain based on a new policy $\pi$, which will always decide on the bet in order to maximize the expected gain, and the $VoI$ under four cases: (1) $r \le 1.5$; (2) $1.5 < r \le 2$; (3) $2 < r < 3$; (4) $r \ge 3$. Let $\pi_I$ be the same decision policy, but also includes the possibility of having information $I$.

1. $r \le 1.5$:

   Based on Equation 2.15, since $E[G(\pi_0)] \le -0.25c < 0$, you will not make the bet under policy $\pi$ if no information is given. Hence, $E[G(\pi)] = 0$. Also, since $E[G(\pi_0)|I=H] \le 0$ and $E[G(\pi_0)|I=T] \le -0.5c < 0$, you will not make the bet no matter what information you receive under policy $\pi_I$. Hence, $E[G(\pi_I)] = 0$. Therefore, $VoI = E[G(\pi_I)] - E[G(\pi)] = 0$.

2. $1.5 < r \le 2$:

   Since $E[G(\pi_0)] \le 0$, you will not make the bet if no information is given. Hence, $E[G(\pi)] = 0$. On the other hand, $E[G(\pi_0)|I=H] \ge 0$, but $E[G(\pi_0)|I=T] < 0$. This means that you will make the bet if $I=H$, but you will not make the bet if $I=T$. Since you do not know which information you will receive, your expected gain is:

   $$E[G(\pi_I)] = E[G(\pi_I)|I=H]P(I=H) + 0\cdot P(I=T) = c\left(\frac{r}{3}-\frac{1}{2}\right) \qquad (2.20)$$

   Therefore, $VoI = E[G(\pi_I)] - E[G(\pi)] = c(r/3-1/2) > 0$. $E[G(\pi_I)] \ne E[G(\pi)]$ because it is conditional on you receiving the information, even though you do not know whether the

previous flip was a head or a tail.

3. $2 < r < 3$:

   Since $E[G(\pi_0)] > 0$, you will make the bet if no information is given. Hence, $E[G(\pi)]$ takes the value in Equation 2.15. On the other hand, $E[G(\pi_0)|I = H] > 0$, but $E[G(\pi_0)|I = T] < 0$. This means that you will make the bet if $I = H$, but you will not make the bet if $I = T$. Similar to case 2, $E[G(\pi_I)]$ takes the value in Equation 2.20. Therefore, $VoI = E[G(\pi_I)] - E[G(\pi)] = c(1/2 - r/6) > 0$.

4. $r \geq 3$:

   Since $E[G(\pi_0)] > 0$, you will make the bet if no information is given. Hence, $E[G(\pi)]$ takes the value in Equation 2.15. Also, since $E[G(\pi_0)|I = H] > 0$ and $E[G(\pi_0)|I = T] \geq 0$, you will make the bet no matter what information is given.

$$E[G(\pi_I)] = E[G(\pi_I)|I = H]P(I = H) + E[G(\pi_I)|I = T]P(I = T) = c\left(\frac{r}{2} - 1\right) \tag{2.21}$$

   Therefore, $VoI = E[G(\pi_I)] - E[G(\pi)] = 0$.

Note that for both Case 1 and 4, $VoI = 0$. This is consistent with the definition because the information does not change the decision, and so the information has no added value. In contrast, for Case 2 and 3, $VoI > 0$. Hence, you should be willing to pay for the information up to the value of $VoI$ obtained from the calculation. To conclude, based on the theory of value of information, the decision to make a bet or not, depending on the return rate $r$, will be:

1. $r \leq 1.5$: You should not buy the information and never make a bet.
2. $1.5 < r \leq 2$: You should buy the information with the price up to $VoI = c(r/3 - 1/2)$ and make a bet only if the previous flip was a head.
3. $2 < r < 3$: You should buy the information with the price up to $VoI = c(1/2 - r/6)$ and make a bet only if the previous flip was a head.
4. $r \geq 3$: You should not buy the information and always make a bet.

Note that this conclusion is based on the chosen uniform prior on $x$. After the first bet, you will obtain the result of the flip. Then, a more appropriate betting strategy is to make the decision based on the posterior of $x$ using the information that you have just obtained.

### 2.6.2 Engineering example: Soil contamination detection

Many science or engineering problems involve design of an optimal experiment or a monitoring system due to limited resources or other constraints. The theory of value of information allows a quantitative comparison between different designs. For example, consider a simple hypothetical scenario: a landlord is threatened by a soil contamination problem in his land. A treatment of the contamination at a site costs $c_t$. He will be charged for a penalty $c_p$ and the treatment cost $c_t$ if an investigator discovers that the soil contamination level at a site exceeds the legal threshold $y_{legal}$. He has performed measurements to check the current contamination level at three sites and Figure 2.3 shows the result. Given the cost of each measurement $c_m$, how many more measurements should he perform and where will be the optimal locations to do so? To solve this problem, I use a Gaussian Process to model the uncertainty of spatial contamination level and the theory of value of information for design optimization.

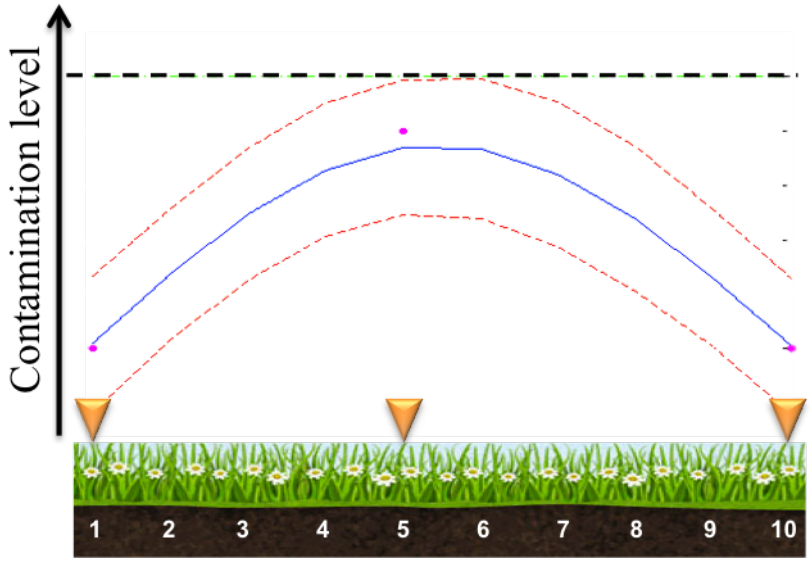


Figure 2.3: Hypothetical scenario with three measurements at location 1, 5, 10 (purple dots). Black dotted line shows the legal threshold of the contamination level. Blue and red curves show the mean and standard deviation from Gaussian Process.

#### 2.6.2.1 Problem setup and solution

For simplicity, I only consider a small set of 10 discrete locations of interest in this example. Let $X_{1:10} = \{x_i | i = 1, ..., 10\}$ be the set of locations and $Y_{1:10} = \{y_i | i = 1, ..., 10\}$ be the set of

contamination levels at the corresponding locations. To apply the theory of value of information, the gain function $G$ in this case is the negative of the cost function $C$ for a given decision policy $\pi$, i.e., $G(\pi) = -C(\pi)$, where $\pi$ is the decision of whether a treatment is performed at a site or not based on a set of contamination level information. Let $Y_0$ be the set of prior information (purple dots in Figure 2.3), $\pi_0$ be the decision based on the prior information, and $\pi_{0,i}$ be the decision based on a new measurement $\hat{y}_i$ at $x_i$ and the prior information. The value of information is:

$$\begin{aligned} VoI_i &= E[C(\pi_0)|Y_0] - E[C(\pi_{0,i})|Y_0] \\ &= E[C(\pi_0)|Y_0] - \int E[C(\pi_{0,i})|Y_0, \hat{y}_i] p(\hat{y}_i|Y_0)\, \mathrm{d}\hat{y}_i \end{aligned} \tag{2.22}$$

$p(\hat{y}_i|Y_0)$ is estimated by a Gaussian Process model (Mackay, 1998) with mean and standard deviation represented by the blue and red curves, respectively, in Figure 2.3. $E[C(\pi)|Y] = \sum_{i=1}^{10} E[C(\pi)|Y, x_i]$ for any policy $\pi$ and information $Y$, and $E[C(\pi)|Y, x_i]$ is calculated as ($N_m$ = number of measurements performed to obtain $Y$):

$$\begin{aligned} &E[C(\pi)|Y, x_i] = N_m c_m + f(\pi, x_i) \\ &\text{where } f(\pi, x_i) = \begin{cases} c_t & ,\pi = \text{do treatment} \\ (c_t + c_p) P(y_i \geq y_{legal}|Y) & ,\pi = \text{no treatment} \end{cases} \\ &\text{and } P(y_i \geq y_{legal}|Y) = \int_{y_{legal}}^{\infty} p(y_i|Y)\, \mathrm{d}y_i \end{aligned} \tag{2.23}$$

The algorithm to find the optimal number of measurements and the corresponding optimal locations is: (1) for each number of new measurements, calculate $VoI$ of all possible combination of measurement locations and pick the one with maximum $VoI$, (2) Pick the number with the maximum value of $VoI$. To reduce computational effort, a suboptimal algorithm is:

1. Calculate $VoI$ for adding a new measurement at each not measured location using Equation 2.22.

2. Pick the location with maximum $VoI$ and repeat step 1 with the new measurement location included in the set of measured locations.

3. Repeat step 2 until the total $VoI$ reduces.

#### 2.6.2.2 Results and discussion

Let us assume that the penalty $c_p$ is twice the treatment cost $c_t$ and a single measurement cost $c_m$ is 2% of $c_t$. The expected values in $VoI_i$ calculations can be estimated by MCS using samples drawn from the Gaussian Process model. Figure 2.4 shows that the optimal location to perform one more measurement is at location 6. This is reasonable because it has the highest chance of exceeding the legal threshold based on the Gaussian Process model (Figure 2.3).

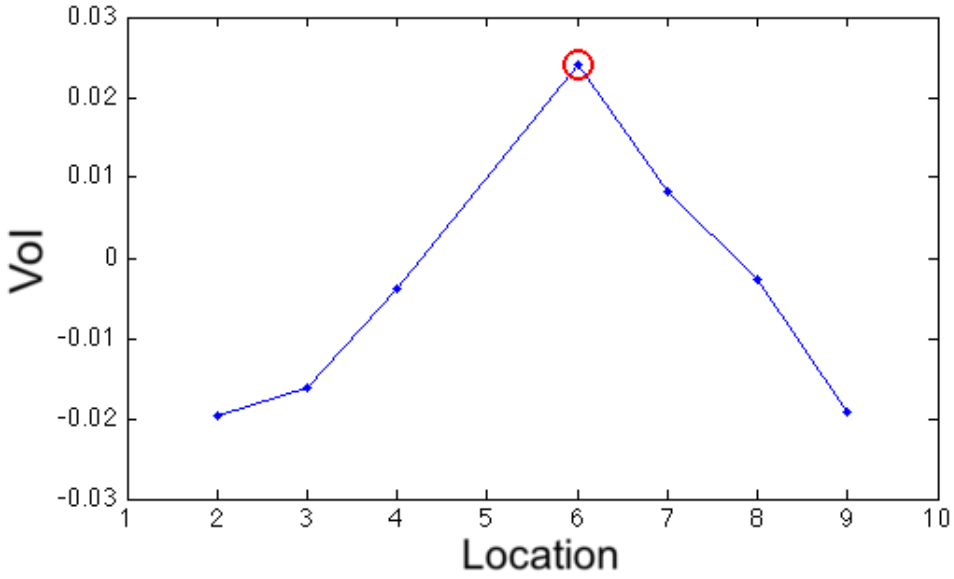


Figure 2.4: Value of information for performing a measurement at each location without any measurement.

By doing the same analysis for $N_m = 1, ..., 7$, the optimal location and its $VoI$ value can be found for each $N_m$. Figure 2.5 shows that it is optimal to perform three more measurements at location 4, 6 and 7 in order to avoid the high cost of penalty $c_p$ based on the prior information and the Gaussian Process model. This is also a reasonable result because location 4, 6 and 7 have the highest risk of exceeding the legal threshold and once measurements are performed at those three locations, the uncertainty in the remaining locations will be further reduced. The expected risk of exceedance will be low enough that the benefit from reducing uncertainty further cannot be compensated by the cost of an extra measurement.

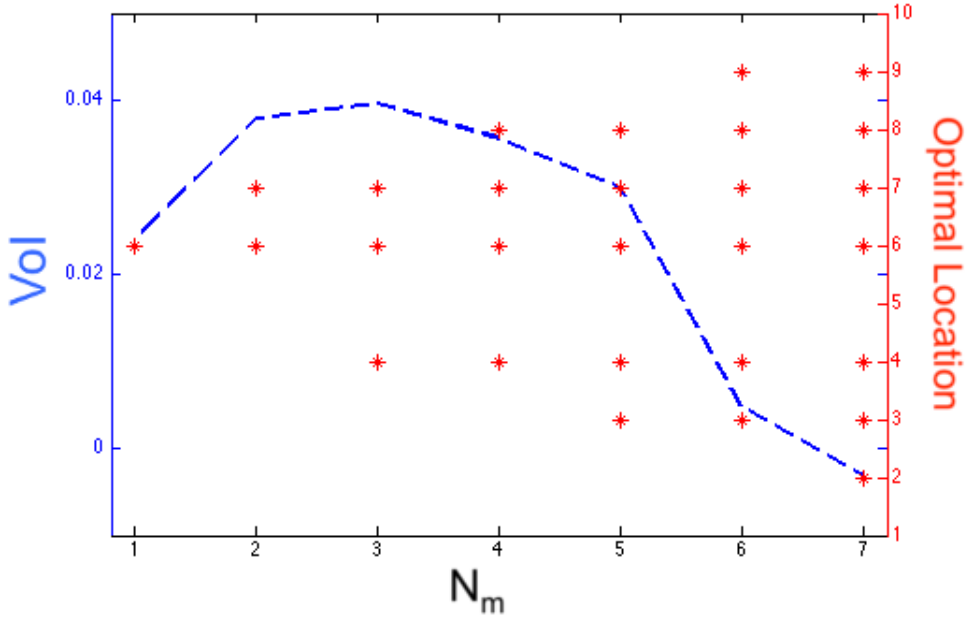


Figure 2.5: Value of information and the optimal locations for performing measurements for a given number of measurements $N_m$ to be performed.

# Chapter 3

# Multi-Events Recognition in EEW

## 3.1 Introduction

Earthquake early warning (EEW) systems have shown promising performance in many countries in the past decade. For example, the EEW system operated by the Japan Meteorological Agency (JMA) in Japan broadcasted the first early warning 5.4s after the first P-wave detection during the 2011 M9 Tohoku earthquake (Hoshiba et al., 2011). However, there remains some limitations to the existing EEW systems, such as unreliable warnings in regions without a dense seismic network and the lack of a finite fault model for large events. Another major problem was observed after the 2011 Tohoku mega earthquake: an enormous number of aftershocks broke a common assumption of many EEW system that an earthquake is a sparse event. As a result, the greatly increased frequency of earthquake occurrence led to a significant increase of false alarms. JMA observed that over 70% of the false alarms recorded two months after the main shock in March 2011 were because the current EEW system cannot properly handle concurrent events happening within a short time frame or spatially close to each other (abbreviated as *multi-events* in this thesis) (JMA, 2013a,b).

Motivated by this incident, this study investigates the possibility of applying a Bayesian probabilistic approach to an existing EEW system and proposes an algorithm to properly handle multi-events. A Bayesian probabilistic approach allows EEW to evaluate the probability of having more than one earthquake given the current data set obtained from the seismic network. The most probable number of concurrent events is found under the Bayesian model class selection framework. Then, the earthquake parameters (e.g., hypocenter location, origin time and magnitude) of each event is estimated through the process of Bayesian inference. The JMA EEW system is used in this

chapter to illustrate the application of Bayesian methodologies to EEW and to demonstrate the effectiveness of the proposed algorithm using historical data. The methodology can also be applied to other EEW systems.

After a short review of the current JMA EEW system and some recent approaches to improve the system, I derive the theories embedded in the proposed algorithm starting from basic Bayesian model class selection theory. A simple numerical estimation method to establish the posterior probability density function (PDF) is presented, called here the Rao-Blackwellized Importance Sampling (RBIS) with sequential proposal PDFs. Practical modifications of the algorithm are suggested based on empirical experience. Finally, the proposed algorithm is tested with the 2011 Tohoku event sequence, including the foreshock on March 9, mainshock on March 11 and the aftershocks until April 30, using the Japan Meteorological Agency (JMA) EEW system as an example. Many false alarms have been observed for the existing JMA EEW system because it lacks the ability to identify multi-events cases. To verify that the proposed algorithm can handle such cases, I run it on a roughly two months waveform data set (March 9 to April 30, 2011) and record all identified earthquakes. The algorithm's performance is addressed by comparing the results with the official catalogue database from JMA (NIED, 2014). Then, this performance is compared with the existing JMA EEW system (JMA, 2013b).

## 3.2 Background on JMA EEW

Started in 2007, the JMA EEW system in Japan is the first country-wide EEW system, and it broadcasts warning to the public when the expected intensity measure is greater than 5− (in JMA seismic intensity scale). The current system employs a mixture of deterministic methods for earthquake detection and parameter estimation, mainly based on a continuous data stream from around 300 JMA seismic stations and 700 Hi-net stations located all around Japan (Hoshiba et al., 2008). First, the hypocenter location and origin time is estimated based on the picking time information from triggered stations. Then, the magnitude estimate is calculated based on the estimated hypocenter location and origin time using the JMA ground motion prediction equation (GMPE) (Kamigaichi, 2004; JMA, 2010, 2012), which will be shown in Section 3.3.2.2. Finally, the estimate of seismic intensity at each site is evaluated based on the estimated magnitude and hypocenter location.

The current system has difficulty in detecting more than one earthquake within a short period of time. The magnitude estimate of an event is primarily based on the maximum displacement amplitude recorded at the stations and the distance of the stations from the potential hypocenter. During the period of active seismicity after 2011 Tohoku earthquake, the JMA EEW system treated the data from multiple events as a single earthquake. Many near source stations of a small event were treated as far source stations of a large event (Figure 3.1). This led to a significant overestimate of magnitude and caused many false alarms (JMA, 2013a,b).

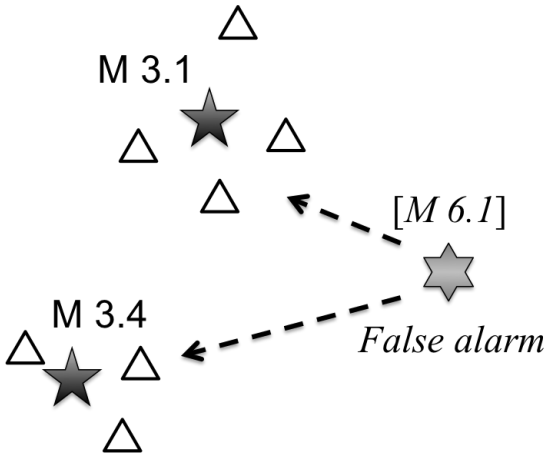


Figure 3.1: Near source stations of two small events falsely treated as far source stations from a large event. Triangle: triggered seismic station, 5-point star: real event, 6-point star: false alarm event.

To improve the system for handling multi-events, two approaches were proposed recently: (1) Hoshiba (2013) (Hoshiba, 2013) proposed a real-time ground motion prediction methodology based on wave propagation theory. Instead of estimating ground motion from hypocenter location and magnitude, this method directly estimates ground motion, which indirectly avoided the problem of not being able to identify multi-events, (2) Yamada et al. (2012) and Liu and Yamada (2014) proposed a multi-events recognition algorithm based on the idea of using a particle filter algorithm. This method attempted to estimate earthquake magnitude, hypocenter location and origin time from maximum displacement amplitude only. Motivated by method (2), this chapter presents a Bayesian probability framework to include multiple data features for earthquake parameter estimation. The Rao-Blackwellized Importance Sampling (RBIS) method, a simple numerical simulation scheme, is used to provide fast and accurate estimation. The idea is to maximize the portion of the solutions that can be done analytically under a given probabilistic model in order to reduce sampling size and improve the accuracy of the estimates. I apply the method to a model with two

features: P-wave picking time and maximum displacement amplitude, as an example. Figure 3.2 demonstrates the two chosen features.

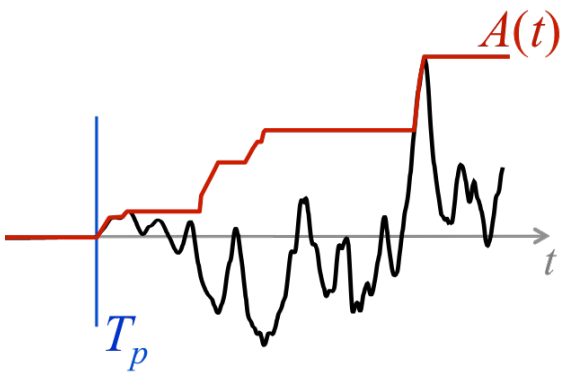


Figure 3.2: Two chosen features in this paper extracted from waveform data (black line): (1) $A(t)$—maximum displacement amplitude as a function of time $t$, (2) $T_p$—P-wave picking time.

## 3.3 Bayesian approach for multi-events EEW

In this chapter, I propose to use the Bayesian probability framework to solve the multi-events EEW problem. This section demonstrates how to apply the Bayesian model class selection framework with Bayesian inference to an existing deterministic EEW method. The JMA EEW system is used as an illustrative example. First, I explain the detail of the Bayesian model class selection in the context of EEW, starting from the two fundamental outputs of EEW: number of concurrent events and their parameters (e.g., magnitude, hypocenter location, origin time, etc.). Second, I propose an efficient numerical sampling method, the Rao-Blackwellized Importance Sampling (RBIS), to estimate earthquake parameters under the Bayesian approach, and derive the expressions needed for calculating the output.

### 3.3.1 Bayesian model class selection for multi-events

#### 3.3.1.1 Major notation

The EEW system receives and processes seismic network data continuously to provide updated warning and earthquake information. In the case of multi-events, the EEW system needs to identify the number of concurrent events given the current data set, as well as their information, in order

to broadcast accurate warnings to the users. For the ease of derivation, this chapter adopts the following notation:

- $\mathcal{D}_{1:t} = \{D_j(1:t)|j = 1, ..., N_{st}\}$—set of waveform data for $N_{st}$ stations from initial time step 1 to time step $t$
- $\mathcal{F}_t = \{F_j(t)|j = 1, ..., N_{st}\}$—set of vectors of data features, which are extracted from the waveform data $\mathcal{D}_{1:t}$, for each of the $N_{st}$ stations, and used for parameter estimation
- $\mathcal{M}_n$—model class for assuming $n$ concurrent events are captured within the current data set $\mathcal{D}_{1:t}$
- $\Theta = \{\theta_l|l = 1, ..., n\}$—set of vectors of earthquake parameters $\theta_l$ for each of the $n$ events given $\mathcal{M}_n$ (Assumption A1: $\Theta$ is independent of time $t$, i.e., it is a static variable)

#### 3.3.1.2 Probability approach of EEW

Based on the notation in Section 3.3.1.1, in this section the two outputs of EEW are expressed in a mathematical form based on fundamental probability theory.

Starting from some initial time step 1, at every time step $t$:

1. Find the most probable number of events that explain the current data set at time $t$, i.e., Find $\hat{n} = \text{argmax}_n\{P(\mathcal{M}_n|\mathcal{D}_{1:t})\}$.

   This optimization problem is often referred to as Bayesian model class selection in the literature (Beck, 2010). To solve $\hat{n}$ with a more explicit expression, one can consider a simple sequential model of Bayesian Network: $(\mathcal{D}_{1:t}) \rightarrow (\mathcal{F}_t) \rightarrow (\Theta/\mathcal{M}_n)$

$$P(\mathcal{M}_n|\mathcal{D}_{1:t}) = \int P(\mathcal{M}_n|\mathcal{F}_t)p(\mathcal{F}_t|\mathcal{D}_{1:t})\,\mathrm{d}\mathcal{F}_t \tag{3.1}$$

   $p(\mathcal{F}_t|\mathcal{D}_{1:t})$ is the PDF that includes error in finding features from the original waveform data. Assumption A2: For simplicity, take a deterministic model for finding $\mathcal{F}_t$ from a given data set up to time $t$, $\mathcal{D}_{1:t}$. As a result, $P(\mathcal{M}_n|\mathcal{D}_{1:t}) = P(\mathcal{M}_n|\mathcal{F}_t)$, where $\mathcal{F}_t$ is a function of $\mathcal{D}_{1:t}$. By Bayes' theorem:

$$P(\mathcal{M}_n|\mathcal{F}_t) = \frac{p(\mathcal{F}_t|\mathcal{M}_n)P(\mathcal{M}_n)}{p(\mathcal{F}_t)} \propto p(\mathcal{F}_t|\mathcal{M}_n)P(\mathcal{M}_n) \tag{3.2}$$

Assumption A3: non-informative prior $P(\mathcal{M}_n) = constant\ \forall n$, to avoid imposing any bias on any model class before the data is collected. Hence:

$$\begin{aligned} &P(\mathcal{M}_n|\mathcal{F}_t) \propto p(\mathcal{F}_t|\mathcal{M}_n) \\ &\Rightarrow \hat{n} = \text{argmax}_n\{P(\mathcal{M}_n|\mathcal{F}_t)\} = \text{argmax}_n\{p(\mathcal{F}_t|\mathcal{M}_n)\} \end{aligned} \tag{3.3}$$

where by the Total Probability Theorem:

$$p(\mathcal{F}_t|\mathcal{M}_n) = \int p(\mathcal{F}_t|\Theta, \mathcal{M}_n)p(\Theta|\mathcal{M}_n)\,\mathrm{d}\Theta \tag{3.4}$$

The models for $p(\mathcal{F}_t|\Theta, \mathcal{M}_n)$ and $p(\Theta|\mathcal{M}_n)$ are introduced later.

2. Find earthquake parameter values $\Theta$ for all events given $\mathcal{M}_{\hat{n}}$,
   i.e., Find $p(\Theta|\mathcal{M}_{\hat{n}}, \mathcal{D}_{1:t})$, the posterior PDF of $\Theta$.
   This is the Bayesian inference problem under a specified model class. By Bayes' theorem (with Assumption A2 applied):

$$\begin{aligned} p(\Theta|\mathcal{M}_{\hat{n}}, \mathcal{D}_{1:t}) &= p(\Theta|\mathcal{M}_{\hat{n}}, \mathcal{F}_t) \\ &= \frac{p(\mathcal{F}_t|\Theta, \mathcal{M}_{\hat{n}})p(\Theta|\mathcal{M}_{\hat{n}})}{p(\mathcal{F}_t|\mathcal{M}_{\hat{n}})} \\ &\propto p(\mathcal{F}_t|\Theta, \mathcal{M}_{\hat{n}})p(\Theta|\mathcal{M}_{\hat{n}}) \end{aligned} \tag{3.5}$$

   Note that the evidence function $p(\mathcal{F}_t|\mathcal{M}_{\hat{n}})$ is the same one used for finding $\hat{n}$. Hence, one can simply calculate the posterior of the parameters of each possible model class and pick the one with maximum evidence value.

#### 3.3.1.3 Practical implementation to handle multi-events

An effective EEW system should provide regular updates of the warning using the continuous seismic data stream. For example, the JMA EEW system provides a warning update every second. Hence, there is limited time to perform the full model class selection scheme through calculating the evidence functions of all possible model class $\mathcal{M}_{\hat{n}}$. From our experience, existing methods to calculate or estimate the evidence function $p(\mathcal{F}_t|\mathcal{M}_n)$ may not be fast enough for this purpose. This motivates the need of a suboptimal model class selection scheme that is efficient yet robust.

Earthquakes happen in sequence. Therefore, $\mathcal{M}_{\hat{n}}$ is a monotonically increasing function of time $t$. Exploiting this pattern, instead of searching for an optimal $\hat{n}$ at every second, one may start with $\hat{n} = 0$ and increase $\hat{n}$ by one every time a fast calculated criterion is met. Intuitively, $\hat{n}$ should be increased by one when the current data set $\mathcal{D}_{1:t}$ cannot be explained by any of the identified events given the currently selected model class $\mathcal{M}_{\hat{n}}$. In other words, let $\mathcal{M}_{\hat{n}} = \{M_l | l = 1, ..., \hat{n}\}$ where $M_l$ represents each event identified within $\mathcal{M}_{\hat{n}}$, one may increase $\hat{n}$ by one when the following criterion is met (with Assumption A2 applied):

$$p(\mathcal{F}_t | M_l) < \tau_{new} \ \ \forall l = 1, ..., \hat{n} \tag{3.6}$$

Here, $\tau_{new}$ is some empirical threshold (possibly depending on $\hat{n}$) for how well the current data set features $\mathcal{F}_t$ are explained by an event $M_l$, and $p(\mathcal{F}_t | M_l)$ is calculated by Equation 3.4.

Note that with this new approach, $\theta_l$ is only dependent on $M_l$ within $\mathcal{M}_{\hat{n}}$. Hence, the posterior of each $\theta_l \in \Theta$, $p(\theta_l | \mathcal{M}_{\hat{n}}, \mathcal{D}_{1:t}) = p(\theta_l | M_l, \mathcal{D}_{1:t})$, can be found separately. For notational simplicity, $M_l$ will be left as implicit whenever $\theta_l$ appears in the rest of this chapter. Hence, the posterior of parameters for each event becomes:

$$p(\theta_l | \mathcal{F}_t) = \frac{p(\mathcal{F}_t | \theta_l) p(\theta_l)}{p(\mathcal{F}_t | M_l)} \propto p(\mathcal{F}_t | \theta_l) p(\theta_l) \tag{3.7}$$

Equation 3.6 involves calculations with the complete feature set $\mathcal{F}_t$. One can further simplify the criterion by calculating with only one set of features $F_j(t)$ that is extracted from a single station $j$. Because most earthquakes have only one first triggered station, each event can be represented by its first triggered station. One can continuously search for newly triggered stations that have a low probability to be caused by any of the existing events in $\mathcal{M}_{\hat{n}}$. Those stations are likely to be the first triggered stations of new events. As a result, a more efficient criterion is:

$$p(F_j(t) | M_l) < \tau_{new} \text{ for newly triggered station } j \ \& \ \forall l = 1, ..., \hat{n} \tag{3.8}$$

As will be discussed in Section 3.3.2, this study adopts a simple numerical method, called the Rao-Blackwellized Importance Sampling (RBIS), to estimate the posterior PDF of the earthquake parameters. Under this method, calculation of $p(F_j(t) | M_l)$ may involve integrating information from all samples $\tilde{\theta}^{(i)}$ for $i = 1, ..., N_s$. To further reduce computational effort, one may estimate

$p(F_j(t)|M_l)$ with an optimal value $\hat{\theta}_l$ based on the assumption that the posterior PDF of $\theta_l$, $p(\theta_l|\mathcal{F}_t)$, has a narrow peak. For example, $\hat{\theta}_l$ can be the mean or maximizer of $p(\theta_l|\mathcal{F}_t)$. Hence, the criterion can be changed to:

$$p(F_j(t)|\hat{\theta}_l) < \tau_{new} \text{ for newly triggered station } j \ \& \ \forall l = 1, ..., \hat{n} \tag{3.9}$$

### 3.3.2 Estimation of earthquake parameters using RBIS

Given a model class $\mathcal{M}_{\hat{n}}$, the posterior PDF of earthquake parameters $p(\theta_l|\mathcal{F}_t)$ of each event $M_l \in \mathcal{M}_{\hat{n}}$ is needed for broadcasting appropriate warning. In practice, a numerical scheme is often needed to estimate the posterior PDF. This section demonstrate the RBIS method for this purpose (the reason for using RBIS is explained in Section 3.3.2.1). For illustrative purposes, two commonly used features, $F_j(t) = [F_{p,j}(t), F_{a,j}(t)]$, are chosen for each station $j$: $F_{p,j}$—P-wave picking time and $F_{a,j}$—log of maximum displacement amplitude (Figure 3.2). Also, five earthquake parameters, $\theta_l = [lat_l, lon_l, d_l, m_l, t0_l]$, are needed for each event $M_l$: $lat$—hypocenter latitude, $lon$—hypocenter longitude, $d$—hypocenter depth, $m$—earthquake magnitude and $t0$—origin time. As an example, this chapter applies the existing JMA EEW model as a basis for calculating the likelihood functions in the Bayesian approach. Details are explained in Section 3.3.2.2.

#### 3.3.2.1 Rao-Blackwellized Importance Sampling

Figure 3.3 shows the variable dependency between the chosen data features and earthquake parameters. Based on this model and Assumption A4: the predictions of the station data are independent of each other, the likelihood function $p(\mathcal{F}_t|\theta_l)$ in Equation 3.7 is expressed as:

$$p(\mathcal{F}_t|\theta_l) = \prod_{j=1}^{N_{st}} [p(F_{p,j}(t)|\theta_l)p(F_{a,j}(t)|\theta_l)] \tag{3.10}$$

Because there are few choices of likelihood model that have a completely analytical solution in the EEW problem, a numerical estimation of the posterior PDF is needed. A simple numerical scheme, such as importance sampling, is preferred for real-time running of EEW. Other choices of numerical sampling methods are feasible depending on the choice of the feature set and the likelihood models. Based on the structure shown in Figure 3.3, I observe that $m$ can be analytically

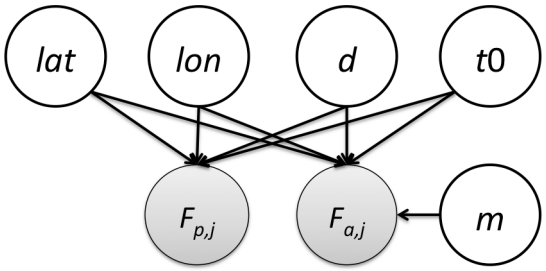


Figure 3.3: Bayesian network model of probabilistic dependency between the data features $\mathcal{F}_t$ and earthquake parameters $\Theta$.

treated without significantly increasing the complexity of the equations (I found that analytically treating $t0$ will induce large complexity into the problem). Hence, $\theta_l$ is separated into $[m, \tilde{\theta}_l]$, where $\tilde{\theta}_l$ includes all the other sampled parameters. A set of sequential proposal PDFs based on the posterior PDF from the previous time step can be implemented for the sake of efficient convergence of the samples in the importance sampling scheme (Section 3.4.3 shows an example). To conclude, I use the Rao-Blackwellized Importance Sampling (RBIS) method as follow:

$$\begin{aligned} p(\theta_l|\mathcal{F}_t) &= p(m|\tilde{\theta}_l, \mathcal{F}_t)p(\tilde{\theta}_l|\mathcal{F}_t) \approx \sum_{i=1}^{N_s} w_i p(m|\tilde{\theta}_l^{(i)}, \mathcal{F}_t)\delta(\tilde{\theta}_l - \tilde{\theta}_l^{(i)}) \\ &\text{where } \tilde{\theta}_l^{(i)} \sim q(\tilde{\theta}_l), N_s = \text{number of samples,} \\ w_i &\propto \frac{p(\tilde{\theta}_l^{(i)}|\mathcal{F}_t)}{q(\tilde{\theta}_l^{(i)})} \text{ and } \sum_{i=1}^{N_s} w_i = 1 \end{aligned} \tag{3.11}$$

In order to exploit the information from previous time step, one can choose $q(\tilde{\theta}_l^{(i)})$ to be $p(\tilde{\theta}_l^{(i)}|\mathcal{F}_{t-1})$ or a constrained uniform distribution based on $p(\tilde{\theta}_l^{(i)}|\mathcal{F}_{t-1})$. For example, let $q(\tilde{\theta}_l^{(i)}) = p(\tilde{\theta}_l^{(i)}|\mathcal{F}_{t-1})$, then Bayes' Theorem simplifies the weights $w_i$ to be:

$$w_i \propto \frac{p(\mathcal{F}_t|\tilde{\theta}_l^{(i)})}{p(\mathcal{F}_{t-1}|\tilde{\theta}_l^{(i)})} \tag{3.12}$$

$$\text{where } p(\mathcal{F}_t|\tilde{\theta}_l^{(i)}) = \int p(\mathcal{F}_t|\theta_l^{(i)})p(m)\,\mathrm{d}m,\ \theta_l^{(i)} = [\tilde{\theta}_l^{(i)}, m] \tag{3.13}$$

#### 3.3.2.2 Gaussian likelihood implementation

A Gaussian model is chosen for both features $F_{p,j}$ and $F_{a,j}$ because of the ease in analytical derivation for $m$ and overall model simplicity:

1. Gaussian likelihood for pick time:

$$p(F_{p,j}(t)|\theta_l) = \frac{1}{\sigma_{p,j}(\theta_l)}\phi\left(\frac{F_{p,j}(t) - \mu_{p,j}(\theta_l)}{\sigma_{p,j}(\theta_l)}\right) \tag{3.14}$$

   where $\mu_{p,j}(\theta_l)$ = theoretical P-wave arrival time at station $j$ given $\theta_l$
   and $\sigma_{p,j}(\theta_l)$ = empirical standard deviation for the P-wave arrival time model

2. Gaussian likelihood for log of maximum displacement amplitude:

$$p(F_{a,j}(t)|\theta_l) = \frac{1}{\sigma_{a,j}(\theta_l)}\phi\left(\frac{F_{a,j}(t) - \mu_{a,j}(\theta_l)}{\sigma_{a,j}(\theta_l)}\right) \tag{3.15}$$

   where $\mu_{a,j}(\theta_l)$ = attenuation equation for $F_{a,j}$ at station $j$ given $\theta_l$
   and $\sigma_{a,j}(\theta_l)$ = empirical standard deviation for the attenuation model

In general, a Gaussian likelihood model with either a Gaussian prior or an uniform prior will result in a Gaussian posterior, which is an analytical solution, if the mean of the likelihood function is a linear function of the model parameters. However, in the case of EEW, $\mu_{a,j}(\theta_l)$ is often a nonlinear function of the parameters $\theta_l$, and so the analytical solution cannot be obtained. Using JMA attenuation equations (Kamigaichi, 2004; JMA, 2010, 2012) as an illustrative example, let $S_s$ be the set of indices of S-wave arrived stations, $S_p$ be the set of indices of P-wave arrived stations, and $S_n$ be the set of indices of no wave-arrival stations, then the mean of maximum displacement amplitude:

$$\mu_{a,j} = \begin{cases} \mu_{noise,j} & j \in S_n \\ 0.72m - 1.2\log R - 0.0005R + 0.005d - 0.46 & j \in S_p \\ 0.87m - \log R - 0.0019R + 0.005d - 0.98 & j \in S_s \end{cases} \tag{3.16}$$

Here, $R$ is the hypocenter-to-site distance (km) as a function of $lat$, $lon$ and $d$; $\mu_{noise,j}$ and $\sigma_{a,j}$ are determined empirically based on the historical data; $t0$ plays a role in deciding which set $j$ belongs to based on a traveling wave model.

#### 3.3.2.3 Analytical treatment of magnitude

Although a fully analytical solution is often not available, the likelihood function is likely to be a linear function of earthquake magnitude $m$ given the other parameters $\tilde{\theta}_l$. Hence, one can apply

the idea of RBIS on $m$ to obtain a partially analytical solution that improves both the accuracy and efficiency of the original numerical simulation scheme.

EEW requires the mean (expected value) and standard deviation of the earthquake parameters given the current data set, i.e., $E[\theta_l|\mathcal{F}_t]$ and $Var[\theta_l|\mathcal{F}_t]$, in order to release appropriate warnings. Note that $Var[\theta_l] = E[\theta_l^2] - (E[\theta_l])^2$ and based on Equation 3.11, for any function of $\theta_l$, $f(\theta_l)$:

$$\begin{aligned} E[f(\theta_l)|\mathcal{F}_t] &= \int f(\theta_l) p(\theta_l|\mathcal{F}_t)\,\mathrm{d}\theta_l \\ &\approx \int f(\theta_l) \sum_{i=1}^{N_s} w_i p(m|\tilde{\theta}_l^{(i)}, \mathcal{F}_t)\delta(\tilde{\theta}_l - \tilde{\theta}_l^{(i)})\,\mathrm{d}\theta_l \\ &= \sum_{i=1}^{N_s} w_i \int f(m, \tilde{\theta}_l^{(i)}) p(m|\tilde{\theta}_l^{(i)}, \mathcal{F}_t)\,\mathrm{d}m \end{aligned} \tag{3.17}$$

Combining with Equation 3.11, I can then derive the following expressions:

$$\begin{aligned} E[\tilde{\theta}_l|\mathcal{F}_t] &= \sum_{i=1}^{N_s} w_i \tilde{\theta}_l^{(i)} \\ Var[\tilde{\theta}_l|\mathcal{F}_t] &= \sum_{i=1}^{N_s} w_i (\tilde{\theta}_l^{(i)})^2 - (E[\tilde{\theta}_l|\mathcal{F}_t])^2 \end{aligned} \tag{3.18}$$

$$\begin{aligned} E[m|\mathcal{F}_t] &= \sum_{i=1}^{N_s} w_i \int m\, p(m|\tilde{\theta}_l^{(i)}, \mathcal{F}_t)\,\mathrm{d}m \\ Var[m|\mathcal{F}_t] &= \sum_{i=1}^{N_s} w_i \int m^2 p(m|\tilde{\theta}_l^{(i)}, \mathcal{F}_t)\,\mathrm{d}m - (E[m|\mathcal{F}_t])^2 \end{aligned} \tag{3.19}$$

As a result, I need analytical results for $p(m|\tilde{\theta}_l^{(i)}, \mathcal{F}_t)$ and $w_i$ (or $p(\mathcal{F}_t|\tilde{\theta}_l^{(i)})$). After that, I can also derive the analytical expression for $p(\mathcal{F}_t|M_l)$ in Equation 3.6 or 3.8. For notation simplicity, $l$ is omitted whenever $(i)$ occurs since the sample index $i$ is always linked with the earthquake index $l$:

1. $p(m|\tilde{\theta}^{(i)}, \mathcal{F}_t)$

   Note that $m$ only depends on $F_{a,j}$ for $j = 1, ..., N_{st}$, i.e., $p(m|\tilde{\theta}^{(i)}, \mathcal{F}_t) = p(m|\tilde{\theta}^{(i)}, F_{a,1}, ..., F_{a,N_{st}})$.

   Again, by Bayes' Theorem (with assumption A4 applied):

$$p(m|\tilde{\theta}^{(i)}, F_{a,1}, ..., F_{a,N_{st}}) \propto p(F_{a,1}, ..., F_{a,N_{st}}|\theta^{(i)}) p(m) = p(m) \prod_{j=1}^{N_{st}} p(F_{a,j}|\theta^{(i)}) \tag{3.20}$$

The JMA model is used as an example to show the steps of the analytical derivation. Applying Equation 3.15 with a modification to Equation 3.16, I can rewrite the expression of $p(F_{a,j}|\theta^{(i)})$ to be:

$$p(F_{a,j}|\theta^{(i)}) = \begin{cases} \frac{1}{\sigma_{a,j}^{(i)}}\phi\left(\frac{F_{a,j}-\mu_{noise,j}}{\sigma_{a,j}^{(i)}}\right) & j \in S_n \\ \frac{1}{\sigma_{a,j}^{(i)}}\phi\left(\frac{m-f_{JMA,j}^{(i)}}{\sigma_{a,j}^{(i)}}\right) & j \in S_p \cup S_s \end{cases}$$
$$\text{where } f_{JMA,j}^{(i)} = \begin{cases} (F_{a,j} + 1.2\log R^{(i)} + 0.0005R^{(i)} - 0.005d^{(i)} + 0.46)/0.72 & j \in S_p \\ (F_{a,j} + \log R^{(i)} + 0.0019R^{(i)} - 0.005d^{(i)} + 0.98)/0.87 & j \in S_s \end{cases} \tag{3.21}$$

Here, $R^{(i)}$ and $d^{(i)}$ are obtained from $\tilde{\theta}^{(i)}$; $\mu_{noise,j}$ depends on station $j$; $\sigma_{a,j}^{(i)}$ depends on sample $\tilde{\theta}^{(i)}$ and station $j$. By the well-known property of product of Gaussian functions, I can derive the following expression:

$$\prod_{j\in S_p\cup S_s} \frac{1}{\sigma_{a,j}^{(i)}}\phi\left(\frac{m-f_{JMA,j}^{(i)}}{\sigma_{a,j}^{(i)}}\right) = \frac{z^{(i)}}{\sigma_m^{(i)}}\phi\left(\frac{m-\mu_m^{(i)}}{\sigma_m^{(i)}}\right)$$
$$\text{where } \left(\sigma_m^{(i)}\right)^2 = \left(\sum_{j\in S_p\cup S_s} \frac{1}{\left(\sigma_{a,j}^{(i)}\right)^2}\right)^{-1},\ \mu_m^{(i)} = \left(\sigma_m^{(i)}\right)^2 \left(\sum_{j\in S_p\cup S_s} \frac{f_{JMA,j}^{(i)}}{\left(\sigma_{a,j}^{(i)}\right)^2}\right) \tag{3.22}$$
$$\text{and } z^{(i)} = \frac{\sqrt{2\pi\left(\sigma_m^{(i)}\right)^2}}{\prod_{j\in S_p\cup S_s}\sqrt{2\pi\left(\sigma_{a,j}^{(i)}\right)^2}} \exp\left[\frac{1}{2}\left(\frac{\left(\mu_m^{(i)}\right)^2}{\left(\sigma_m^{(i)}\right)^2} - \sum_{j\in S_p\cup S_s}\frac{\left(f_{JMA,j}^{(i)}\right)^2}{\left(\sigma_{a,j}^{(i)}\right)^2}\right)\right]$$

As a result, I conclude that:

$$\prod_{j=1}^{N_{st}} p(F_{a,j}|\theta^{(i)}) = \frac{z^{(i)}}{\sigma_m^{(i)}}\phi\left(\frac{m-\mu_m^{(i)}}{\sigma_m^{(i)}}\right) \prod_{j\in S_n}\frac{1}{\sigma_{a,j}^{(i)}}\phi\left(\frac{F_{a,j}-\mu_{noise}}{\sigma_{a,j}^{(i)}}\right) \tag{3.23}$$

2. $p(\mathcal{F}_t|\tilde{\theta}^{(i)})$

First, I find an analytical expression for $p(\mathcal{F}_t|\theta^{(i)})$ by combining Equation 3.10, 3.14 and 3.23:

$$p(\mathcal{F}_t|\theta^{(i)}) = \frac{z^{(i)}}{\sigma_m^{(i)}}\phi\left(\frac{m-\mu_m^{(i)}}{\sigma_m^{(i)}}\right) \prod_{j\in S_n}\frac{1}{\sigma_{a,j}^{(i)}}\phi\left(\frac{F_{a,j}-\mu_{noise,j}}{\sigma_{a,j}^{(i)}}\right) \prod_{j=1}^{N_{st}}\frac{1}{\sigma_{p,j}^{(i)}}\phi\left(\frac{F_{p,j}-\mu_{p,j}^{(i)}}{\sigma_{p,j}^{(i)}}\right) \tag{3.24}$$

where $\mu_{p,j}^{(i)}$ and $\sigma_{p,j}^{(i)}$ depends on sample $\tilde{\theta}^{(i)}$ and station $j$ as well.

Combining Equation 3.13 and 3.24:

$$p(\mathcal{F}_t|\tilde{\theta}^{(i)}) = z^{(i)} \prod_{j \in S_n} \frac{1}{\sigma_{a,j}^{(i)}} \phi\left(\frac{F_{a,j} - \mu_{noise,j}}{\sigma_{a,j}^{(i)}}\right) \prod_{j=1}^{N_{st}} \frac{1}{\sigma_{p,j}^{(i)}} \phi\left(\frac{F_{p,j} - \mu_{p,j}^{(i)}}{\sigma_{p,j}^{(i)}}\right) \int \frac{p(m)}{\sigma_m^{(i)}} \phi\left(\frac{m - \mu_m^{(i)}}{\sigma_m^{(i)}}\right) \mathrm{d}m \tag{3.25}$$

3. Choice of prior $p(m)$

   The integral in Equation 3.25 can be solved analytically only for some specific choices of the prior $p(m)$, for example, a Gaussian prior or a uniform prior. In the case of EEW, when a potential earthquake is detected based on the triggering of any seismic stations, no bias in the magnitude estimate should be introduced prior to extracting further information from the waveform data. Therefore, a uniform prior is chosen instead of a prior for the well-known Gutenberg-Richter law:

$$p(m) = \begin{cases} 0 & m < a \ \& \ m > b \\ 1/(b-a) & a \leq m \leq b \end{cases} \tag{3.26}$$

   A reasonable choice for the parameters would be $a = 0$ and $b = 10$ because this is the likely range of earthquake magnitudes.

   As a result, the integral in Equation 3.25 is related to the Gaussian CDF and Equation 3.25 becomes:

$$\begin{aligned} p(\mathcal{F}_t|\tilde{\theta}^{(i)}) &= \frac{z^{(i)} c_0^{(i)}}{b-a} \prod_{j \in S_n} \frac{1}{\sigma_{a,j}^{(i)}} \phi\left(\frac{F_{a,j} - \mu_{noise,j}}{\sigma_{a,j}^{(i)}}\right) \prod_{j=1}^{N_{st}} \frac{1}{\sigma_{p,j}^{(i)}} \phi\left(\frac{F_{p,j} - \mu_{p,j}^{(i)}}{\sigma_{p,j}^{(i)}}\right) \\ \text{where } c_0^{(i)} &= \Phi\left(\frac{b - \mu_m^{(i)}}{\sigma_m^{(i)}}\right) - \Phi\left(\frac{a - \mu_m^{(i)}}{\sigma_m^{(i)}}\right) \end{aligned} \tag{3.27}$$

   Note that in most cases, $c_0^{(i)} \approx 1$ because the Gaussian PDF with $\mu_m^{(i)}$ and $\sigma_m^{(i)}$ should have most of its density between the chosen prior value $a$ and $b$. In other words, $c_0^{(i)}$ is a discounting factor that penalizes the likelihood function putting probability density outside the predetermined magnitude range. Also, if $S_p$ and $S_s$ are both a null set $\emptyset$, the factor $\frac{z^{(i)} c_0^{(i)}}{b-a}$ is deleted from Equation 3.27.

4. $\int m\, p(m|\tilde{\theta}^{(i)}, \mathcal{F}_t)\, \mathrm{d}m$ and $\int m^2 p(m|\tilde{\theta}^{(i)}, \mathcal{F}_t)\, \mathrm{d}m$

   These two integrals in Equation 3.19 are simply the first and second moment of the uniform PDF if $S_p$ and $S_s$ are both a null set $\emptyset$, or the first and second moment of the truncated Gaussian PDF otherwise. Their analytical expressions can be written as follow:

$$\begin{aligned}
\int m\, p(m|\tilde{\theta}^{(i)}, \mathcal{F}_t)\, \mathrm{d}m &\equiv \tilde{\mu}_m^{(i)} \\
&= \begin{cases} \frac{a+b}{2}, & S_p \cup S_s = \emptyset \\ \mu_m^{(i)} + \frac{\sigma_m^{(i)}}{c_0^{(i)}} \left[ \phi\left( \frac{a-\mu_m^{(i)}}{\sigma_m^{(i)}} \right) - \phi\left( \frac{b-\mu_m^{(i)}}{\sigma_m^{(i)}} \right) \right], & \text{otherwise} \end{cases} \\
\int m^2 p(m|\tilde{\theta}^{(i)}, \mathcal{F}_t)\, \mathrm{d}m &= \left(\tilde{\mu}_m^{(i)}\right)^2 + \left(\tilde{\sigma}_m^{(i)}\right)^2 \\
\text{where } \left(\tilde{\sigma}_m^{(i)}\right)^2 &= \begin{cases} \frac{(b-a)^2}{12}, & S_p \cup S_s = \emptyset \\ \left( \frac{\sigma_m^{(i)}}{c_0^{(i)}} \right)^2 \tilde{c}^{(i)}, & \text{otherwise} \end{cases}
\end{aligned} \tag{3.28}$$

$$\begin{aligned}
\tilde{c}^{(i)} = &\left(c_0^{(i)}\right)^2 + \frac{c_0^{(i)}(a-\mu_m^{(i)})}{\sigma_m^{(i)}} \phi\left( \frac{a-\mu_m^{(i)}}{\sigma_m^{(i)}} \right) - \frac{c_0^{(i)}(b-\mu_m^{(i)})}{\sigma_m^{(i)}} \phi\left( \frac{b-\mu_m^{(i)}}{\sigma_m^{(i)}} \right) \\
&- \left( \phi\left( \frac{a-\mu_m^{(i)}}{\sigma_m^{(i)}} \right) - \phi\left( \frac{b-\mu_m^{(i)}}{\sigma_m^{(i)}} \right) \right)^2
\end{aligned} \tag{3.29}$$

Now, I can obtain the analytical expression for the last missing part in this problem, i.e., $p(\mathcal{F}_t|M_l)$ in Equation 3.6 or 3.8, which is simply the evidence function of the earthquake parameter posterior PDF given $M_l$. Under the simplified notation, $p(\mathcal{F}_t|M_l) \to p(\mathcal{F}_t)$ for each earthquake index $l$. By applying the Total Probability Theorem with importance sampling using the posterior PDF as the proposal PDF (Newton, 1994):

$$p(\mathcal{F}_t) = \int p(\mathcal{F}_t|\theta_l) p(\theta_l) \mathrm{d}\theta \approx \frac{1}{N_s} \left( \sum_{i=1}^{N_s} \frac{1}{p(\mathcal{F}_t|\tilde{\theta}^{(i)})} \right)^{-1} \tag{3.30}$$

where $p(\mathcal{F}_t|\tilde{\theta}^{(i)})$ is calculated by Equation 3.27.

## 3.4 Multi-events EEW algorithm

Actual implementation of the proposed probabilistic approach faces some practical challenges that reduce its efficiency. For instance, it is often difficult to maintain a large seismic network. Unexpected noisy data caused by station damage or human activities may not be well described by any probability model that can be calculated fast. Also, because of the sparse network on the sea floor, offshore events require longer time to be identified and have a larger prediction variance. In this section, several suggestions are provided based on our experience on running the EEW system with historical data. These suggestions seek for a balance between a fast algorithm due to the short time available for computation and a robust prediction under the practical challenges. At the end, a summary of the algorithm is presented, which integrates the theory in Section 3.3 and the practical improvements in this section.

### 3.4.1 Creating, merging and canceling events

Empirical experience shows that there are often noise triggers caused by equipment error or false picking. This type of error cannot be described by typical probability models, such as the Gaussian model used as an example in this study, that yield a fast-computable result for EEW. In order to filter out these triggers that may lead to error in the trigger-based algorithm (e.g., criterion based on Equation 3.8 or 3.9), extra constraints can be added before an event is actually created:

1. Filter small events: Many small events or far away offshore events that do not cause intense shaking in the region of interest may be neglected for the sake of EEW. One may consider adding a lower threshold for the waveform amplitude of the first triggered station of a potential event to filter out events that have minimal influence.

2. Filter large local noise: Human activities or equipment error may sometimes appear as an large impulsive signal. A check based on wave propagation is effective for filtering out such an event. For example, one may require more than one consecutive trigger of stations close by before an actual event is created in the algorithm. Such a method is especially effective for a dense seismic network because the induced time delay in waiting to verify an event will be minimal. For example, the Japan JMA EEW system may integrate the Hi-net stations and the JMA stations under the same system to significantly increase the network density.

Although $\mathcal{M}_{\hat{n}}$ is a monotonically increasing function of time, the noisy environment of the seismic network may create artificial events. A merging or canceling event criterion that allows stepping $\mathcal{M}_{\hat{n}}$ backward is necessary to improve robustness of the system. Here are two suggestions:

1. Deleting based on picking time alignment: After the trigger of the first few stations of an event, the hypocenter and origin time estimates will start to converge. From this moment, if the observed picking times of the stations deviate from the theoretical P-wave arrival times based on the current parameter estimates, this event is likely to be falsely identified and can be deleted from the algorithm.

2. Merging based on hypocenter and origin time estimate: To avoid false alarm due to a duplicated event caused by noise data, it is beneficial to maintain a unique set of event records in the algorithm. Two events are merged if their converged hypocenter and origin time estimates are reasonably close. In some cases, even if the two events are actually not identical events, it is beneficial to merge them within the EEW system in order to avoid confusing warning.

### 3.4.2 Selective data subset

Theoretically, in the absence of noise, four independent pieces of information are enough to pinpoint the location and origin time of an earthquake. In most earthquakes, their parameters can be accurately identified based on data from around five to ten stations closest to the hypocenter. Furthermore, due to the attenuation effect of the seismic waves, information from stations that are far from the hypocenter has negligible contribution to the posterior PDF. Instead of using all stations for every event, $\mathcal{F}_t$ is reduced to include only information from stations within the *effective range* of the first triggered station (the theoretically closest location to the hypocenter) of an event. This is equivalent to assuming $p(F_j(t)|\theta_l) = 1$ for all station $j$ outside the *effective range* for event $M_l$.

Distance is not the only factor for selecting a subset of the stations to be used for an earthquake. For offshore earthquakes, stations are often available on only the land side of the event. A wide azimuth coverage can significantly improve the estimation of hypocenter and origin time. Combining both factors, a fixed number of stations based on a newly triggered station can be selected in two steps:

1. Select a subset of stations that have the closest distance to the triggered station.

2. Select the remaining stations one-by-one that lead to the most increase of azimuth coverage from the existing set of stations.

Using Japan as an example, Figure 3.4 shows the station selection for both inland and coastline stations. The proposed two-step selection scheme will automatically result in a purely distance-based selection for the inland case, and a combine-factors selection in the coastline case.

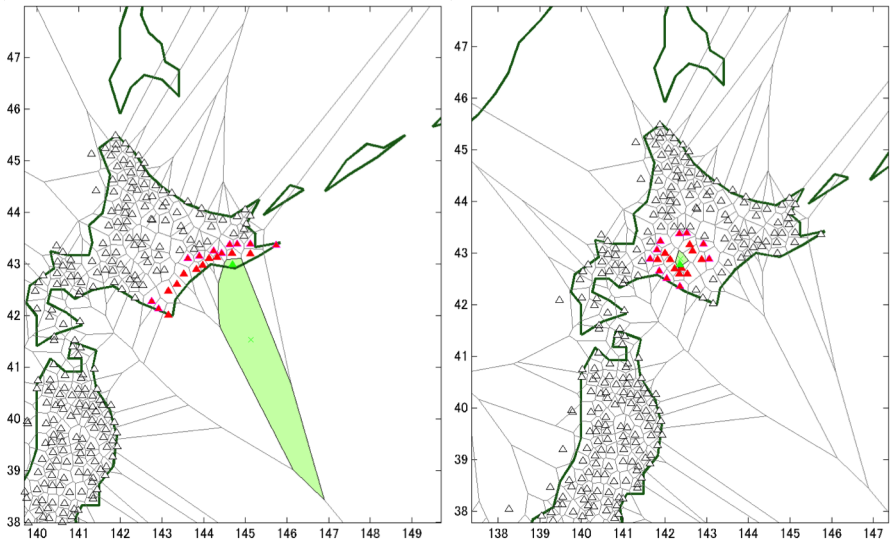


Figure 3.4: Example of station selection in Japan for coastline (left) and inland (right) station. Seismic stations are denoted in triangles. The green area represents the Voronoi cell of the newly triggered station. The red stations are selected stations for the newly triggered station (green triangle).

### 3.4.3 Sample prior and update

From empirical experience, even if noise is included, it is highly probable to obtain a likelihood function $p(\mathcal{F}_t|\tilde{\theta}_l)$ that is peaked around the true earthquake parameter values soon after the first triggered (P-wave picked) station occurs, especially for inland earthquakes. The speed of convergence increases as the network density increases. For example, it only takes a few seconds to converge to an inland earthquake under the combined network of JMA and Hi-net stations in Japan. As a result, instead of using a prior (the initial proposal PDF in RBIS) that covers all possible space and time within the region of interest, one may sample from a uniform distribution around the first triggered station of a new event, and a reduced time range depending on the spatial area of the location prior. The spatial extent of the uniform distribution can be determined based on the Voronoi cell methodology.

Because of the lack of station coverage on the sea, the Voronoi cell of a station on the coastline can be very large. Instead of using the large Voronoi cell as a prior, one may use a smaller cell around the station and add a sample updating scheme. When it is an offshore event, the updating scheme will guide the samples to converge toward the hypocenter after each time step. A possible updating scheme conditioning on the hypocenter estimate from the previous time step is:

1. Shift samples toward the direction of the new expected hypocenter location if the change of estimate from the previous time step is large

2. Resample based on the sample weights from the previous time step for better convergence of the hypocenter estimate if the change of the estimate from the previous time step is small

### 3.4.4 Algorithm summary

Actual implementation of the method can be summarized as a two-step algorithm at each given time step $t$ (Figure 3.5). Starting from an initial step $t = 1$, first, earthquake parameters of each existing event are updated based on the newly received seismic data from the network. Second, the number of concurrent events is updated by the suboptimal model class selection scheme with the predetermined creating, merging and deleting criteria. The process is repeated until the termination of the system.

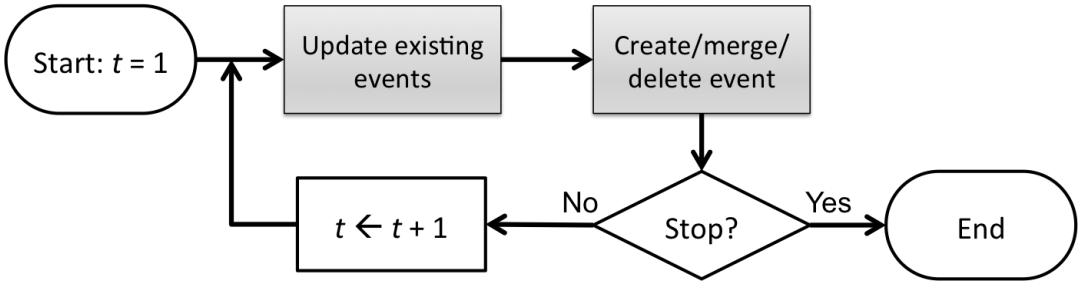


Figure 3.5: Flowchart of a two-step RBIS EEW algorithm at each time step $t$.

The update of the earthquake parameters of each existing event $n$ can be broken down into three parts and the algorithm may stop after all $\hat{n}$ events are updated (Figure 3.6):

1. Extract information from the waveform data to update the features used in event $n$.

2. Update samples based on new information and earthquake parameter estimates from the previous time step (suggested method in Section 3.4.3).

3. Update all earthquake parameter estimates using the RBIS method explained in Section 3.3.2.

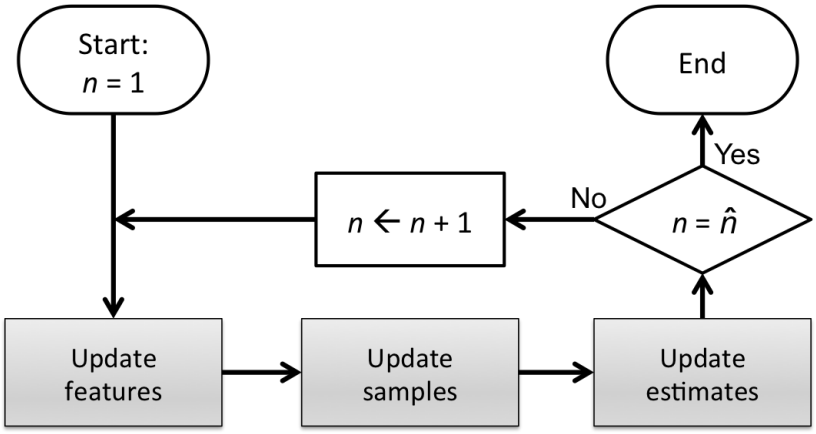


Figure 3.6: Flowchart of a three-step earthquake parameter updating scheme for each event $n$ based on RBIS. Terminate when all $\hat{n}$ events processed.

The update of the number of concurrent events can also be broken down into three parts (Figure 3.7):

1. Merge existing events (reduce number of concurrent events) that have similar converged estimates of earthquake parameters.

2. Delete existing events (reduce number of concurrent events) that have inconsistent theoretical P-wave arrival times comparing to the observed P-wave picking times from the current data.

3. Create a new event (increase number of concurrent events) with a newly triggered station as the theoretical first triggered station for the event if all three criteria are met: (a) Equation 3.6, 3.8 or 3.9; (b) waveform amplitude of the first triggered station exceeds the predetermined threshold; (c) More than one consecutive trigger of stations close by the first triggered station.

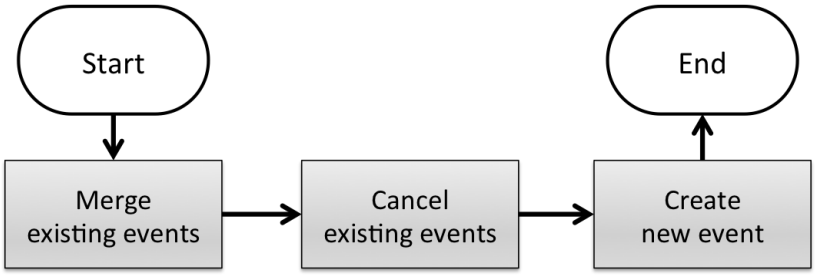


Figure 3.7: Flowchart of a three-step updating scheme for the number of concurrent event.

## 3.5 Data description for the test

After the 2011 Tohoku earthquake, the seismic activity around Japan increased significantly. There were thousands of earthquakes larger than M4 recorded in Japan (both inland and offshore) in March and April, 2011. This high seismic activity level is extremely challenging for most of the existing EEW systems because of the fundamental assumption of only one event happening within a short period of time and the noise caused by interferences between multiple earthquakes. The JMA EEW system releases a warning when the maximum value of the expected Japanese seismic intensity level exceeds 5−. During those two months, there were around 70 warnings released by the JMA EEW system, but 60% of them where false alarms, and many of those cases are due to the confusion caused by multi-events. In this test, I choose the seismic data from March 9 to April 30, 2011. This period includes the Tohoku foreshock that happened on March 9, the mainshock on March 11 and the major aftershock sequence that has sustained for around two months. After that, the seismic activity slowly reduced.

While the existing JMA EEW system relies heavily on JMA seismic stations, this study integrates the data from Hi-net stations with the data from JMA stations as one data set, which helps investigate the effect of a denser seismic network on an EEW system. There are around 300 JMA stations and 700 Hi-net stations, giving around a thousand stations to be used in this study. Different from the JMA seismic stations, which are accelerometers, the Hi-net seismic stations are high-sensitivity velocimeters. They have a smaller response for long-period waves and suffer from large amplitude saturation. In order to integrate the information from both seismic networks, the following corrections are performed based on Yamada et al. (2014):

1. Add a bias term of 0.3 to the mean magnitude calculated from Hi-net stations

2. Add a filter based on Allen (1978) to improve P-wave picking time

The original seismic waveform data within the selected period of time is obtained from the National Research Institute for Earth Science and Disaster Prevention (NIED) webpage. The proposed algorithm processes this data and the resulting performance is compared with the performance of the existing JMA EEW system. The warning data of the JMA EEW system during the selected period of time is obtained from the JMA report on 2011 Tohoku earthquake (JMA, 2013b) and a recent study from Tamaribuchi et al. (2014).

## 3.6 Detail for applying the algorithm to the test

When applying the algorithm (Section 3.3.1) to the seismic data within the selected period of time (March 9 to April 30, 2011), specific models and parameters have to be chosen. This section presents the details of applying the algorithm to this test, including the topics in Section 3.4, a reduction in the sampling space to increase computational efficiency and the Arrived/Not-arrived picking time model for calculating the Gaussian likelihood for P-wave picking time.

### 3.6.1 Reduction of the sampling space

In the proposed RBIS-based EEW algorithm in Section 3.3.1, the earthquake magnitude is estimated by an analytical solution. Hence, the sampling space is in four dimensions: latitude, longitude, depth and origin time of an earthquake. The number of samples needed to accurately represent a PDF exponentially increases proportional to the dimension of the sampling space. Therefore, reduction of the sampling space is always desired. In this case, I observed from empirical experience that the uncertainty in origin time is very small when the hypocenter location is known. This means that the posterior PDF of origin time given the hypocenter location often peaks around one value. Instead of drawing many samples for the origin time as a separate sampling dimension, I can estimate the peaked PDF by only one sample calculated based on a deterministic model for each sample of hypocenter location. The single sample value is found by minimizing the residual between the observed P-wave picking time and the theoretical P-wave arrival time from all triggered stations in an event. The theoretical P-wave arrival time can be calculated from a simple 1D wave traveling model underground.

### 3.6.2 Arrived/Not-arrived picking time model

The main question for using Equation 3.14 is what value to use for $F_{p,j}(t)$ when a station is not triggered, i.e., no picking information. Some previous studies suggest not to include those stations in the likelihood calculation. However, the fact that a P-wave has not yet arrived is also an important piece of information. Motivated by the Arrived/Not-arrived picking time model, I let $F_{p,j}(t)$ be equal to current time when a station has not yet been triggered, but the theoretical arrival time suggests the opposite. For this specific case, I suggest adding a lower limit for the likelihood function to avoid a single malfunctioned station that will never be triggered driving the final likelihood value

of an event to zero. I suggest using a minimum value of 0.004 that represents a three standard deviation error probability under a Gaussian model. If a station has not yet been triggered and the theoretical arrival time suggests the same, $p(F_{p,j}(t)|\theta_l) = 1$, meaning that no information is extracted from this station. Table 3.1 shows a summary for using the Arrived/Not-arrived picking time model when a station is not triggered.

| $\mu_{p,j}(\theta_l)$ | $F_{p,j}(t)$ | $p(F_{p,j}(t)\|\theta_l)$ |
|---|---|---|
| $< t_{now}$ | $t_{now}$ | has min. value |
| $\geq t_{now}$ | - | 1 |

Table 3.1: Summary on values of $F_{p,j}(t)$ and $p(F_{p,j}(t)|\theta_l)$ when a station is not triggered based on the Arrived/Not-arrived picking time model ($t_{now}$ = current time).

### 3.6.3 Station selection

Because seismic waves attenuate when traveling through the ground, information from stations that are far from the hypocenter make insignificant contributions to estimation of the earthquake parameters. In most earthquakes, the parameters can be accurately identified based on data from around ten stations closest to the hypocenter. Based on empirical experience, a subset of 20 closest stations to the estimated hypocenter is selected from the complete seismic network (including both JMA and Hi-net stations) in order to ensure certain robustness to the algorithm through redundancy. When a station is identified as a potential first triggered station of a new earthquake, the 20 stations are chosen by the following steps:

1. Pick 10 closest stations to the center of the Voronoi cell of the first triggered station based on the assumption that the hypocenter is most likely to be around that center point without any further information given.

2. For the remaining 10 stations, select each station one by one based one a criterion related to azimuth coverage: select the station that leads to a maximum increase in azimuth coverage to the center of the Voronoi cell of the first triggered station. If there are multiple such stations (e.g., in an inland case, the first 10 stations may have a complete azimuth coverage of $360^o$ already), pick the one closest to the center of the Voronoi cell of the first triggered station.

When an inland station is identified as a potential first triggered station of a new earthquake, this method is the same as selecting 20 closest stations to the center of the Voronoi cell of the first triggered station. However, in the case of an offshore earthquake, the seismic stations are often located only on the land side of the earthquake. A wider azimuth coverage is important for a quick and accurate estimation of the hypocenter location and origin time of the potential earthquake. The above method can result in a wide azimuth coverage when a station close to the offshore is identified as a potential first triggered station of a new earthquake (e.g., Figure 3.4).

### 3.6.4 Details of the suboptimal model class selection

A full Bayesian model class selection approach cannot guarantee to obtain a solution within the limited time (around one second) available for computation in the case of EEW. The suboptimal scheme in Equation 3.9 is used to improve the efficiency in this test. By assuming the P-wave picking times and the maximum displacement amplitudes are independent data, $\hat{n}$ is increased by one and a new event is created when:

$$p(F_{p,j}(t)|\hat{\theta}_l)p(F_{a,j}(t)|\hat{\theta}_l) < \tau_{new} \text{ for newly triggered station } j \text{ and } \forall l = 1, ..., \hat{n} \tag{3.31}$$

I select $\tau_{new} = 0.004$, which represents a three standard deviation error tolerance for both P-wave picking time and maximum displacement amplitude data under the Gaussian model. This value is chosen to preserve a relatively conservative criterion for creating new events in order to suppress the number of false alarms under a very noisy environment, especially when seismic waves from multiple concurrent events interfere with each other. An alternative is to use a smaller $\tau_{new}$ when more than one close by event is predicted. To further improve the robustness of the suboptimal scheme and filter out small events that are not significant for the purpose of EEW, two extra criteria are added on creating new events:

1. $F_{a,j}(t) > 0.005$cm: this filters out small local events.
2. 2 out of 5 of the closest stations to the triggered station have to be triggered within the time range of theoretical P-wave travel time: this filters out large amplitude local noise.

Because the Gaussian model cannot capture some unexpected sources of noise, such as equipment deficiency, a criterion for deleting an event is added to remove unexpectedly created false

events and a criterion for merging two events is added to correct the case of triggering two new events from a single actual event:

1. Delete an event when more than 1/3 of $N_{st}$ stations have an observed P-wave picking time that is inconsistent with the theoretical value based on the estimated earthquake parameters. (Empirical experience shows that noisy data is a relatively rare case, and 1/3 is a conservative ratio to avoid incorrectly deleting a real event in the early stage)

2. Merge an event when the mean epicenter locations of two events are within 10km radius and the expected origin times are less than three seconds apart (three standard deviation error tolerance on origin time). The depth is not included in this criterion because empirical experience shows a much larger error expected for the depth estimate. This criterion is set such that even if there are actually two earthquakes happening, only the larger magnitude one is relevant for the purpose of EEW.

### 3.6.5 Proposal PDF and sample updating

The proposed algorithm estimates earthquake parameters based on a set of samples drawn from a proposal PDF. The proposal PDF is constructed based on a prior PDF when an event is first created. After that, it is constructed based on information from the posterior PDF of the earthquake parameters from the previous time step. As described in Section 3.6.1, the sampling space is reduced to latitude, longitude and depth, i.e., the hypocenter location of the earthquake. The prior on the latitude and longitude is selected to be a uniform distribution on the Voronoi cell area of each station. In the case of a station closed to the coastline, the Voronoi cell will be very large to cover the offshore events. In order to maintain the efficiency of the algorithm, the prior for both latitude and longitude is limited to a maximum width of one unit. An adaptive proposal PDF is introduced below to converge the samples to the actual offshore epicenter location. The prior on the depth is selected to be a uniform distribution between 0km to 100km. An alternative to the depth prior is to include information about Japan's subduction zone profile underground.

For the construction of the proposal PDF based on the posterior PDF of the earthquake parameters from the previous time step, I divide it into two cases:

1. If the distance between the mean epicenter location at the current and the previous time step exceeds some predetermined ratio of the range of the prior on the latitude and longitude, the

new proposal PDF for the epicenter is constructed by shifting the center of the uniform prior to the mean of the epicenter obtained from the current time step (Figure 3.8).

2. Otherwise, a new proposal PDF is constructed based on the resampling scheme described in Liu and Yamada (2014).

Case 2 is for reducing the variance of importance sampling, and so to improve the efficiency of the algorithm. Most of the inland earthquakes fall into this case. Case 1 is designed to cover the case of an offshore earthquake. In such an event, a smaller prior is used to maintain computational efficiency (as mentioned above). The new proposal PDF allows fast convergence to the actual epicenter location when it is away from the area of the current samples. I suggest using a ratio of 50% for both latitude and longitude based on empirical experience considering a trade-off between the efficiency of importance sampling convergence and the variance of the expected value after new data is collected.

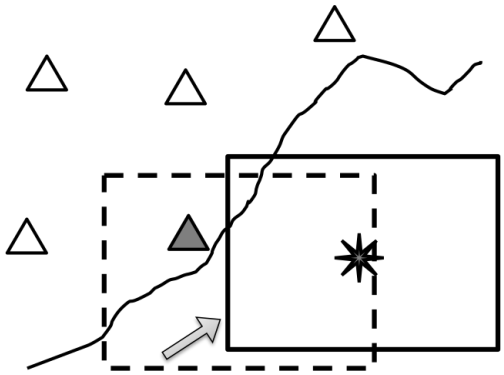

Figure 3.8: Example of shifting the proposal PDF in Case 1. Triangles are seismic stations. Solid triangle is the triggered station for a potential new event. Dotted rectangle is the uniform prior PDF with a mean epicenter estimated at the black star. The new uniform proposal PDF is shifted to the solid rectangle.

## 3.7 Test results and discussion

### 3.7.1 Single large event

First, I illustrate some details of the proposed algorithm by studying the foreshock that happened on March 9, 2011. This single large event occurred in the Pacific ocean outside the Tohoku region in Japan, close to the location of the mainshock on March 11. Table 3.2 shows the details of this event.

| Origin Time | Latitude | Longitude | Depth(km) | Magnitude |
|---|---|---|---|---|
| 11:45:13 | 38.33 | 143.28 | 8.28 | M7.3 |

Table 3.2: Detail of the Tohoku foreshock on March 9, 2011.

Figure 3.9 shows three snapshots of the distribution of weighted samples for this event. One can observe that the selected stations for this event spread across the coastline, instead of clustering around the closest point to the actual epicenter. This allows a wider azimuth coverage for better estimating the detail of the offshore event as explained in Section 3.6.3. After the earthquake begins at 11:45:13, its P-wave first arrives the coastline around 30 seconds later and a new event is triggered in the system at 11:45:41. The first set of samples is created using the prior based on Voronoi cell information. As explained in Section 3.6.5, a maximum width is set when a coastline station is triggered to avoid too large of a prior area. Then, the samples migrate toward the actual epicenter after one time step (1 sec later), and the samples converge stably (by a resampling step with a soft boundary) 5 seconds after the event is triggered. Note that sample weights in Figure 3.9 are in log scale (same scale is used for Figure 3.10 and 3.12). The actual posterior distribution represented by the weighted samples are actually very peak around the actual epicenter.

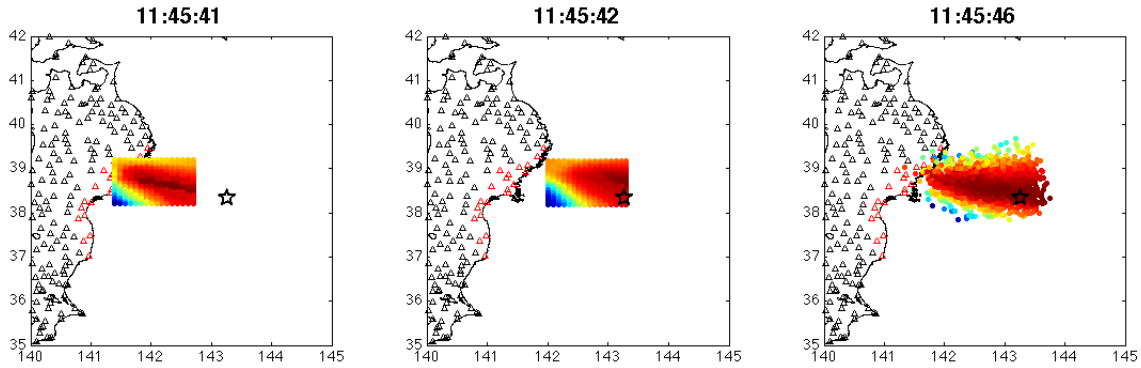


Figure 3.9: Weighted samples distribution for the foreshock on March 9, 2011. Color of the samples is proportional to ln(weight) with higher value in red and lower value in blue. Black star indicates the actual epicenter location. Black triangles are seismic stations, and red ones are selected stations for this event.

Figure 3.10 shows a breakdown of the weight calculation, which is composed of the P-wave picking time ($F_p$) part and the maximum displacement amplitude ($F_a$) part. One can observe that when the event is first triggered, the values of the picking time part are relatively close to each other compared to a few seconds later. At this early stage, there is not enough picking

time information from the stations to fully constrain the hypocenter location. The maximum displacement amplitude part helps refine the convergence to a smaller region. After that, the picking time part becomes reliable enough to dominate the weight contribution and the amplitude part becomes not so important.

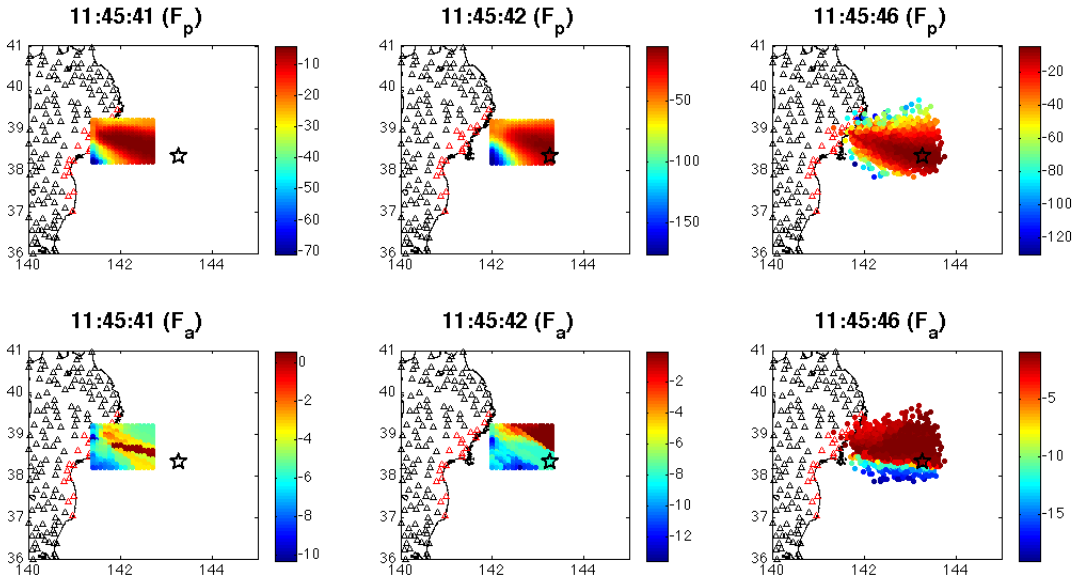


Figure 3.10: Distribution of the P-wave picking time ($F_p$) part and the maximum displacement amplitude ($F_a$) part of the sample weights for the foreshock on March 9, 2011. Color of the samples is proportional to ln(weight) with higher value in red and lower value in blue. Black star indicates the actual epicenter location. Black triangles are seismic stations, and red ones are selected stations for this event.

Figure 3.11 shows a summary of the convergence of the five earthquake parameters (latitude and longitude are combined to calculate the error of epicentral distance $R$). The algorithm takes a relatively longer time to converge because it is an offshore event. As expected, the depth convergence is not as good as the other parameters.

### 3.7.2 Two overlapped events

Next, I would like to study a challenging case with two concurrent events overlapping each other within a short period of time. The two events occurred on March 19, 2011, at the Ibaraki Prefecture. The two hypocenters were at the same location and the origin time of the two events were only 28 seconds apart from each other. This makes it very difficult to separate the two events in the case of EEW. Table 3.3 shows the detail of both events.

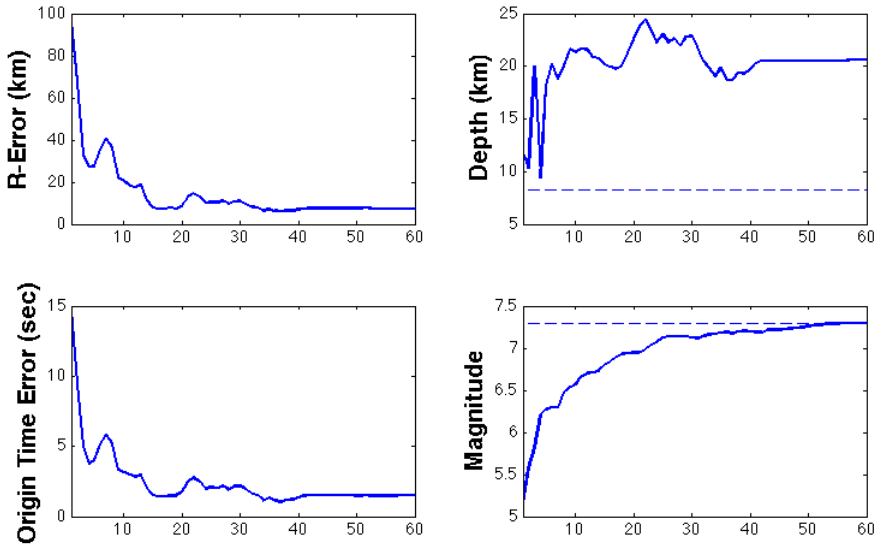


Figure 3.11: Convergence summary of the new algorithm for the foreshock on March 9, 2011. R-Error is the epicentral distance error between the estimated epicenter and the actual epicenter. The horizontal dotted lines are actual parameter values of the earthquake. X-axis shows the time (sec) after the event is triggered.

| Origin Time | Latitude | Longitude | Depth(km) | Magnitude |
|---|---|---|---|---|
| 18:56:20 | 36.78 | 140.57 | 5.76 | M4 |
| 18:56:48 | 36.78 | 140.57 | 5.37 | M6.1 |

Table 3.3: Detail of the two overlapped concurrent events on March 19, 2011.

Figure 3.12 shows four snapshots of the distribution of weighted samples for the two overlapping events. The first event begins at 18:56:20 and a new event is triggered in the system 3 seconds later. Because it is an inland earthquake, the prior sample set is already well converged to the actual epicenter. The samples are completely stable after few seconds later. The second event begins at the exact same location at 18:56:48 and a new event is successfully triggered in the system 3 seconds later. Again, the prior sample set is already well converged at the time the second event is triggered and the samples are completely stable after a few seconds later. It is important to point out that the system starts calculation of both events right after the first P-wave arrival to a station in the network 1 second after the earthquakes begin. The extra two seconds delay to officially trigger a new event in the system is due to the selected triggering criteria explained in Section 3.6.4 in order to filter out potential false alarms. Therefore, this delay does not affect the speed of convergence for the earthquake parameters.

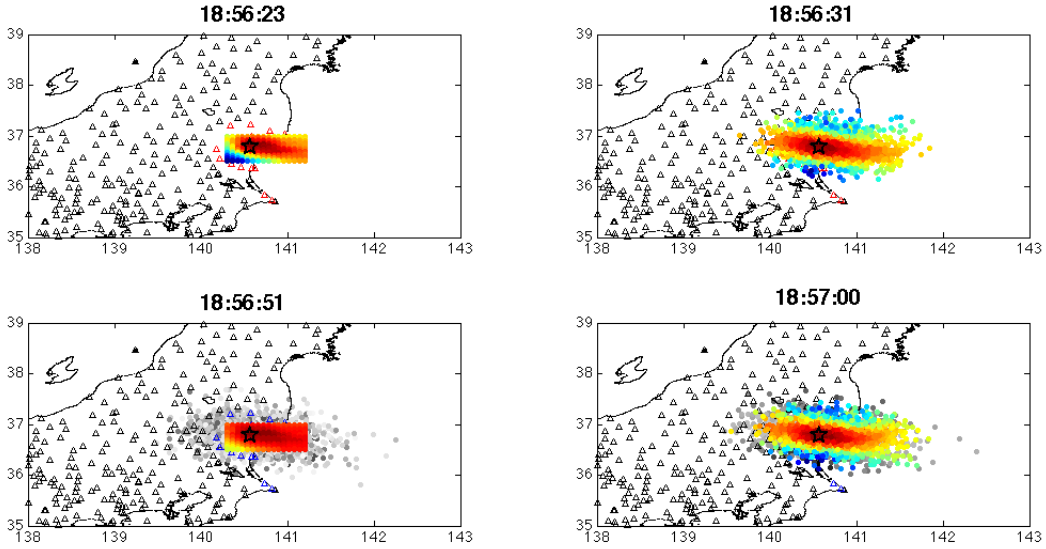


Figure 3.12: Weighted samples distribution for the two concurrent events on March 19, 2011. Colored samples in the upper two plots represent the first event. Gray and colored samples in the lower two plots represent the first and second event, respectively. Color of the samples is proportional to ln(weight) with higher value in black/red and lower value in white/blue. Black star indicates the actual epicenter location for both events. Black triangles are seismic stations, and red and blue ones are selected stations for the first and second event, respectively.

Figure 3.13 shows a summary of the convergence of the five earthquake parameters. Comparing to the single event on March 9 (Figure 3.11), the error of all parameters are small at the time the events are first triggered. Fast convergence is expected for the case of an inland earthquake. The only problem is that the magnitude estimate of the first event is affected by the seismic waves generated by the second event. After the trigger of the second event, the magnitude estimate of the first event converges to the value of the second event. However, no false alarm is triggered for the purpose of EEW because the two events are close enough in time and space. Although one can set a more sophisticated convergence criterion to appropriately stop estimating the parameters for an event 30 seconds after it is triggered, this is likely to increase the error for many other events. Therefore, it may not be practical to do so for the purpose of EEW.

### 3.7.3 Summary of March to April events

In this section, I verify the performance of the proposed algorithm by the two months data (March 9 to April 30) that includes the foreshock, mainshock and aftershock sequence of the 2011 Tohoku earthquake. The main comparison is divided into two parts: (1) compare the earthquake param-

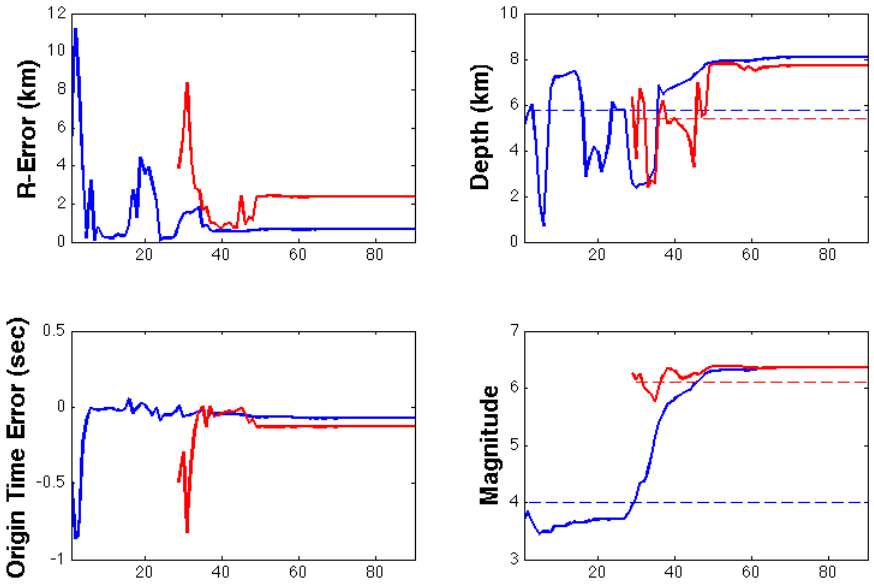


Figure 3.13: Convergence summary of the new algorithm for the two concurrent events on March 19, 2011. Blue lines and red lines correspond to the first and second event, respectively. R-Error is the epicentral distance error between the estimated epicenter and the actual epicenter. The horizontal dotted lines are actual parameter values of the earthquakes. X-axis shows the time (sec) after the first event is triggered.

eters estimated by the algorithm with the catalogue data to verify the ability of the algorithm to accurately predict an earthquake in the case of EEW; (2) compare the performance of the algorithm as an actual EEW system based on expected maximum intensity measure used by the JMA EEW with the performance of JMA EEW during the two months period.

*First comparison*: I verify the ability of the proposed EEW algorithm to accurately predict earthquake parameters. All seismic data (JMA and Hi-net stations) from March 9 to April 30 are used except the ten hours data from 15:00 to 23:59 on March 11. In that period, the significant increase of seismicity around the region results in a very complicated seismic data set that is hard to identify individual earthquakes from. The catalogue in that period is not complete and, thus, not reliable enough to be compared with. Although the high seismicity continued for a long time and the catalogue is still missing some events after that specific time range, the missing set is in a manageable size that we can make a reasonable comparison with. A total of 895 earthquakes have been identified by the new algorithm. Among them, 45 events are removed from the comparison due to one of the following reasons:

1. The catalogue missed the identified event.

2. The event is part of two concurrent events that are very close to each other in space and time, such that the smaller event is insignificant for the purpose of EEW.

Figure 3.14 shows the catalogue magnitude distribution for all the earthquakes in this comparison.

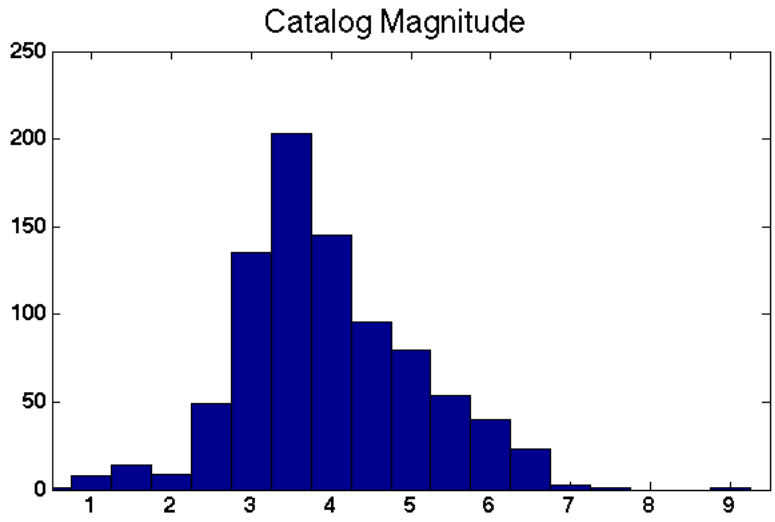


Figure 3.14: Catalogue magnitude distribution for the 850 earthquakes between March 9 and April 30 used for performance verification of the proposed algorithm.

Figure 3.15 shows the histograms of the residuals of latitude, longitude, depth, origin time, magnitude and Japanese seismic intensity calculated by subtracting the catalogue values from the new EEW algorithm estimates. The following conclusions are drawn:

1. The relatively peaked histograms verify that the proposed algorithm can predict the earthquake parameters accurately.

2. Due to its geographical shape, Japan has a more uniform station distribution along the latitude direction than along the longitude direction. Therefore, a lower variance is observed for latitude estimation than longitude. Most of the larger errors in longitude are due to offshore events, which there is a lack of seismic station coverage along the longitudinal direction.

3. As one may expect, the depth shows the largest variance among the three components of the hypocenter location estimate. Again, the larger errors in depth are mostly due to offshore events, where the errors in longitude directly affect the errors in depth.

4. Although there is a bias towards overestimation for magnitude estimates, most of those cases are actually small events that are insignificant for the purpose of EEW (as shown in Figure 3.16). This argument can be further verified by the second comparison.

5. The proposed algorithm demonstrates an acceptable performance for the Japanese seismic intensity estimate based on the JMA standard, where +/- 1 unit of error for EEW seismic intensity estimates is expected.

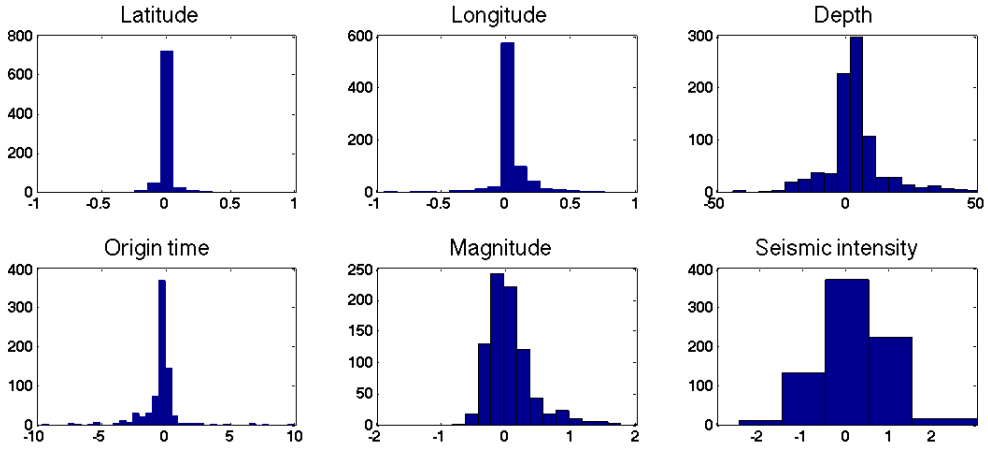


Figure 3.15: Residual histogram of latitude (deg), longitude (deg), depth (km), origin time (sec), magnitude and Japanese seismic intensity. X-axis shows the residual calculated by: new EEW algorithm estimates – Catalogue values. Y-axis shows the number of earthquakes.

*Second comparison*: I verify the performance of the algorithm as an actual EEW system. Based on Tamaribuchi et al. (2014), there were 71 warnings released by the JMA EEW system within the period of March 11 to April 30. I compare the proposed algorithm's accuracy of releasing a warning with the existing JMA EEW system using the JMA EEW criterion based on Japanese seismic intensity. Warnings are released for intensity above 5− with an expected error of +/- 1 unit. Appendix A lists the details of all events with results of the seismic intensity estimates from the catalogue, JMA EEW system, an algorithm proposed by Tamaribuchi et al. (2014) and the proposed algorithm in this chapter. The new algorithm corrects almost all false alarm cases by the existing JMA EEW except the following three cases:

1. Event 2: This earthquake is initially identified accurately, but is deleted before the convergence criterion is met due to the interference of multiple aftershocks around that period.

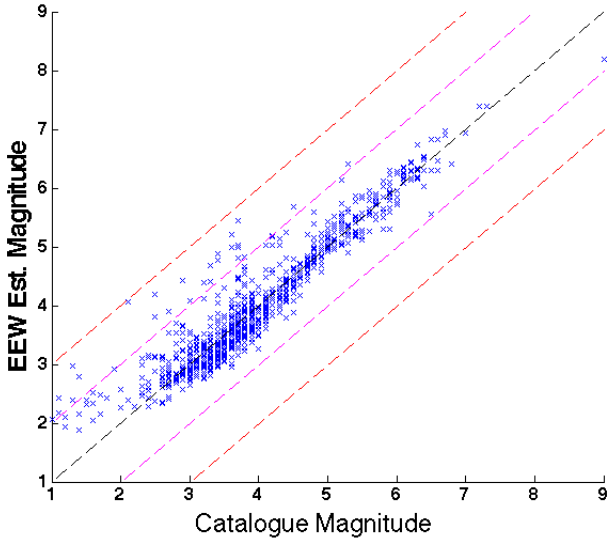


Figure 3.16: Plot of EEW estimated magnitudes (final) versus catalogue magnitudes. The dotted black line indicates the case of perfect prediction. The dotted purple and red lines indicate the +/- 1 and 2 magnitude error bounds, respectively.

Although the seismic intensity estimate is accurate initially, the warning is incorrectly cancelled. Referring to Section 3.6.4, a more sophisticated deletion criterion may fix this problem.

2. Event 34: This is the two overlapping concurrent earthquakes case described in Section 3.7.2. The overestimation is due to the inference of the second event. However, for the purpose of EEW, the incorrect seismic intensity estimate for the smaller event is expected and it will not cause a false alarm in this case.

3. Event 46: The proposed algorithm actually estimates the hypocenter location, origin time and magnitude of this earthquake accurately. The underestimated seismic intensity is because of a deficiency to estimate the actual maximum seismic intensity based on only JMA and Hi-net stations. This problem can be solved by implementing a better algorithm for estimating seismic intensity.

Figure 3.17 shows the histograms of seismic intensity residual for the three EEW systems based on the 71 selected earthquakes. It verifies that the proposed algorithm significantly improves the performance of EEW based on seismic intensity compared to the existing JMA EEW system that cannot handle multi-events cases.

Finally, I would like to discuss the importance of a denser seismic network by comparing the

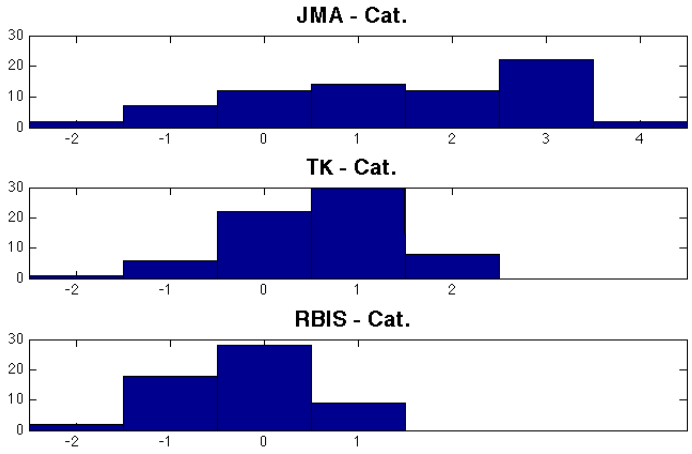


Figure 3.17: Histogram showing the performance of seismic intensity estimate for the existing JMA EEW system (JMA), an algorithm proposed by Tamaribuchi et al. (2014) (TK) and the new algorithm proposed in this chapter (RBIS) based on the selected 71 earthquakes. X-axis shows the error of the Japanese seismic intensity calculated by: EEW estimates - Catalogue values.

results from Tamaribuchi et al. (2014) and the proposed algorithm in this chapter. Figure 3.17 shows that the algorithm proposed in this chapter slightly improves the seismic intensity estimate from the one proposed by Tamaribuchi et al. (2014). In fact, both algorithms use a probabilistic approach to solve the multi-events cases. One important difference is that the algorithm in this work includes Hi-net stations data for estimating all earthquake parameters, but the other does not. The use of a denser seismic network results in faster and more accurate estimates. Almost the same performance is achieved by using only two features (P-wave picking time and maximum displacement amplitude) in the new algorithm, as compared to the algorithm proposed by Tamaribuchi et al. (2014), which uses a total of four features. Although some treatment of the data is needed in order to integrate data from the two different seismic networks, which may increase the uncertainty in the process, the resulting benefits make it worthwhile to do so.

## 3.8 Conclusion

Motivated by the increased false alarm rate of the JMA EEW system after the 2011 Tohoku earthquake in Japan, this study proposes a probability-based EEW algorithm to identify concurrent earthquakes (multi-events). The Bayesian model class selection framework is applied to solve for the number of concurrent events in the EEW multi-events problem. Because of the short time

limitation of EEW, a simple numerical method, Rao-Blackwellized Importance Sampling with a set of sequential proposal PDFs, is used to estimate the earthquake parameters and the necessary equations are derived analytically as much as possible. Also, some suggestions are given to improve the algorithm for practical use.

For illustration purposes, the existing JMA EEW system is taken as an example to demonstrate the process of applying the proposed probabilistic method to an existing deterministic EEW model. Two features, the P-wave picking time and the maximum displacement amplitude, are chosen for earthquake parameter estimation. A Gaussian model is used for the likelihood function of both features. A real example based on two months data (March 9 to April 30, 2011) around the time of the 2011 Tohoku earthquake is studied to verify the proposed algorithm. The algorithm is able to accurately identify multiple concurrent events. Significant improvement is shown in comparison with the existing JMA EEW system. Also, the importance of having a denser network is demonstrated in the test. The inclusion of the Hi-net stations greatly enhances the average warning lead time and accuracy of the EEW predictions.

# Chapter 4

# ePAD: Framework for Automated Decision-Making for EEW Applications

Since EEW predicts earthquake parameters based on incomplete waveform data, high uncertainty is expected from the broadcast warning. Although the uncertainty may reduce as more data is collected, the reduced lead time may not be enough to complete a mitigation action. The decision of what the optimal action is and when to perform the action involves a complicated trade-off between potential missed and false alarms due to the uncertainty of EEW prediction and lead time. In this chapter, I propose an earthquake probability-based automated decision-making (ePAD) framework that can handle this problem. It is designed to include the contributions of lead time and uncertainties from the selected models and EEW information in the automated decision-making based on a cost-benefit model. This framework, which can be flexibly implemented for specific applications, allows users to easily pick their desired decision behavior (i.e., to control how uncertainty influences the decision).

Applying a performance-based earthquake early warning (PBEEW) methodology (Grasso, 2005; Iervolino, 2011), which is a combination of performance-based earthquake engineering (PBEE) (Porter, 2003) and EEW, ePAD separates the EEW information input from all the pre-calculable user-specific models (e.g., decision model, structural model and/or ground motion prediction equation (GMPE)), and combines the latter into a single function called the *Decision Function* (DF). This leads to a simpler representation during calculation and an easier way of performing analyses, as well as allowing the possibility of replacing the pre-calculable function with a surrogate model

for fast computing. The lead time contribution is embedded in the framework in two ways: an incomplete action model and a value of information model. The former considers the case where the benefit and cost of a mitigation action may change if it is not completed before the arrival of the damaging seismic waves; the latter considers the case where a decision may be delayed if there is to be future updates of EEW information and the predicted lead time is more than enough to complete a mitigation action.

This chapter is based on my previous publication in Wu et al. (2012, 2013). First, I start with a brief review on the recently proposed decision methods for EEW applications. Then, the basic theory and details of the ePAD framework is presented. Finally, various decision criteria are compared under the ePAD framework and an illustrative example is presented based on a PEER benchmark office building.

## 4.1 Review of EEW decision-making methods

The state-of-the-art decision-making method for most of the existing EEW applications in practice is based on the classical threshold method, which takes an action when the probability of a ground shaking intensity measure ($IM$) exceeding some pre-set threshold $im_0$ is greater than some fixed value $P_0$. In many cases, engineers may simply set a threshold value for the expected value of $IM$, ignoring most of the influence from the $IM$ uncertainty. In these methods, calibration of the decision parameter values plays an important role. Researchers have converged on the idea of using cost-benefit analysis as a basis for determining an appropriate value for the parameters. Moreover, some researchers suggest directly using the a cost-benefit analysis for the decision criterion. This idea motivated the development of PBEEW, which uses the PEER PBEE model to perform cost-benefit analysis for decision making of EEW applications.

In Grasso et al. (2007), the authors introduced a trade-off between the expected loss due to false alarm and the expected loss due to missed alarm to determine $P_0$ when $im_0$ has already been determined by some engineering study. An action is taken when the expected loss due to a missed alarm is larger than the expected loss due to a false alarm. They showed that this is equivalent to the probability of $IM$ exceeding a specified threshold $im_0$ being greater than a value $P_0$ that depends on these expected losses.

Iervolino et al. (2007) examined a decision framework to decide when to trigger an earthquake alarm. Instead of the threshold-based method, an expected-loss-based decision criterion using the PBEE approach is considered. In this approach, a thorough loss assessment is performed and the decision is made by monitoring the expected loss due to taking action and no action.

These methods make a significant contribution to automating decisions for mitigation actions. However, there are still limitations for practical usage. One of the most important limitations is that the decision for most EEW applications is time sensitive due to a short and uncertain lead time, and this uncertainty should be explicitly treated in decision making, including the fact that the ground shaking may start before the mitigation action is completed. The ePAD decision framework presented next provides a flexible platform for further development of the models used in the decision-making process. It includes a model for explicit lead time treatment in the real-time decision process. Also, the concepts embedded in this framework can be used to analyze the differences between previously published decision methods for EEW applications.

## 4.2 ePAD framework

### 4.2.1 Decision-making by cost-benefit model

Given EEW information, the ePAD framework must be able to robustly and rapidly choose an optimal action from a set of possible mitigation actions $\Omega_a = \{a_0, a_1, ..., a_n\}$, where $a_i$ denotes initiating a certain action for $i = 1...n$, and $a_0$ denotes not to initiate any action. Taking an action often leads to some kind of interruption to the operation of the facility, business, or society, whereas not taking an action induces a risk of hazardous losses. To compare possibly disparate consequences, they need to be converted into a single metric, called here a Decision Variable ($DV$). Without loss of generality, we assume that larger values of $DV$ are preferred. Once we have a consistent metric for trade-off comparisons, ePAD uses a rational decision-making procedure based on fundamental decision theory (Von Neumann and Morgenstern, 1944; Raiffa and Schlaifer, 1961):

$$\text{Take optimal action } \hat{a} = \text{argmax}_{a \in \Omega_a} E[U(DV)|D(t), a] \tag{4.1}$$

where $U(DV)$ denotes the utility of $DV$, $E[X|Y, a]$ denotes the expected value of $X$ given $Y$ for action $a$, and $D(t)$ is the seismic data from EEW as a function of time $t$.

Decisions based on expected utility can be categorized into three risk attitudes: risk-neutral, risk-averse, and risk-taking, where risk-neutral $U(DV)$ is a linear function, risk-taking $U(DV)$ is a convex function, and risk-averse $U(DV)$ is a concave function (see Section 2.4 for more details). In EEW applications, decision criteria can be further simplified if a risk-neutral approach is taken. It increases the efficiency of decision-making process substantially especially when $\Omega_a$ is a large set. Let $DV = (DV_B - DV_C) - DV_E$, where $DV_B$ is the beneficial change in $DV$ due to the mitigation action, and $DV_C$ corresponds to the cost for implementing the action. $DV_E$ corresponds to the earthquake-induced loss that would occur in the absence of any mitigation action and so it is independent of any action $a$. A linear utility function implies that $U(DV) = U(DV_B) - U(DV_C) - U(DV_E)$. Hence:

$$E[U(DV)|D(t), a] = E[U(DV_B)|D(t), a] - E[U(DV_C)|D(t), a] - E[U(DV_E)|D(t)] \tag{4.2}$$

Because $E[U(DV_E)|D(t)]$ is a constant with respect to $a$, it can be dropped out from the maximization problem in Equation 4.1. The new decision criterion becomes:

$$\hat{a} = \text{argmax}_{a \in \Omega_a} \{E[U(DV_B)|D(t), a] - E[U(DV_C)|D(t), a]\} \tag{4.3}$$

For example, if $DV = L_B - L_C - L_E$ with a risk-neutral utility function, where $L_B$ denotes the reduction in economic loss due to a mitigation action (e.g., alleviated machine damage), $L_C$ denotes the induced economic cost after implementing the action (e.g., interruption to business [downtime] or liability [lawsuits]), and $L_E$ denotes the expected economic loss due to earthquake (dropped in the optimization as explained above), then Equation 4.3 becomes:

$$\hat{a} = \text{argmax}_{a \in \Omega_a} \{E[L_B|D(t), a] - E[L_C|D(t), a]\} \tag{4.4}$$

### 4.2.2 Performance-Based Earthquake Early Warning

In most EEW applications, the calculation of expected utility is complex. ePAD uses a cost-benefit analysis based on a PBEE model to calculate the expected utility, giving the PBEEW approach. A major benefit of using a PBEE model is that it provides a relatively simple platform to include multiple engineering submodels, and at the same time, most of the submodels can be precalculated as they are independent of the EEW information under the PBEE model.

Most of the current EEW systems provide magnitude and epicenter information from the seismic data $D(t)$, preferably $p(M, R|D(t))$, where $M$ and $R$ are the magnitude and site-to-source distance of the incipient earthquake (note that from the epicenter estimation and the site coordinates, vector $R$ can be directly inferred). Figure 4.1 shows the PBEEW model where all the pre-calculable parts are shown in larger boxes, $IM$ is the ground shaking intensity measure (possibly a vector); $EDP$ is a vector of engineering demand parameters; and $DM$ is a damage state measure for all the vulnerable components in the structure. Recently, an EEW method has been developed that directly infers site-specific $IM$ information from the seismic data (Hoshiba, 2013). Without loss of generality, derivations in the rest of this chapter assume that EEW provides $IM$ estimation, giving $p(IM|D(t))$. If the EEW system provides $M$ and $R$ information instead, then $p(IM|D(t))$ can be generated from a probabilistic ground-motion prediction equation $p(IM|M, R)$ combined with $p(M, R|D(t))$ by taking their product and integrating over $M$ and $R$.

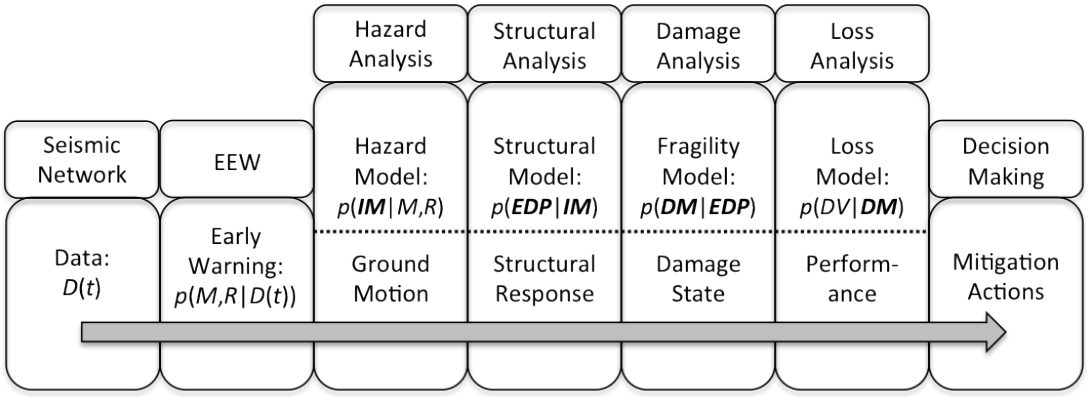


Figure 4.1: Probability model of PBEEW assuming EEW provides $M$ and $R$ prediction.

Using the Total Probability Theorem, the PBEEW model in Figure 4.1 leads to the following expressions:

$$E[U(DV)|D(t), a] = \int E[U(DV)|IM, a]p(IM|D(t))\,\mathrm{d}IM \tag{4.5}$$

where $E[U(DV)|IM, a]$

$$= \int U(DV)p(DV|DM, a)p(DM|EDP, a)p(EDP|IM, a)\,\mathrm{d}DV\mathrm{d}DM\mathrm{d}EDP \tag{4.6}$$

PBEEW lays a foundation for robust and rapid automated decision making in EEW applications. Precalculated parts can be tabulated for efficient use in real time. For continuous variables

and higher dimension problems, a surrogate model approach is more efficient. Related concepts are discussed in the next section.

### 4.2.3 Concept of decision function, decision contour, and surrogate model

#### 4.2.3.1 Decision function

A decision function (DF) is defined as a function of EEW information, for example, $IM$ information, that includes all the pre-calculable parts in the decision-making process. Equation 4.1 can be rewritten as:

$$\text{Take optimal action } \hat{a} = \text{argmax}_{a \in \Omega_a} E[DF|D(t), a] \tag{4.7}$$

$$\text{where } E[DF|D(t), a] = \int DF(IM, a) p(IM|D(t))\, \mathrm{d}IM \tag{4.8}$$

In the case of risk-neutral decision making, the decision function using Equation 4.3 is defined as:

$$DF(IM, a) = E[U(DV_B)|IM, a] - E[U(DV_C)|IM, a] \tag{4.9}$$

Note that based on the definition of $DV_B$ and $DV_C$ in Section 4.2.1, $DF(IM, a_0) = 0$, because taking no action will induce no extra benefit or cost (this will be changed in the value of information model for lead time in Section 4.2.4.2).

As a result of Equation 4.8, one can treat the decision function as a special utility function based on the information provided by EEW ($IM$ in this example) that represents a specific decision behavior of an EEW user. In fact, in Section 4.3, I show that previously published decision criteria, such as threshold-based methods, can be rewritten into the form of Equations 4.7 and 4.8. Hence, the concept of decision function can be used to compare different decision criteria when combined with the concept of decision contour, which will be introduced in the next section.

#### 4.2.3.2 Decision contour

EEW systems require efficient transmission of warning information due to the short lead time available for emergency response. Therefore, it is likely that the probabilistic EEW information will be reduced into some low dimension space $\mathbb{R}^n$. In this case, one can predetermine the decision

for any point in this domain using Equation 4.7. Hence, a decision map is obtained by separating the $\mathbb{R}^n$ domain into multiple regions, where each region represents a different optimal action $\hat{a} \in \Omega_a$. The decision contours are defined as the curves or boundaries that separate each region. For example, if the probability of a scalar $IM$ at a single site is modeled as a log-normal distribution, $p(IM|D(t))$ can be perfectly represented in $\mathbb{R}^2$ by the mean and the standard deviation of the log-normal distribution. Figure 4.2 shows an example for a decision map in $\mathbb{R}^2$ for this case. For a given mean and standard deviation of $IM$, the location of the corresponding point in $\mathbb{R}^2$ gives the optimal action to take.

Given a specific probability model for the EEW information, different decision functions will lead to different decision contours, where each represents a different decision behavior. Thus, the user may choose a type of decision contour that reflects the desired decision behavior, which corresponds to a specific type of decision function, or, equivalently, a specific choice of decision criterion. A comparison between different decision criteria utilizing the concept of decision function and decision contour is presented in Section 4.3.

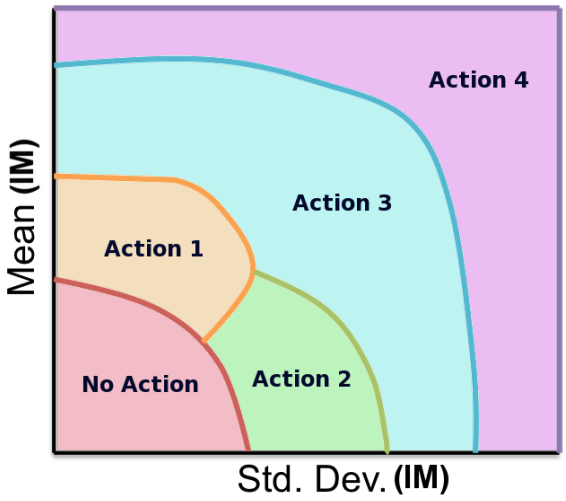


Figure 4.2: Example of a decision map in $\mathbb{R}^2$.

#### 4.2.3.3 Surrogate model and relevance vector machine

A computationally efficient decision-making system is essential for EEW applications due to the short lead time available. Therefore, calculation of Equations 4.7 and 4.8 needs to be optimized. If the EEW information can be reduced into a low-dimensional space, decision contours can be

utilized. In many practical cases, it is unlikely that an analytical form for the decision contours can be obtained. In this case, a surrogate model can be used to approximate the decision contours with another simpler functional form. This allows almost instant decision making once the EEW information is given because the optimal action can be directly determined from the decision map defined by the decision contours with an approximate analytical form.

On the other hand, if EEW information cannot be reduced into a low-dimension space, real-time calculation of the integral in Equation 4.8 is needed. Multiple strategies to store $DF$ for the sake of efficient integration are available. One could find its exact analytical form, if possible; or store a table of the functions values for a discrete set of $IM$ values; or construct an analytical approximation. In our case, a tabular approach would require a very fine mesh to get a reasonable estimate of the integral. Because an analytical form is unlikely to be obtained, a set of basis functions is chosen for a basis expansion to approximate $DF$. If appropriate basis functions can be chosen based on the selected probability model for the EEW information, then the integral in Equation 4.8 can be evaluated to give an analytical functional form. For example, if a Gaussian model is chosen for the EEW information, one can construct a kernel basis expansion for $DF$ using Gaussian kernels. In this case, the relevance vector machine (RVM) (Tipping, 2001) is a robust regression technique suitable for creating the surrogate model using a kernel basis expansion because of its ability to provide a sparse and accurate regression model, as explained in Section 2.5. The sparse surrogate model allows a substantial reduction in the computation time of the expected $DF$ estimation.

### 4.2.4 Lead time contribution in ePAD

Due to the uncertain nature of EEW information, decisions for mitigation actions can be sensitive to the amount of time left for action. For example, if the lead time is too short for completing a high benefit action, you may decide to take a quicker action with lower benefit; or if you are very certain that the lead time is more than enough to finish a mitigation action, you will probably delay taking the action with the hope that updated EEW information will allow a more reliable decision in the next second or so. In general, the longer you wait, the more seismic wave data the EEW system collects, and so the more accurate the EEW information will be. The decision problem is more than a cost-benefit trade-off. It also depends on the trade-off between the probability of

not being able to finish an action and the probability of obtaining more accurate information from EEW if one chooses to wait for another second before making a decision. Therefore, when the lead time is not perfectly determined, it is not only a limiting factor for possible EEW applications, but also a crucial trade-off factor in the decision-making process. Recently proposed decision-making methods have not emphasized lead time as part of the dynamic decision making. In fact, it is not easy to include this extra factor into classical cost-benefit analyses.

In the ePAD framework, we separate the treatment of the lead time and its uncertainty into two models: incomplete action model and value of information model. As mentioned in Section 1.2, there are two general types of EEW system. One provides only a single warning, and the other provides multiple warnings (continual updates). For EEW systems that provide only one-time warning information, there is only one decision to be made. The only time concern is whether an action can be completed before the earthquake arrives. Hence, a model for benefit and cost of incomplete actions is added to the original cost-benefit analysis to solve the problem (referred as the incomplete action model). On the other hand, for EEW systems that provide continual updates on warning information, instead of choosing to take no action, one can choose to delay the decision to wait for future EEW updates. A new model is needed to approximate the benefit and cost of delaying a decision, besides the incomplete action model.

Modeling the contribution of lead time to the expected utility in a general framework can be a complicated problem. For simplicity, this article develops a lead time model under the assumption of risk-neutral utility functions. The case of risk-taking and risk-averse is left for future research. Recall that in the risk-neutral case, decision criterion can be simplified to only consider $DV_B$ and $DV_C$, and then $DF$ is defined as Equation 4.9. Let $T_{lead}$ denote the lead time before the arrival of the earthquake, then the decision criterion is still given by Equation 4.7 but Equations 4.8 and 4.9 are modified to be:

$$E[DF|D(t), a] = \int DF(IM, T_{lead}, a) p(IM, T_{lead}|D(t)) \, \mathrm{d}IM \, \mathrm{d}T_{lead} \tag{4.10}$$

where the decision function is defined as:

$$DF(IM, T_{lead}, a) = E[U(DV_B)|IM, T_{lead}, a] - E[U(DV_C)|IM, T_{lead}, a] \tag{4.11}$$

For ease of illustration, we adopt the following notation for the action sets:

1. $\Omega_a = \{a_0, a_1, ..., a_n\}$ is the set of alternative mitigation actions or operations, where $a_i$ denotes initiating the $i^{th}$ action for $i \in [1, n]$ and $a_0$ denotes not initiating any action at a given time $t$, in other words, temporarily not taking any action.

2. $\Omega_A = \{A_0, A_1, ..., A_n\}$ is the same set of alternative mitigation actions or operations, but $A_i$ denotes the completion of the $i^{th}$ action for $i \in [1, n]$ and $A_0$ denotes permanently not taking any action.

#### 4.2.4.1 Incomplete action model

The time factor raises the question of how much benefit an incomplete action has as a function of the lead time. Hence, for all $i \in [1, n]$, we introduce benefit and cost reduction factors $\beta_i, \gamma_i \in \mathbb{R}$, which are functions of $T_{lead}$ to model $DF(IM, T_{lead}, a_i)$ as a function of $T_{lead}$:

$$DF(IM, T_{lead}, a_i) = \beta_i(T_{lead})E[U(DV_B)|IM, A_i] - \gamma_i(T_{lead})E[U(DV_C)|IM, A_i] \tag{4.12}$$

In most cases, $\beta_i \in [0, 1]$ is an increasing function of $T_{lead}$ that indicates a partial to complete benefit of a mitigation action as $T_{lead}$ increases; whereas $\gamma_i$ equals to constant 1 because once an action is taken, the cost of implementing the action is usually independent of $T_{lead}$. Because $A_0$ is not taking any action, both $E[U(DV_B)|IM, A_0]$ and $E[U(DV_C)|IM, A_0]$ are equal to 0, so $DF(IM, T_{lead}, a_0)$ is equal to 0.

#### 4.2.4.2 Value of information model

For many EEW systems based on a regional network, a warning is continually updated at some fixed time interval, $\Delta t$. In this case, the decision problem need no longer be a single decision in time because one may choose not to initiate any action at time $t$, then another decision may be made at $t + \Delta t$ when the updated EEW information may have less uncertainty. A more general version of this problem can arise in optimal policy searching for control or robotics problems, or optimal stopping time for option pricing. A standard methodology is to develop a dynamic model for the evolution of the state of interest and pick a policy that optimizes a predetermined cost function. However, in the case of EEW, because of the extremely short lead time, there will be

no turning back once an action is initiated. Hence, except $a_0$ (no action initiated), all actions will lead to a state termination. This simplifies the problem to identify the extra benefit (or cost) of $a_0$ due to a possibly better (or worse) decision made at $t + \Delta t$ based on all future EEW information, rather than a full optimal policy searching algorithm. In other words, the same decision criterion as shown in Equation 4.7 can be used, but $E[DF|D(t), a_0]$, which is originally equal to 0 because not taking any action induces zero benefit and cost, has an added value due to the potential change of EEW information in the future:

$$E[DF|D(t), a_0] = VoI \tag{4.13}$$

where, motivated by the theory of the value of information (Howard, 1966), I model the added value $VoI$ as the expected performance of the decision criterion over the domain of $p(IM, T_{lead}|D(t + n\Delta t))$ for all $n > 0$ minus the original expected performance of $a_0$ (which equals zero).

Applying the theory of value of information (Section 2.6) to the case of multiple EEW warning, the gain function $G(\pi)$ is related to $DF(IM, T_{lead}, a)$, where the decision policy $\pi$ is simply the chosen decision criteria. The information $I$ is related to the future updated EEW information $D(t + n\Delta t)$ for integer $n > 0$. Technically, $I = \{D(t + n\Delta t)|\forall n > 0\}$:

$$E[G(\pi_I)|I] = \max_{a \in \Omega_a} \{E[DF|a, D(t), D(t + \Delta t), ...]\} \tag{4.14}$$

$$p(I) = p(D(t + \Delta t), D(t + 2\Delta t), ...|D(t)) \tag{4.15}$$

However, modeling of $p(I)$ in this case refers to modeling the probability of all possible future seismic data based on the current seismic data, which is extremely difficult. An alternative is to choose a model for estimating future EEW information. For example, if one models the EEW information $p(IM, T_{lead}|D(t))$ as a product of two independent log-normal PDFs with means $\mu_E(t), \mu_T(t)$, and standard deviations $\sigma_E(t), \sigma_T(t)$, an intuitive choice of modeling future EEW information can be made by fixing the mean values but reducing the standard deviation values,

that is for some real value $\nu$ and for all $n > 0$:

$$\mu_E(t + n\Delta t) = \mu_E(t),\ \mu_T(t + n\Delta t) = \mu_T(t)$$
$$\sigma_E(t + n\Delta t) = \frac{\sigma_E(t)}{\nu^n},\ \sigma_T(t + n\Delta t) = \frac{\sigma_T(t)}{\nu^n}$$

In general, for any model chosen for estimating future EEW information with a vector of parameters $\nu$:

$$E[G(\pi_I)] = \int E[DF|\nu]p(\nu|D(t))\,\mathrm{d}\nu \tag{4.16}$$

Many models can be used to estimate $p(I)$, but most of them will lead to a complex $E[DF|\nu]$ that becomes impossible to evaluate. In this study, I propose a simple model based on the assumption of perfect information.

The most ideal assumption one can make on future EEW information is to assume that in the next EEW update, $D(t + \Delta t)$ will provide enough information to perfectly determine $IM$ (or $M$ and $R$ depending on the EEW system). Although this is an impractical assumption that can never be achieved, it provides important insights into the influence of uncertain lead time on decision making for EEW applications. Insights and possible improvement of this model for practical use are discussed in the example in Section 4.4. The perfect information assumption implies that $I = \{I\hat{M}, \hat{T}_{lead}\}$, where $I\hat{M}$ and $\hat{T}_{lead}$ represent the true $IM$ and $T_{lead}$ values, respectively, and:

$$p(I) = p(I\hat{M}, \hat{T}_{lead}) = p(IM, T_{lead}|D(t)) \tag{4.17}$$

which is the current EEW information because it reflects the current belief on the true $IM$ and $T_{lead}$ values. Meanwhile:

$$E[G(\pi_I)|I] = \max_{a\in\Omega_a} E[DF|IM, T_{lead} - \Delta t, a] \tag{4.18}$$

Note that $\Delta t$ is subtracted from $T_{lead}$ because $E[G(\pi_I)|I]$ refers to the expected value under decision made at $t + \Delta t$, where the current estimate of $T_{lead}$ will be reduced by $\Delta t$.

As $E[G(\pi)] = E[DF|D(t), a_0] = 0$ because it represents the expected value of not taking any action at time $t$ when no future information is available, the added value due to the uncertain lead

time equals $VoI$:

$$\begin{aligned} VoI &= E[G(\pi_I)] - 0 \\ &= \iint_{\Delta t}^{\infty} \max_{i\in[0,n]} E[DF|IM, T_{lead} - \Delta t, a_i] p(IM, T_{lead}|D(t))\, \mathrm{d}T_{lead}\mathrm{d}IM \end{aligned} \tag{4.19}$$

where for $i \in [1, n]$:

$$E[DF|IM, T_{lead} - \Delta t, a_i] = DF(IM, T_{lead} - \Delta t, a_i) \tag{4.20}$$

because expected value of $DF$ is simply $DF$ when $IM$ and $T_{lead}$ are given.

For the case $i = 0$:

$$E[DF|IM, T_{lead} - \Delta t, a_0] = DF(IM, A_0) = 0 \tag{4.21}$$

Note that when $T_{lead}$ is between 0 and $\Delta t$, no new decision can be made, meaning that $E[G(\pi_I)|I] = 0$. Therefore the integral in Equation 4.19 excludes $T_{lead}$ values between 0 and $\Delta t$.

In summary, this model can be simply represented by a single DF:

$$\begin{aligned} &DF(IM, T_{lead} - \Delta t, a_0) \\ &= \begin{cases} \max_{i\in[1,n]}\{0, E[DF|IM, T_{lead} - \Delta t, a_i]\}, & T_{lead} > \Delta t \\ 0, & T_{lead} \le \Delta t \end{cases} \end{aligned} \tag{4.22}$$

In practice, large earthquakes usually induce losses that are substantially larger than the cost of a mitigation action. Therefore, a decision maker is likely to prefer avoiding a missed alarm to a false alarm. $DF$ without a lead time model, which is the basic cost-benefit analysis case, will usually give a substantially larger risk of a false alarm than a missed alarm. In this sense, the value of information model aims at reducing the false alarm rate while maintaining a low missed alarm rate. However, the perfect information model may suppress the false alarm too much so that it leads to an unacceptable increase in the missed alarm rate. To compensate the "overconfidence" from assuming perfect information at the next EEW update, $\Delta t$ could be artificially increased to reduce the influence of the $VoI$ model (as shown in Section 4.4.2.2). This is equivalent to assuming perfect information at a larger $\Delta t$ value, but the decision will be re-done before the assumed perfect

information is obtained. Hence, the decision is made based on nearly perfect information instead of perfect information, which indirectly compensates for the overconfidence while maintaining a relatively low computational effort for practical purposes. Other practical models for estimating future EEW information to calculate Equation 4.16 are left for future research.

### 4.2.5 ePAD framework summary

Based on the received EEW information, ePAD makes a decision with Equations 4.7, 4.8 and 4.9. Calculation of each term in the equations depends on the chosen model and user-specific decision behavior. Below shows a typical procedure for setting up the framework:

Step (1). *Define problem*

i. Action—select a set of mitigation actions of interest, estimate loss models (i.e., benefit and cost models: $E[DV_B|IM, A]$ and $E[DV_C|IM, A]$) and incomplete action model (i.e., reduction factors $\beta(T_{lead})$ and $\gamma(T_{lead})$ in Equation 4.12 for each action.

ii. Structure—determine models for other PBEE components shown in Figure 4.1: GMPE for the site (if necessary), structural response model, and damage fragility model.

iii. EEW—select a PDF form for EEW information (e.g., Gaussian distribution) and determine the use of incomplete action model and value of information model depending on the EEW type (single or multiple warning system).

Step (2). *Framework setup*

i. Precalculate $DF(IM, T_{lead}, a_i)$ for all $i \in [1, n]$ based on PBEE methodology and Equation 4.11 or 4.12.

ii. Set $DF(IM, T_{lead}, a_0)$ to be 0 for single warning EEW, or determine a model for it using the concept of value of information (e.g., Equation 4.19) for multiple warning EEW.

iii. If the PDF of EEW information can be parameterized in a low-dimension space, calculate the decision contours and develop an appropriate surrogate model for them. Otherwise, develop a surrogate model for $DF$ to reduce computational effort.

Step (3). *Framework validation*

i. If the PDF of EEW information can be parameterized in a low-dimension space, verify that the decision behavior represented by the resulting decision contours is consistent with the users desired rational decision making.

ii. Check the decisions made by running ePAD with past earthquake data (if available) to confirm that a desired decision behavior is obtained. If it is not obtained, adjust models in Steps 1 and 2, then re-do the procedure.

## 4.3 Comparisons of decision criteria

For the convenience of comparison, let us consider a simplified case where only one possible mitigation action is considered (i.e., $\Omega_a = \{a_0, a_1\}$), $IM$ is a scalar such as the acceleration response spectral value $SA$ at a structure's fundamental period, and the utility function $U(DV)$ is independent of $T_{lead}$. This is consistent with the decision frameworks mentioned in Section 4.1. For this simplified case, the previous decision criterion in Equation 4.1 becomes:

$$\text{Take action if } E[U(DV)|D(t), a_1] > E[U(DV)|D(t), a_0] \tag{4.23}$$

This is be rewritten in the following form based on the PBEEW framework:

$$\text{Take action if } \int \left(E[U(DV)|IM, a_1] - E[U(DV)|IM, a_0]\right) p(IM|D(t))\, \mathrm{d}IM > 0 \tag{4.24}$$

Now, define the ePAD Decision Function:

$$DF_{ePAD}(IM) = E[U(DV)|IM, a_1] - E[U(DV)|IM, a_0] \tag{4.25}$$

Then, $DF_{ePAD}$ is effectively a utility function for $IM$ that is used for the decision-making (take action when the expected utility is greater than zero). This is the decision function appropriate for the decision criterion of Iervolino et al. (2007) where a PBEE methodology is used to evaluate the expected values.

For the threshold-based method mentioned in Section 4.1, one would determine fixed thresholds

$im_0$ and $P_0$, perhaps based on engineering judgment, and the decision criterion would be:

$$\text{Take action if } P(IM > im_0|D(t)) > P_0 \tag{4.26}$$

Using the Heaviside step function $H(x)$, this can be rewritten in the following form:

$$\text{Take action if } \int (H(IM - im_0) - P_0)\, p(IM|D(t))\, \mathrm{d}IM > 0 \tag{4.27}$$

Thus, the decision function becomes for the threshold method:

$$DF_{TM}(IM) = H(IM - im_0) - P_0 \tag{4.28}$$

For Grasso et al. (2007), given a pre-specified threshold $im_0$ for $IM$ that is set by the designers or operators of the facilities being protected, action is taken if and only if the expected cost of no action is greater than the expected cost of action. Two important expected costs are introduced: 1) An expected cost, $C_{fa}$, due to a false alarm is assumed if the mitigation action is taken but the $IM$ at a site is less than $im_0$; 2) An expected cost, $C_{save}$, due to a missed alarm, and so a missed opportunity for mitigating the expected earthquake economic loss by $C_{save}$, is assumed if no action is taken but the $IM$ at a site is larger than $im_0$. As a result, the decision criterion can be written as:

$$\text{Take action if } C_{save}P(IM > im_0|D(t)) > C_{fa}P(IM \leq im_0|D(t)) \tag{4.29}$$

This can be rewritten in the following form:

$$\text{Take action if } \int \left( H(IM - im_0) - \frac{C_{fa}}{C_{save} + C_{fa}} \right) p(IM|D(t))\, \mathrm{d}IM > 0 \tag{4.30}$$

If we take $P_0 = C_{fa}/(C_{save} + C_{fa})$ under this method, then its decision function is the same as $DF_{TM}(IM)$.

Another possible method is to take action if the occurrence of a specific damage state ($DM_S$) exceeds a certain threshold probability. For example, one may take a mitigation action when the probability of severe building damage exceeds $P_{DM}$. The decision criterion can be written as follow:

$$\text{Take action if } P(DM_S|D(t)) > P_{DM} \tag{4.31}$$

This can be rewritten in the following form:

$$\text{Take action if } \int (P(DM_S|IM) - P_{DM})\, p(IM|D(t))\, \mathrm{d}IM > 0 \tag{4.32}$$

Thus, the decision function for this case is:

$$DF_{DM}(IM) = P(DM_S|IM) - P_{DM} \tag{4.33}$$

As explained in Section 4.2.3.2, different types of decision function result in different shapes of decision contour, thus represent different decision behaviors. Figure 4.3 shows a general shape of each decision function mentioned above.

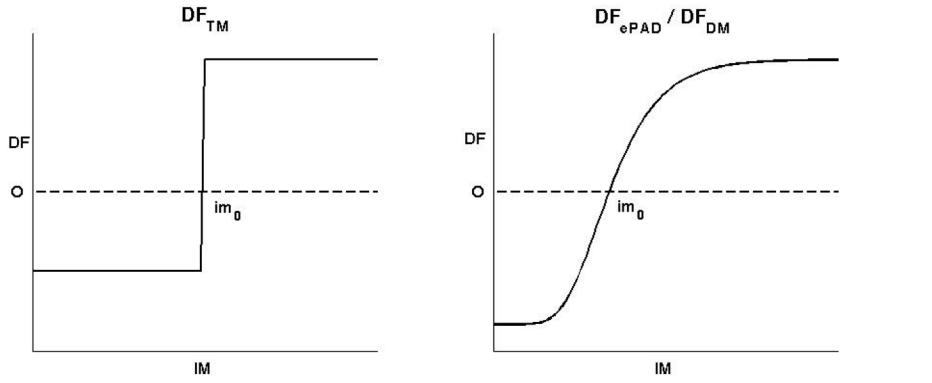


Figure 4.3: General shapes of decision functions $DF_{TM}$ and $DF_{ePAD}/DF_{DM}$.

In civil structure applications, $P(DM_S|IM)$ can be represented by a fragility curve, which is usually a type of sigmoid function, and $DM_S$ is usually a vector of discrete damage states instead of a single damage state. Also, $DF_{ePAD}$ can be viewed as a linear combination of sigmoid functions, which is also a sigmoid function, because $E[U(DV)|IM, a] = \sum_k E[U(DV)|DM_k, a]P(DM_k|IM, a)$, where $E[U(DV)|DM_k, a]$ is known once a loss model is defined for each $DM_k$. Therefore, one can determine $P_{DM}$ by fitting $DF_{ePAD}$ with $DF_{DM}$ of any chosen $DM_S$. The regression problem can be solved by optimizing an objective function, for example, least-squares matching between the decision contours of $DF_{ePAD}$ and $DF_{DM}$.

## 4.4 Example: Evacuation warning

Real EEW applications may involve complex loss models and the activation of special engineering systems for mitigating the economic losses and life-safety threat of an earthquake. For the purpose of illustrating the previously presented framework and models, a simplified example based on a previously studied benchmark office building is chosen and only a single action is considered—whether to broadcast an earthquake alert or not. Hence, the action only influences the loss model, whereas the structural model is independent of the action. A similar type of example is presented in Iervolino et al. (2007) to demonstrate the benefit of using a basic cost-benefit analysis for decision making. In this study, I focus on analyzing the newly proposed lead time model to validate its ability to mimic rational human decision making and to discuss some possible adjustments of the models for practical use.

### 4.4.1 Problem setup

#### 4.4.1.1 Structural, loss, and lead time models

The PEER benchmark office building studied in Goulet et al. (2007) and Haselton et al. (2007) is taken as the target structure for our example. It is a hypothetical four-story reinforced concrete moment-frame building designed according to the 2003 International Building Code, located on deep sediment near the center of the Los Angeles basin, at 33.996N, 118.162W, south of downtown Los Angeles. The above-mentioned references include the details of the structural models, fragility functions, and annual loss assessment. In this example, only a single action $A_1$ is considered: broadcasting an earthquake alarm to alert people inside the building to move to the closest safe location. The value of the alarm is saving building occupants lives if they successfully move to the safe location. Hence, a complete action corresponds to all occupants have moved to the safe location, instead of just the completion of broadcasting the alarm. In this case, $DV$ is defined based on economic loss $L$ and a risk-neutral model is used for utility function. The decision criterion becomes the one shown in Equation 4.4, or Equation 4.7 when it is in terms of $DF$.

For the structural model, using the same definition as in Haselton et al. (2007), the two damage states related to the cost-benefit analysis for our chosen action are global collapse ($C$) and local collapse ($LC$). The scalar $IM$ chosen is the fundamental period spectral acceleration ($SA$). Figure

4.4 shows the fragility curves for both damage states, which are a simplification of the component-wise fragility functions of the benchmark building that match the damage state definitions. A log-normal CDF is used for each fragility curve.

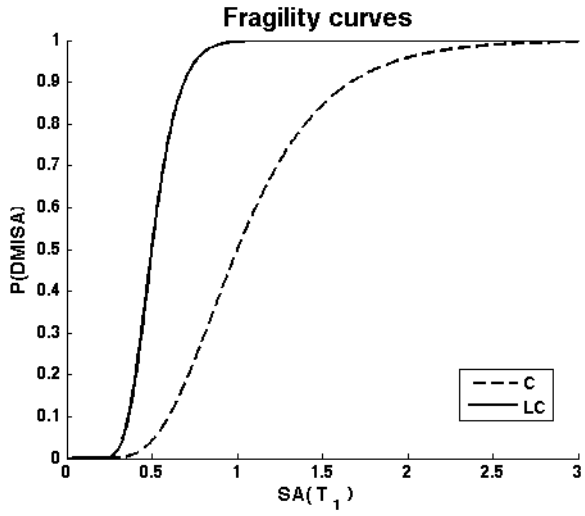


Figure 4.4: Fragility curves for structural model ($C$: global collapse, $LC$: local collapse).

The expected life loss is taken as 20 in the case of global collapse and an equivalent life loss (including the consideration of injuries) of 2 in the case of local collapse based on the previous study in Haselton et al. (2007). To model the action benefit, an 80% life-saving ratio is assumed for $A_1$, giving expected life savings of 16 and 1.6 in the case of global collapse and local collapse, respectively. The cost of action is assumed to be the induced business downtime of the building due to the disturbance caused by the action, which is a constant value independent of the damage state of the building. To measure all benefit and costs in a common unit, the value of a statistical life is often used in cost-benefit analysis involving decision making related to life-saving issues. In this case, the two constant values can be reduced to a single factor, $r$, which represents the ratio of downtime cost to the value of statistical life. The value of $r$ can be adjusted based on the judgment of the decision maker(s) responsible for approving the warning system installation in the building. A reasonable choice is $r = 0.2$ based on the loss analysis in Haselton et al. (2007), but the results are found to be not sensitive to small changes of the value of $r$. Table 4.1 lists all the other predetermined parameter values in the structural and loss models for our example structure.

| Damage states ($DM$) | Fragility function model | | | Loss Model | |
|---|---|---|---|---|---|
| | Type | Mean | Std. dev. | Life loss | Life-saving ratio |
| Global collapse ($C$) | Log-normal CDF | $\mu_1$ | $\sigma_1$ | 20 | 0.8 |
| Local collapse ($LC$) | Log-normal CDF | $\mu_2$ | $\sigma_2$ | 2 | 0.8 |

Table 4.1: Choice of parameter values for fragility function models and loss models.

Next, a lead time model for the action is constructed. A rough estimate of 20 to 25 seconds for people to move to the closest safe location is assumed. As mentioned in Section 4.2.4.1, $\beta$ is typically an increasing function of $T_{lead}$ between 0 and 1. In this example, the functional form taken for the benefit reduction factor, $\beta_1(T_{lead})$, in Equation 4.12 is a log-normal CDF function with mean $\mu_\beta = \ln(10)$ and standard deviation $\sigma_\beta = 0.35$ which is plotted in Figure 4.5. The other factor, $\gamma_1 = 1$, because we assume that once the alarm is triggered, the downtime cost is induced regardless of the outcome.

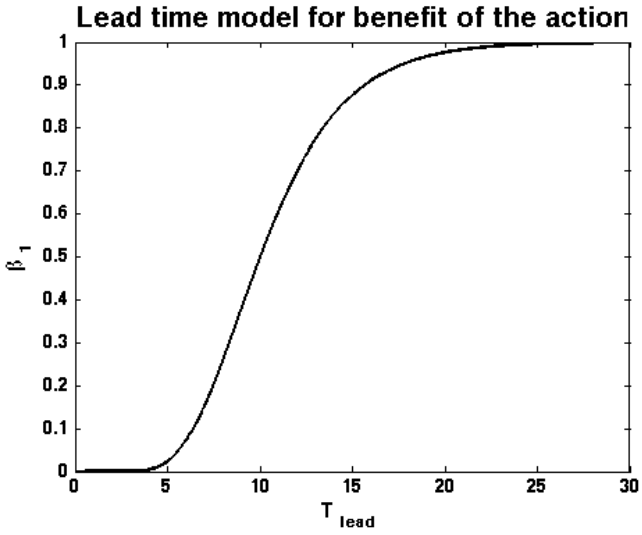


Figure 4.5: Lead time model $\beta_1$ for the action $a_1$.

#### 4.4.1.2 EEW model and expected value calculation

Considering the high efficiency needed for EEW information transmission, the PDFs of EEW information are usually parameterized in a low-dimensional space. For simplicity, in this example, I model $T_{lead}$ and $SA$ as two independent log-normal distributions given $D(t)$. Hence,

$p(IM, T_{lead}|D(t))$ in Equation 4.10 becomes:

$$p(SA, T_{lead}|D(t)) = \phi\left(\frac{\ln(SA) - \mu_E(t)}{\sigma_E(t)}\right)\phi\left(\frac{\ln(T_{lead}) - \mu_T(t)}{\sigma_T(t)}\right) \tag{4.34}$$

Using the structural and loss models as illustrated in Section 4.4.1.1, and letting $DM_1 = C$ and $DM_2 = LC$, the decision function in Equation 4.12 can be written as:

$$DF(SA, T_{lead}, a_1) = \beta_1(T_{lead})\sum_{i=1}^{2} E[L_B|DM_i, A_1]P(DM_i|SA) - r \tag{4.35}$$

$$\text{where } \beta_1(T_{lead}) = \Phi\left(\frac{\ln(T_{lead}) - \mu_\beta}{\sigma_\beta}\right), P(DM_i|SA) = \Phi\left(\frac{\ln(SA) - \mu_i}{\sigma_i}\right)$$

Also, recall that $E[L_C|SA, A_1] = r$ is a constant, which is the ratio of downtime cost to the value of statistical life. Here, $(L_B, L_C) = (16, 0.2)$ for $DM_1 = C$ and $(1.6, 0.2)$ for $DM_2 = LC$. Note that the PDF of $DM_i$ is independent of action $a_1$ because in this example, the action—evacuation—will only influence the loss model, but not the structural model.

To efficiently calculate Equation 4.10 for this example, one can show the following result for the Gaussian CDF and PDF:

$$\int \Phi\left(\frac{X - \mu_c}{\sigma_c}\right)\phi\left(\frac{X - \mu_p}{\sigma_p}\right)\,\mathrm{d}X = \Phi\left(\frac{\mu_p - \mu_c}{\sqrt{\sigma_c^2 + \sigma_p^2}}\right) \tag{4.36}$$

Hence, the closed form expression for $E[DF|D(t), a_1]$ is:

$$E[DF|D(t), a_1] = -r + \Phi\left(\frac{\mu_T - \mu_\beta}{\sqrt{\sigma_T^2 + \sigma_\beta^2}}\right)\sum_{i=1}^{2} E[DV_B|DM_i, A_1]\Phi\left(\frac{\mu_E - \mu_i}{\sqrt{\sigma_E^2 + \sigma_i^2}}\right) \tag{4.37}$$

Based on Equation 4.19, $E[DF|D(t), a_0]$ equals the value of information:

$$E[DF|D(t), a_0] = \iint_{\Delta t}^{\infty} \max\{DF(SA, T_{lead} - \Delta t, a_1), 0\}p(SA, T_{lead}|D(t))\,\mathrm{d}T_{lead}\mathrm{d}SA \tag{4.38}$$

Because this integral cannot be evaluated in a closed form, a Monte Carlo sampling technique is

used to estimate the integral. Now, the single action decision criterion can be simplified as:

$$\text{Take action if and only if } E[DF|D(t), a_1] > E[DF|D(t), a_0] \tag{4.39}$$

In summary, Table 4.2 lists the values for all parameters in the models.

| Parameter | Value | Parameter | Value |
|---|---|---|---|
| $E[DV_B\|DM_1, A_1]$ | $20 \times 0.8$ | $E[DV_B\|DM_2, A_1]$ | $2 \times 0.8$ |
| $\mu_1$ | $\ln(1)$ | $\sigma_1$ | 0.4 |
| $\mu_2$ | $\ln(0.5)$ | $\sigma_2$ | 0.25 |
| $\mu_\beta$ | $\ln(10)$ | $\sigma_\beta$ | 0.35 |
| $\mu_E$ | From EEW | $\sigma_E$ | From EEW |
| $\mu_T$ | From EEW | $\sigma_T$ | From EEW |

Table 4.2: Values for the parameters for reduced expected life loss, the fragility curves $p(DM_i|SA)$, where $DM_1 = C$, $DM_2 = LC$, and $SA$ is in g's, benefit reduction function $\beta$, and PDFs for $SA$ and $T_{lead}$.

### 4.4.2 Analysis and results

As the EEW information is modeled as Equation 4.34, it can be represented in a four-dimension domain with $\mu_E$, $\sigma_E$, $\mu_T$ and $\sigma_T$ at any given time $t$. Hence, the decision contour analysis can be performed. Figures 4.6, 4.7 and 4.8 show a set of decision contours in 2-D domain of $\mu_E$ and $\sigma_E$, for some fixed $\mu_T$ and $\sigma_T$ values. Each curve represents a separating boundary, where the region below the curve means "not to broadcast an alert" and the region above the curve means "broadcast an alert". Each figure is plotted as $\mu_E$ versus $\sigma_E$ to show how the "critical mean $SA$ value" responds to its uncertainty. As a result, a horizontal decision contour means that the critical mean is independent of $SA$ uncertainty, showing an uncertainty neutral decision behavior. Similarly, a decreasing decision contour means that the action is taken at a lower critical mean value as uncertainty increases, thus the uncertainty introduces a negative factor in the decision maker, for example, more fear of the possibility of having a large earthquake. I call it an uncertainty-averse decision behavior. In contrast, an increasing decision contour shows that the uncertainty introduces a positive factor in the decision maker, for example, more hope in the possibility of a small earthquake or delaying the decision, showing an uncertainty-taking decision behavior. Note

that these definitions are different from the risk-averseness because risk-averseness is defined based on the utility function. In this single action case, the "uncertainty-averseness" is a result of making decisions based on the expected value of a utility function on $SA$ defined by the decision function with a Gaussian model on $SA$ given seismic data at time $t$. Recall that a risk-neutral model for $U(DV)$ is assumed in our example (Section 4.1). The different decision behaviors toward uncertainty of EEW information are results of the loss and structural models, as well as the lead time inclusion.

#### 4.4.2.1 Results with ePAD for single warning

First, let us consider the problem from a rational human perspective. How would different lead time estimations change a decision if an incomplete action has less value? In our example, the less lead time we have, the less people can be saved by moving to the closest safe location. An action with less benefit means that one is less likely to take the action. Therefore, an increase in the critical mean $SA$ value is expected after the inclusion of an incomplete action model when the lead time is below the minimum time needed for action completion.

Indeed, Figure 4.6 shows a result that is consistent with this expectation. In this case, the decision contours are calculated with Equations 4.39, 4.37, and $E[DF|D(t), a_0] = 0$ (as explained in Section 4.2.4.1). One can observe that as $\mu_T$, the mean of $T_{lead}$ decreases, the decision contour shifts upward. This means that as the expected time for completing the action is decreasing, the benefit of the action is decreasing, and thus, the system is less likely to trigger the action because the cost stays constant in this case. As the expected time is approaching or exceeding the time limit for completing the action, which is 20–25 seconds in this case (see Figure 4.5), one can observe that the decision contour converges to the same decision contour as if the time factor is not included. This is because the concern of incomplete action vanishes when the lead time is expected to be sufficient. Also, the decision contour for $\mu_T < 6$ seconds does not appear in Figures 4.6, 4.7 and 4.8 because the time is too little to take the action with enough expected benefit to outweigh the cost; thus no action is triggered for any given EEW information. In reality, a backup action, such as warning people to immediately duck, cover, and hold at their current location, is needed to fill the gap between theoretical calculations and practical usage. If the EEW information lies above the decision contour with incomplete action, the original action is triggered; else if it lies between

the decision contour with incomplete action and decision contour without modeling the effects of incomplete action (approximately the curve of $\mu_T = 24$ seconds in Figure 4.6), the backup action that can be done almost instantaneously is triggered instead; otherwise, no action is triggered.

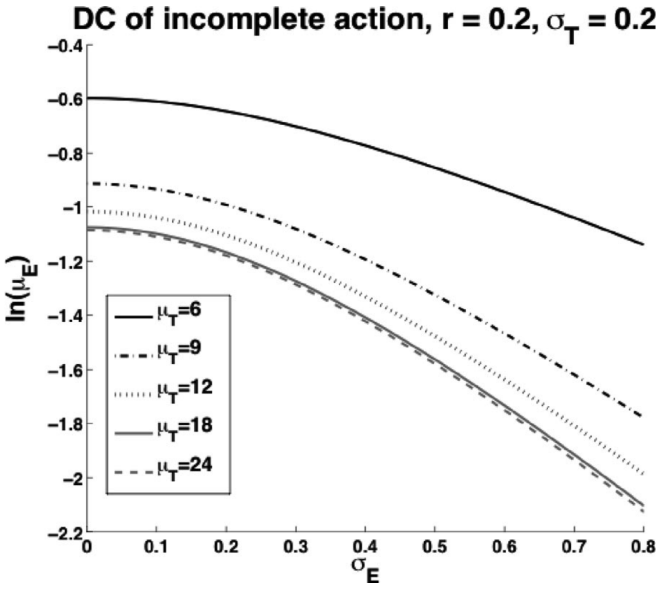


Figure 4.6: Decision contours for the single warning case (with an incomplete action model) with fixed lead time uncertainty (unit of $\mu_E$ and $\sigma_E$: g, unit of $\mu_T$ and $\sigma_T$: seconds).

#### 4.4.2.2 Results with ePAD for multiple-warning

Again, let us first consider the problem from a rational human perspective. How would different lead time estimations change a decision if now one has another chance to make a decision every $\Delta t$ interval? When the lead time is too short to complete the action, the possibility of delaying the decision does not provide any value, thus it should not influence the decision. Therefore, the decision contour should stay the same as in Section 4.4.2.1. On the contrary, when the lead time is more than sufficient to complete the action, the decision should be delayed for potentially better EEW information in the future, unless the $SA$ value is already perfectly determined. Therefore, a significant increase in the critical mean $SA$ value is expected when there is a large $\sigma_E$.

Figure 4.7 shows a result consistent with this expectation. In this case, the decision contours are calculated with Equations 4.39, 4.37, and 4.38. Assuming that there are continual updates of EEW information at every second ($\Delta t = 1$ second), one can observe the following three features from the figure:

1. As the expected lead time $\mu_T$ is close to or exceeds the minimum time needed for action completion (20–25 seconds), the decision behavior changes from uncertainty-averse to uncertainty-taking.

2. As the expected lead time $\mu_T$ decreases below the minimum time needed for action completion (20–25 seconds), the decision contour converges to the one in Figure 4.6.

3. The critical mean $SA$ value stays the same as in Figure 4.6 when $\sigma_E$ approaches zero.

Here is the explanation for the corresponding observed features:

1. The additional risk exposure due to the uncertainty in $SA$ prediction is compensated by the potential value of future information. In other words, the value of waiting for updated EEW information outweighs the risk of not being able to initiate an appropriate mitigation action while waiting.

2. When the expected lead time is insufficient to complete the action, the value of future information diminishes to zero because the benefit of action is already very small. Hence, it has minimal influence on the decision in this case.

3. When there is no uncertainty in $SA$ prediction, a delay in decision provides no extra value. Hence, it is better to make the decision immediately.

Note that the larger $\Delta t$ is, the higher the risk to bear when choosing not to take action at the current time. Hence, it reduces the potential value of future information. Comparing Figures 4.7 and 4.8, an increase in $\Delta t$ leads to an overall reduction of the influence of the value of information, and thus, less risk exposure. As mentioned in Section 4.2.4.2, the perfect information model of value of information used in this article overestimates the true value of future EEW information. This may lead to an over suppression of false alarm and an unacceptable increase of missed alarm. Because the perfect information model is the best possible scenario for the multiple warning case, it can be treated as the upper bound of false alarm rate reduction based on lead time inclusion, and the model in Section 4.2.4.1 without the $VoI$ model, which is equivalent to $\Delta t$ approaching infinity, is the lower bound. Therefore, $\Delta t$ could be treated as an artificial parameter and be adjusted between the true EEW update interval value and infinity to better fit the desired decision behavior

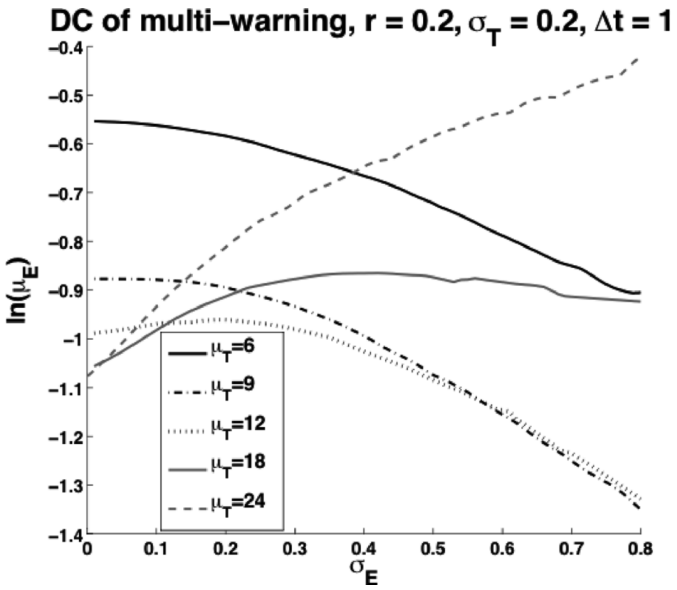


Figure 4.7: Decision contours of multiple warning case (include incomplete action model and value of information model with $\Delta t = 1$ second) with fixed lead time uncertainty (unit of $\mu_E$ and $\sigma_E$: g, unit of $\mu_T$ and $\sigma_T$: seconds).

(e.g., although $\Delta t = 1$ second, the decision contours for $\Delta t = 3$ seconds could be used in practice if it better fits the users situation).

## 4.5 Conclusion and ongoing work

In light of the increasing attention to EEW applications, I propose the ePAD framework that is based on some existing fundamental approaches and some new models to enhance the decision-making process. Especially after the 2011 M9 Tohoku earthquake in Japan, the benefits and feasibility of EEW are becoming more appreciated throughout the world. Despite the expanding engineering development of early warning systems, their applications are developing at a slower pace, partly due to reliability concerns. The uncertain nature of the EEW information leads to an inevitable trade-off between missed warnings and false warnings. Because large earthquakes often induce substantial damage to society, usually a missed warning is more serious than a false warning; however, in some situations, false warnings can be costly. A well-designed decision algorithm will not only offer a fast decision procedure that will make more EEW applications feasible, but will also allow a better trade-off between missed warnings and false warnings.

ePAD aims at providing a platform for further studies in this aspect by laying out a general decision criterion based on fundamental decision theory and an existing cost-benefit analysis ap-

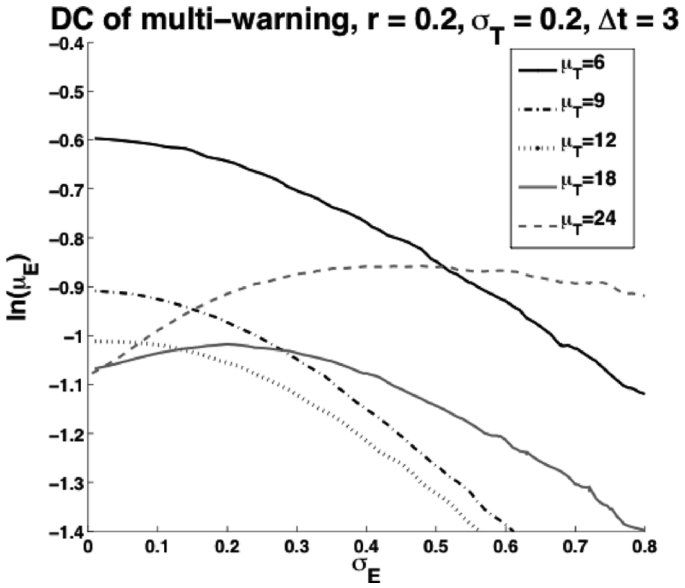


Figure 4.8: Decision contours of multiple warning case (include incomplete action model and value of information model with $\Delta t = 3$ second) with fixed lead time uncertainty (unit of $\mu_E$ and $\sigma_E$: g, unit of $\mu_T$ and $\sigma_T$: seconds).

proach (as shown in Section 4.2). Existing approaches can be improved in two important aspects that can further optimize the trade-off: correlation in multiple-action decisions and the treatment of lead time with its uncertainty. This chapter focuses on the latter aspect to reduce false warnings. The former will be discussed in Chapter 6.

To maximize the benefits of EEW given a short lead time, the concepts of decision function, decision contour, and surrogate model are used to improve the effectiveness of the ePAD framework. If EEW information can be reduced into a low-dimensional space, then an analysis of the decision contours can be done and a surrogate model can directly be applied based on the decision contours to achieve real-time decisions. Otherwise, a surrogate model can be applied to the decision function to improve calculation efficiency during the decision process. This is possible because most of the calculations are independent of the EEW information under the PBEEW model.

From the moment that the EEW system releases warning information, the three main steps in a mitigation application are performing the probabilistic ground motion prediction for the site, the response prediction for the target structure/system, and the loss/damage prediction. Because the last two steps do not involve information from the EEW, they can be done ahead of time and, if necessary, approximated with a robust surrogate model such as the RVM. Combined with the newly proposed lead time model in a real-time decision process, this allows more flexibility for users

to adapt ePAD to correspond to a desired rational decision behavior.

The proposed lead time model is validated in the illustrative example. Rather simple models are assumed for both information from the EEW system and the structural response. The results show that both the incomplete action model and the value of information model are consistent with the rational human decision making. The models capture the change in the decision due to the reduced benefit of an incomplete action and the enhanced benefit of delaying the decision, given potential updates of EEW information. For applications, a user must first apply appropriate probability models, that is, a loss model, structural model, and ground motion model (if necessary), to obtain a baseline decision behavior. Then, the parameters in the models, such as $\beta_i(T_{lead})$, $\gamma_i(T_{lead})$, and $\Delta t$, can be adjusted to fine tune the resulting decision behavior that fits the users needs. This can be efficiently done by using the concepts of decision contours and decision maps as analysis tools. Note that the concept of decision function and decision contour can also be used for comparing different decision-making methods for EEW applications.

Future research could explore new value of information models. It is also important to investigate the challenges in loss model development. For many EEW applications, it is difficult to quantify the benefit of a mitigation action, especially for life-saving purposes. Overestimating the benefit will increase the probability of taking a mitigation action when it should not have been done, whereas underestimating will increase the probability of not acting when it is appropriate to do so, thereby influencing the trade-off between missed response and false response in a detrimental way. Also, typical costs for EEW applications are often in different units than the benefits, and it is a practical challenge to find an appropriate conversion factor between them. Future research could focus on such practical challenges to further extend the scope of the ePAD framework to cover various decision behaviors. It is also of interest to investigate the possibility of an ePAD-like implementation for tsunami or hurricane early warnings. Because the lead time for emergency response is usually longer for these natural hazards, a different set of models is needed for these applications.

# Chapter 5

# Application of ePAD: EEW-based Elevator Control

## 5.1 Motivation and background

Elevators in earthquake zones are often equipped with seismic sensors that can trigger an emergency shutdown to avoid falling or severe damage. However, specialists are required to check the integrity of the elevator and restart the elevator system after an emergency shutdown. Hence, after a large earthquake occurs, there might be significant loss caused by people being trapped in the elevators. One example is an M6.3 earthquake that happened on Oct 31, 2013 in Hualien, Taiwan, where there were reports of people trapped in the elevator (Yahoo News, 2013). Earthquake early warning (EEW) systems, which provide a few seconds to a minute of warning lead time, open a new solution to prevent such tragedies: stop the elevator at the closest floor and open the doors before the arrival of the destructive seismic waves. Due to the uncertainty of EEW information, false alarms may occur, which would lead to unnecessary disruption to the elevator service that may trouble the passengers. Current practice is often to trigger a mitigation action when the expected intensity measure ($IM$) based on EEW information exceeds a pre-set threshold. A common approach for $IM$ estimation is to use a ground motion prediction equation (GMPE) based on the estimated earthquake magnitude and hypocenter location (Boore and Atkinson, 2008; Campbell and Bozorgnia, 2008), although recently a new approach has appeared that directly estimates $IM$ in a large region based on local $IM$ data from seismic network stations (Hoshiba, 2013). However, the shaking experienced in a tall building will be significantly different from that on the ground and it will also differ from one building to another, or even from one floor to another.

During the April 7, 2011 M9.0 Tohoku earthquake in Japan, for example, roof accelerations on some tall buildings in the Tokyo metropolitan area were amplified by a factor of around 3.5 compared to the ground motions (Kasai et al., 2012).

Kubo et al. (2011) investigated combining an EEW system and a real-time strong motion monitoring system which factors in the structural response to the emergency response for a high-rise building. In their approach, elevators are moved to the closest floor and the doors are opened if the expected peak floor acceleration exceeds a pre-set threshold based on a Japanese standard. The expected peak floor acceleration is calculated based on the EEW information, a ground motion prediction equation and a lumped-mass building model. In contrast, Cheng et al. (2014) conducted a study on elevator control that used a performance-based earthquake engineering framework and receiver operating characteristic (ROC) analysis.

In this chapter, I investigate the contributions from the uncertainties in the EEW information and warning lead time to decision-making, which were not included in the previous studies. The dynamic response amplification is addressed and the ePAD framework is applied to control elevator based on uncertain EEW information, a generic structural model and a simple cost-benefit model. A surrogate model is trained based on the relevance vector machine (RVM) from machine learning to emulate the complex cost-benefit model that includes the value of information (VoI). The Japanese and USA standards for stopping elevator based on the ground shaking intensity is compared under the ePAD framework. For illustrative purposes, I also present a case study for a building in downtown Los Angeles and with an earthquake on the San Andreas Fault.

## 5.2 Applying ePAD

### 5.2.1 Basic model (No lead time contribution)

For the elevator control application, examples of possible mitigation actions include immediate stop, stop at the closest floor, move to the ground floor, etc. For this study, a single action is considered: stop the elevator at the closest floor and open the door. For the basic model (decision-making without the influence of lead time), let the action set $\Omega = \{A_0, A_1\}$, where $A_0$ = no action and $A_1$ = take action. A decision is made based on the trade-off between the cost (induced economic cost after taking the action) and the benefit (reduced economic loss after taking the action), $L_C$ and

$L_B$ respectively, given the seismic data $D(t)$ at time $t$. Following the ePAD framework, I use the *decision function*:

$$\text{Take optimal action } \hat{A} = argmax_{A\in\Omega} E[DF|D(t), A] \tag{5.1}$$

$$\text{where } E[DF|D(t), A] = \int DF(IM, A)p(IM|D(t))\,\mathrm{d}IM \tag{5.2}$$

$$\text{and } D(IM, A) = E[L_B|IM, A] - E[L_C|IM, A] \tag{5.3}$$

When no action is taken, there is no benefit and cost corresponding to the action, thus, the expected value of $L_B$ and $L_C$ given $IM$ and $A_0$, $E[L_B|IM, A_0]$ and $E[L_C|IM, A_0]$, are both zero. Hence, $E[DF|D(t), A_0] = 0$. On the other hand, $E[L_B|IM, A_1]$ and $E[L_C|IM, A_1]$ are calculated based on a loss model and a structural model. Let the cost of action be time delay and service interruption from stopping the elevator, which occurs each time the action is taken. Hence, $E[L_C|IM, A_1] = r_{C1}l_{C1} + r_{C2}l_{C2}$, a constant with respect to $IM$, where $l_{C1}$ and $l_{C2}$ represent the expected amount of time delay and service interruption, respectively, affecting the passengers, and $r_{C1}$ and $r_{C2}$ represent the corresponding factors to transfer the loss terms, $l_{C1}$ and $l_{C2}$, to economic loss. Also, let the benefit of action be preventing injury or death for occupants trapped in the elevator after an earthquake. Hence, $E[L_B|IM, A_1] = r_B l_B P(DM|IM, A_1)$, where $P(DM|IM, A_1)$ represents the fragility function of damage state $DM$ and is described in detail in Section 5.2.2. Here, $DM$ represents the state of elevator in danger (defined more specifically in Section 5.3.1), $l_B$ represents the number of injured individuals, and $r_B$ represents a factor to transfer injury to economic loss. The choice of $r_{C1}$, $r_{C2}$ and $r_B$ is directly related to the decision behavior, which will be discussed in detail in Section 5.3.

### 5.2.2 Structural model

A structural model is needed to calculate the fragility function $P(DM|IM, A_1)$. This study adopts a generic structural model developed by Miranda and Taghavi-Ardakan (2005) to readily predict peak floor accelerations ($PFA$), one of the controlling variables for the decision on elevator control, from peak ground acceleration ($PGA$), the chosen $IM$ in this study. The chosen model categorizes buildings by four parameters: fundamental period $T_1$, modal damping ratio $\zeta$, lateral stiffness ratio $\alpha_0$ and lateral stiffness reduction ratio $\delta$. The dimensionless parameter $\alpha_0$ describes the

participation of shear and flexural deformations in the model, which affects the lateral deflected shape of the building. The other dimensionless parameter $\delta$ describes the variation of lateral stiffness along the building height. Taghavi-Ardakan (2006) concluded that lateral stiffness reduction has negligible effect on the prediction of floor responses over a practical range of stiffness reduction, so $\delta = 1$, i.e., uniform stiffness along the height is adopted in this study. A typical value of modal damping ratio $\zeta = 5\%$ is selected. This study considers three values of $\alpha_0$ suggested by Miranda and Reyes (Miranda and Reyes, 2002): $\alpha_0 = 12.5$ is used for moment resisting frame buildings, $\alpha_0 = 3.125$ is used for dual system (e.g., resisting frame and shear wall) buildings, and $\alpha_0 = 1$ is used for shear wall buildings. The fundamental period $T_1$ is predetermined for each building. Figure 5.1 and 5.2 show the mean $\mu_{ST}$ and standard deviation $\sigma_{ST}$ of $\ln(PFA/PGA)$, along the building height. For a set of selected values of the four building parameters in the model, which determines the values of $\mu_{ST}$ and $\sigma_{ST}$, the probability of $PFA$ given $PGA$ is expressed as:

$$p(PFA|PGA) = \phi\left(\frac{\ln\left(\frac{PFA}{PGA}\right) - \mu_{ST}}{\sigma_{ST}}\right) = \phi\left(\frac{\ln PFA - \ln PGA - \mu_{ST}}{\sigma_{ST}}\right) \tag{5.4}$$

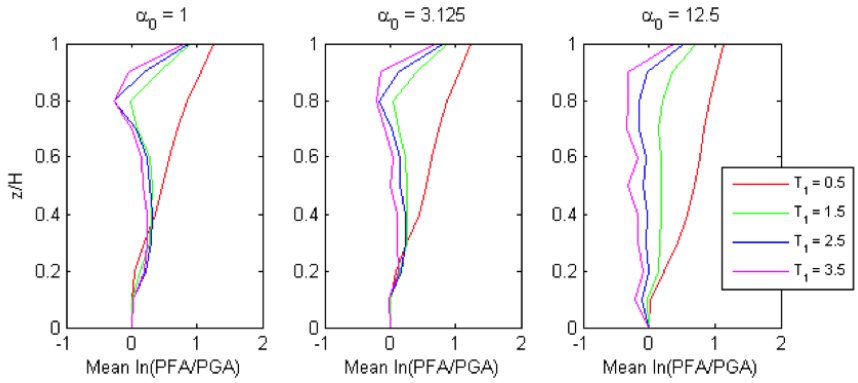


Figure 5.1: Mean of floor acceleration demand (based on Taghavi-Ardakan (2006)). $z$ is the height of the level considered; $H$ is the total height of a building; and $\alpha_0$ is the lateral stiffness ratio.

This continuum model combines a flexural cantilever beam and a shear cantilever beam that inherits some limitations, such as linear elastic behavior and classical damping. Also, tall buildings are more sensitive to long-period acceleration, while short buildings are more sensitive to high-frequency acceleration. Therefore, the estimation of $PFA$ based on $PGA$ by this model may not be the best choice, because $PGA$ is controlled by high-frequency components of the ground motion. This model is selected because a probability distribution for $PFA$ given $PGA$ is available (Taghavi-

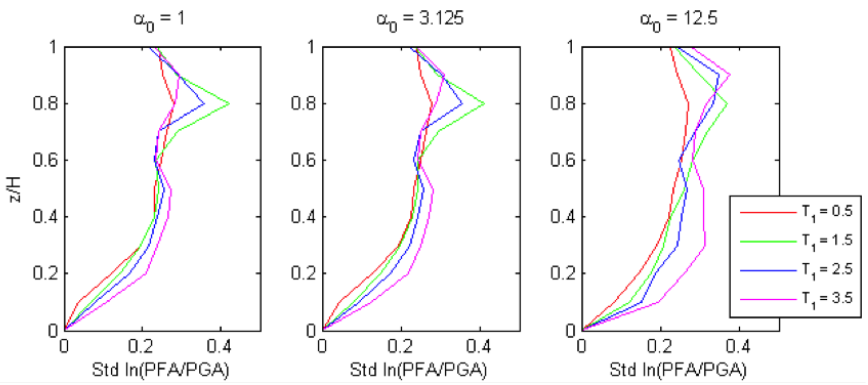


Figure 5.2: Standard deviation of floor acceleration demand (based on Taghavi-Ardakan (2006)). $z$ is the height of the level considered; $H$ is the total height of a building; and $\alpha_0$ is lateral stiffness ratio.

Ardakan, 2006) and the log-normally distributed $PFA$ results in closed form solutions that provide insights into how the uncertainty of different model parameters influences the decision behavior.

### 5.2.3 Incomplete action model

When lead time is too short to complete the action, an incomplete action model is considered by adding a discounting factor to both $L_B$ and $L_C$. These factors, as a function of warning lead time $T_{lead}$, model potential change of benefit and cost of the action due to lack of time. Let $\Omega_a = \{a_0, a_1\}$ be the new set of actions, where $a_0 =$ no action at current time step and $a_1 =$ take action at current time step. From ePAD:

$$\text{Take optimal action } \hat{a} = argmax_{i\in[0,1]} E[DF|D(t), a_i] \tag{5.5}$$

$$\text{where } E[DF|D(t), a_i] = \iint DF(IM, T_{lead}, a_i) p(IM|D(t)) p(T_{lead}|D(t))\, \mathrm{d}IM \mathrm{d}T_{lead} \tag{5.6}$$

$$\text{and } DF(IM, T_{lead}, a_i) = \beta_i(T_{lead}) E[L_B|IM, A_i] - \gamma_i(T_{lead}) E[L_C|IM, A_i] \tag{5.7}$$

Similar to the basic model case, $DF(IM, T_{lead}, a_0) = 0$. $E[L_B|IM, A_1]$ and $E[L_C|IM, A_1]$ are the same as in the basic model, and the discounting factors $\beta$ and $\gamma$ as a function of $T_{lead}$ are chosen as follows:

Let $T_a$ be the amount of time required to finish the action. When $T_{lead} < T_a$, the elevator cannot appropriately stop at the closest floor and open the door for people to evacuate. Thus, $\beta_1$ is assumed to be a step function with value of 0 when $T_{lead} < T_a$, and with value of 1 otherwise. This represents an all-or-nothing benefit model. For the time delay and service interruption cost,

$\gamma_1$ is assumed to be a simple linear function with value between $r_0$ and 1 when $T_{lead} < T_a$, where $r_0$ represents the ratio of fixed cost (independent of $T_{lead}$) over the total cost. In this study, part of the service interruption cost $r_{C2}l_{C2}$ is taken as a fixed cost (e.g., mandatory inspection after emergency stop), thus, $r_0 = r_{C2}l_{C2}/(r_{C1}l_{C1} + r_{C2}l_{C2})$. Figure 5.3 shows the value of $\beta_1$ and $\gamma_1$ as a function of $T_{lead}$. ($\beta_0$ and $\gamma_0$ are not needed because $DF(IM, T_{lead}, a_0) = 0$)

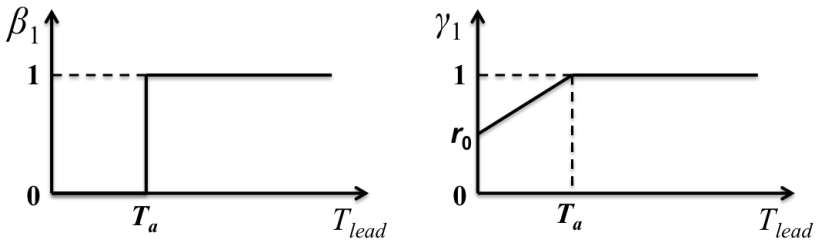


Figure 5.3: $\beta_1$ and $\gamma_1$ as a function of $T_{lead}$.

### 5.2.4 Value of information model

If an EEW system continually provides early warning information, one may want to delay a decision of initiating a mitigation action when the expected warning lead time is sufficiently long and the current EEW information is very uncertain. This is a trade-off between the potential benefit of having less uncertain EEW information and the potential cost of not being able to complete the action. ePAD models this extra cost-benefit factor using a value of information ($VoI$) model (Howard, 1966), which estimates the expected marginal benefit of delaying the decision, or in other words, not to take any action now (action $a_0$). Hence, $E[DF|D(t), A_0] = VoI$ instead of 0. From ePAD (Wu et al., 2013):

$$VoI = \iint_{\Delta t}^{\infty} \max\{DF(IM, T_{lead} - \Delta t, a_1), 0\} p(IM|D(t)) p(T_{lead}|D(t)) \, \mathrm{d}IM \mathrm{d}T_{lead} \tag{5.8}$$

Here, $\Delta t$ is the expected time interval for the next EEW update. With the max-function involved, $VoI$ often does not have a closed form solution and so a numerical approximation must be made. This approximation can be pre-learned by a surrogate model so that it can be rapidly computed as the EEW information arrives. In this study, the relevance vector machine (RVM) from machine learning (Tipping, 2001) is chosen to construct a surrogate model for $VoI$ because of its ability to create a sparse model using a Bayesian approach. Results are shown in Section 5.3.3.

## 5.3 Analyses and Discussion

### 5.3.1 Closed form solution for basic model

In the basic model, the only incoming EEW information is $p(IM|D(t))$, which is typically modeled as a Gaussian distribution with $\mu_{IM}$ and $\sigma_{IM}$ as the mean and standard deviation of $IM$ for $IM = \ln PGA$. This study investigates the influence of each model parameter on decision behavior using the decision contour method introduced in ePAD: a map of action and no-action regions partitioning the 2-D parameter space of $\mu_{IM}$ and $\sigma_{IM}$. The resulting critical contour that separates the two regions, called the *decision contour*, is used to interpret different decision behaviors.

According to the State of California (Cal/OSHA) regulation standards, an earthquake sensing device must be installed in every elevator to trigger an emergency shut down if the detected acceleration is more than 0.5g (Cal/OSHA, 2012). In contrast, Japanese elevator regulation requires elevators to stop operation at a much lower threshold, 0.08g to 0.15g of acceleration depending on building properties and elevator location (Kubo et al., 2011). Let the natural log of the threshold on $PFA$ be $lnpfa_0$; examples in this study use the Cal/OSHA standard, $lnpfa_0 = \ln(0.5)$. Given the chosen structural model (a Gaussian model on $\ln(PFA/PGA)$ depending on structural properties (Equation 5.4)), the fragility functions $P(DM|IM, A_1)$ and $P(DM|D(t), A_1)$ are described as follow:

$$\text{Let } p(IM|D(t)) = \phi\left(\frac{\ln PGA - \mu_{IM}}{\sigma_{IM}}\right) \tag{5.9}$$

$$\begin{aligned}\text{and } P(DM|IM, A_1) &= P(\ln PFA > lnpfa_0 | \ln PGA) \\ &= \Phi\left(\frac{\ln PGA + \mu_{ST} - lnpfa_0}{\sigma_{ST}}\right)\end{aligned} \tag{5.10}$$

$$\begin{aligned}\text{then } P(DM|D(t), A_1) &= \int P(DM|IM, A_1) p(IM|D(t))\, \mathrm{d}IM \\ &= \Phi\left(\frac{\mu_{ST} + \mu_{IM} - lnpfa_0}{\sqrt{\sigma_{ST}^2 + \sigma_{IM}^2}}\right)\end{aligned} \tag{5.11}$$

Here, $\phi(x)$ and $\Phi(x)$ are the standard Gaussian probability density function (PDF) and cumulative density function (CDF), respectively.

Note that Equation 5.1 can be simplified when a single action is considered:

$$\begin{aligned}
&\text{Take action if and only if} \\
&E[DF|D(t), A_1] > 0 \\
&\Leftrightarrow \Phi\left(\frac{\mu_{ST} + \mu_{IM} - lnpfa_0}{\sqrt{\sigma_{ST}^2 + \sigma_{IM}^2}}\right) > \frac{r_{C1}l_{C1} + r_{C2}l_{C2}}{r_B l_B} \triangleq P_0
\end{aligned} \tag{5.12}$$

The decision contour can then be found in closed form by solving Equation 5.12 for $\mu_{IM}$ as a function of $\sigma_{IM}$ in the case of equality:

$$\mu_{IM} = (lnpfa_0 - \mu_{ST}) + \sqrt{2\left(\sigma_{ST}^2 + \sigma_{IM}^2\right)}erf^{-1}(2P_0 - 1) \tag{5.13}$$

Here, $erf^{-1}$ is the inverse error function. Note that $P_0$ is always between 0 and 1, with $P_0$ approaching 0 when benefit dominates cost, and action is always taken. If $P_0$ is greater than or equal to 1, the action is never taken because the benefit cannot cover the cost. This result illustrates the possibility of choosing the type of decision behavior that a user desires based on $P_0$, instead of going through a complete cost-benefit analysis that leads to a fixed decision behavior.

Figure 5.4 shows the influence of $P_0$ on the decision contour (a method to understand how uncertainty influences decision). When $P_0 < 0.5$, the critical mean value of $\ln PGA$ that separates action and no action region decreases as uncertainty (the standard deviation) increases. The elevator will be stopped with a smaller shaking level as the EEW information becomes more uncertain, and it represents a conservative decision behavior, which is also called uncertainty-averse in the ePAD framework (Section 4.4.2). On the contrary, $P_0 > 0.5$ represents a risk taking decision behavior, because the elevator will not be stopped until a higher shaking level is reached as uncertainty increases, which is also called uncertainty-taking in ePAD. In this sense, $P_0 = 0.5$ represents an uncertainty-neutral decision behavior.

Figure 5.5 shows the influence of structural model uncertainty $\sigma_{ST}$ on the decision contour (or the decision behavior). From Equation 5.13, the decision contour approaches a linear function when $\sigma_{ST}$ approaches 0, and the contour approaches a horizontal line when $\sigma_{ST}$ dominates $\sigma_{IM}$. It demonstrates that the decision is less sensitive to the $IM$ uncertainty when $\sigma_{ST}$ dominates.

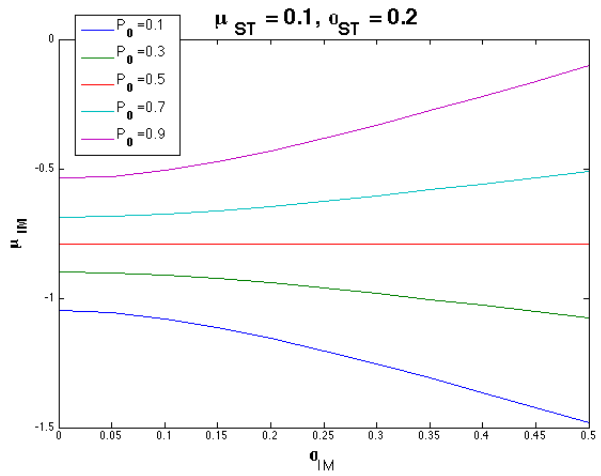


Figure 5.4: Decision contours with fixed $\mu_{ST}$ and $\sigma_{ST}$ values but varying $P_0$ values. Region above the contour represent taking action, and below represent no action.

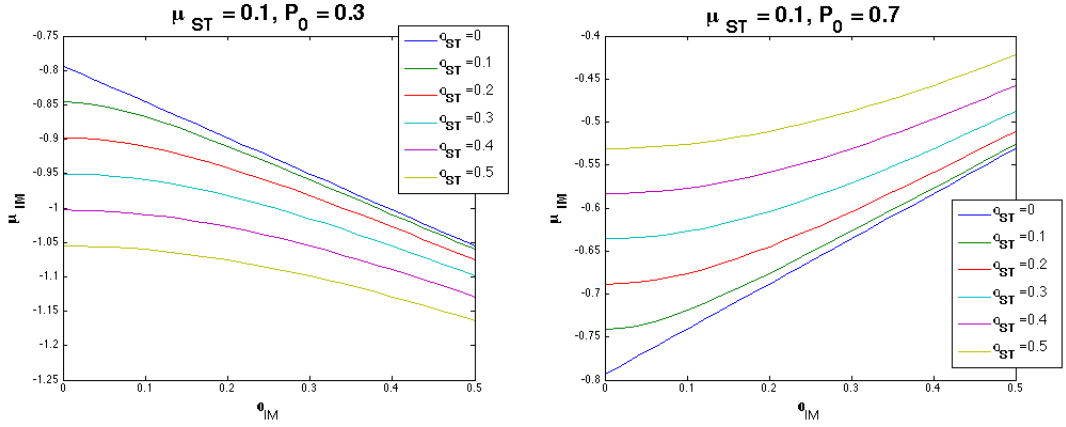


Figure 5.5: Decision contours with fixed $P_0$, $\mu_{ST}$ values and varying $\sigma_{ST}$ values. Region above the contour represents taking action, and below represents no action.

### 5.3.2 Closed form solution for incomplete action model

In the incomplete action model, the influence of insufficient lead time on decision-making is investigated. This model utilizes the lead time information, $p(T_{lead}|D(t))$, from EEW as well. Similar to Section 5.3.1, Equation 5.1 is simplified to:

$$\text{Take action if and only if } E[DF|D(t), a_1] > 0 \tag{5.14}$$

Exploiting the separation of $T_{lead}$ and $IM$ in $DF$ for the incomplete action model (Equation 5.6 and 5.7):

$$E[DF|D(t), a_1] = E[\beta_1|D(t)]E[L_B|D(t), A_1] - E[\gamma_1|D(t)]E[L_C|D(t), A_1] \tag{5.15}$$

The expected values of $\beta_1$ and $\gamma_1$ are found by integrating $\beta_1$ and $\gamma_1$ with $p(T_{lead}|D(t))$, which is taken as log-normally distributed. ($\beta_1(T_{lead})$ and $\gamma_1(T_{lead})$ are shown in Figure 5.3)

$$\text{Let } p(T_{lead}|D(t)) = \frac{1}{T_{lead}}\phi\left(\frac{\ln T_{lead} - \ln\mu_T}{\sigma_T}\right) \tag{5.16}$$

$$\text{then } E[\beta_1|D(t)] = \Phi\left(\frac{\ln\mu_T - \ln T_a}{\sigma_T}\right) \triangleq f_\beta \tag{5.17}$$

$$\begin{aligned}\text{and } E[\gamma_1|D(t)] &= \left\{\frac{1-r_0}{T_a}e^{\ln\mu_T + \frac{\sigma_T^2}{2}}\Phi\left(\frac{\ln T_a - \ln\mu_T}{\sigma_T} - \sigma_T\right) + r_0\right\} + (1-r_0)\Phi\left(\frac{\ln\mu_T - \ln T_a}{\sigma_T}\right) \\ &\triangleq f_\gamma + (1-r_0)f_\beta \end{aligned} \tag{5.18}$$

Following a similar approach to that used in Section 5.3.1 with $P_0$ defined as in Equation 5.12, Equation 5.14 can be rearranged to be:

$$\begin{aligned} &E[DF|D(t), a_1] > 0 \\ &\Leftrightarrow \Phi\left(\frac{\mu_{ST} + \mu_{IM} - lnpfa_0}{\sqrt{\sigma_{ST}^2 + \sigma_{IM}^2}}\right) > \left(\frac{f_\gamma}{f_\beta} + 1 - r_0\right)P_0 \triangleq r_T P_0 \end{aligned} \tag{5.19}$$

As before, the decision contour can then be found in closed form by solving Equation 5.19 in the case of equality for $\mu_{IM}$ as a function of $\sigma_{IM}$:

$$\mu_{IM} = (lnpfa_0 - \mu_{ST}) + \sqrt{2\left(\sigma_{ST}^2 + \sigma_{IM}^2\right)}erf^{-1}(2r_T P_0 - 1) \tag{5.20}$$

If one rearranges the expression for $r_T$ in Equation 5.19, it can be found that $r_T \geq 1$, which means that the incomplete action model in this case introduces an amplification factor $r_T$ for $P_0$ from the basic model. In other words, it always gives a more uncertainty-taking decision. This is because an incomplete action is less beneficial than taking the complete action, which leads to a higher critical $\mu_{IM}$ value compared to the basic model. When $r_T P_0 \geq 1$, the action is never taken. In practice, when the basic model suggests taking action, but the incomplete action model

suggests the opposite, then a backup action is triggered instead. Such back up action should be fast to complete, but will usually come with less benefit. In this case, the backup action could be an immediate stop of the elevator at the current location.

Figure 5.6 shows the value of $r_T$ as a function of $\mu_T$ and $\sigma_T$. Assuming $T_a = 2s$ and $r_0 = 0.5$ in Figure 5.3, $r_T$ increases exponentially as $\mu_T$ approaches and exceeds $T_a$, and its rate of increase reduces as the uncertainty in the lead time $\sigma_T$ increases. On the other hand, the incomplete action model has no influence on the decision when there is sufficient lead time, where $r_T \approx 1$.

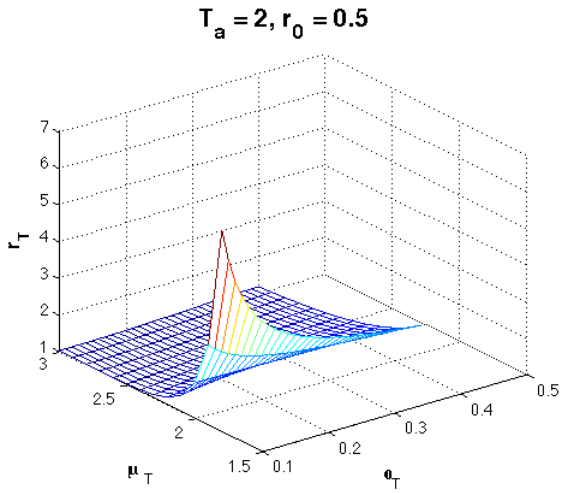


Figure 5.6: Value of $r_T$ as a function of $\mu_T$ and $\sigma_T$ given a fixed $T_a$ and $r_0$.

Figure 5.7 shows the decision contours for $lnpfa_0 = \ln(0.5)$, $\alpha_0 = 3.125$, $T_1 = 2.5s$, and $P_0 = 0.3$, which represents a typical dual system high-rise building with around 20 to 30 floors, and a slightly conservative decision behavior under the US elevator standard. In this case, $\mu_{ST} = 0.82$ and $\sigma_{ST} = 0.22$. The parameter values for lead time models are $T_a = 2s$, $r_0 = 0.5$, $\sigma_T = 0.2$ and $\mu_T$ ranges from 1s to 4s. Note that, when $\mu_T$ is less than 2s, no decision contours are shown in the figure. This is because the action is never taken due to the lack of benefit of an incomplete action, which the backup action is taken instead when necessary. One can observe that as $\mu_T$ decreases, the decision contour deviates from the one without lead time model (same as $\mu_T \approx$ 3s to 4s) and becomes more uncertainty-taking. Consistent with common intuition, this is due to the reduced expected benefit of an incomplete action.

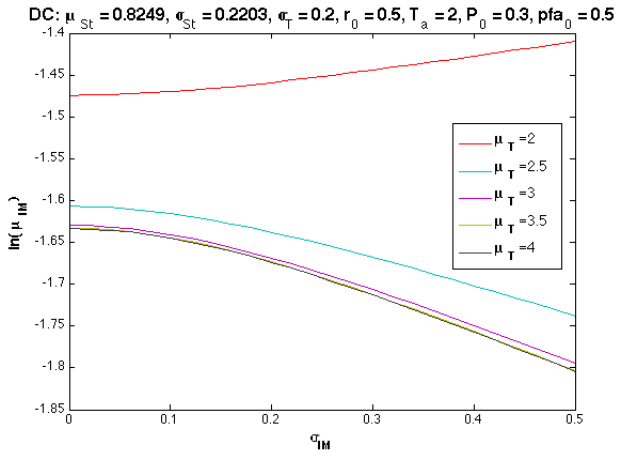


Figure 5.7: Decision contours with incomplete action model.

### 5.3.3 Numerical solution for VoI model using surrogate model

In the value of information model, the influence of adding extra benefit for action $a_0$ on decision-making is investigated. Before directly applying a surrogate model to $VoI$, I first simplify the expression given for the chosen $\beta_1$ and $\gamma_1$ models in Section 5.2.3.

Since $DF(IM, T_{lead} - \Delta t, a_1) < 0$ when $T_{lead} < T_a + \Delta t$, $\max\{DF(IM, T_{lead} - \Delta t, a_1), 0\} = 0$ in this range. Hence, the $T_{lead}$ lower bound of the integral of $VoI$ can be changed to $T_a + \Delta t$ instead of $\Delta t$. Also, in this range, both $\beta_1$ and $\gamma_1$ equal one, which leads to a separation of the double integral on $T_{lead}$ and $IM$ into two single integrals:

$$VoI = \int_{T_a+\Delta t}^{\infty} p(T_{lead}|D(t))\,\mathrm{d}T_{lead} \int \max\{DF(IM, A_1), 0\} p(IM|D(t))\,\mathrm{d}IM \tag{5.21}$$

The first integral in Equation 5.21 is simply the log-normal CDF, which can be rewritten as $\Phi((\ln(\mu_T)\ln(T_a + \Delta t))/\sigma_T)$; $DF(IM, A_1) = r_B l_B P(DM|IM, A_1)(r_{C1} l_{C1} + r_{C2} l_{C2})$. Let us now rearrange Equation 5.1 to be:

Take action if and only if

$$E[DF|D(t), a_1] = E[L_B|D(t), a_1] - E[L_C|D(t), a_1] > VoI \tag{5.22}$$

Dividing the inequality by $r_B l_B$ leads to the following simplified expression:

$$\text{Take action if and only if } \Phi\left(\frac{\mu_{ST}+\mu_{IM}-lnpfa_0}{\sqrt{\sigma_{ST}^2+\sigma_{IM}^2}}\right) > r_T P_0 + r_{VoI} I_{VoI} \tag{5.23}$$

$$\text{where } r_{VoI}(\mu_T,\sigma_T) = \Phi\left(\frac{\ln\mu_T - \ln(T_a+\Delta t)}{\sigma_T}\right)/\Phi\left(\frac{\ln\mu_T - \ln T_a}{\sigma_T}\right) \tag{5.24}$$

$$\text{and } I_{VoI}(\mu_T,\sigma_T) = \int \max\{0, P(DM|IM,A_1) - P_0\}\phi\left(\frac{IM-\mu_{IM}}{\sigma_{IM}}\right) \mathrm{d}IM \tag{5.25}$$

Note that $r_{VoI} I_{VoI} \geq 0$, which means that the value of information model in this case increases the value of $r_T P_0$ from the incomplete action model. In other words, it always gives an even more uncertainty-taking decision. This is because the extra benefit from delaying the decision represented by $VoI$ leads to an even higher critical $\mu_{IM}$ value compared to the incomplete action model with no waiting for more EEW information. Different from this incomplete action model, $VoI$ is not only a function of $\mu_T$ and $\sigma_T$, but is also a function of $\mu_{IM}$ and $\sigma_{IM}$. This is reasonable because, for example, one is more likely to delay a decision when the EEW information is very uncertain. Whereas $r_{VoI}$ can be calculated in closed form from Equation 5.24, an RVM surrogate model is used to calculate $I_{VoI}$.

Figure 5.8 shows an RVM surrogate model for $lnpfa_0 = \ln(0.5)$, $\alpha_0 = 3.125$, $T_1 = 2.5s$, and $P_0 = 0.3$, which are the same values as in Figure 5.7. The data points for generating the surrogate model are obtained from Monte Carlo Simulation (MCS) of the actual integral $I_{VoI}$. In this study, I generated a total of nine surrogate models (three building types: $\alpha_0 = 1, 3.125, 12.5$, and three elevator standards: $lnpfa0 = \ln(0.08), \ln(0.15), \ln(0.5)$) as a function of $P_0, T_1, \mu_{IM}$ and $\sigma_{IM}$. The maximum approximation error among all models is controlled to be under 5%.

Figure 5.9 shows the resulting decision contours of a specific case where $I_{VoI}$ in Equation 5.23 is obtained from the RVM surrogate model and also directly from MCS based on the same parameter values as in Figure 5.7 with $\Delta t = 1s$. The surrogate model estimates the actual decision contours well. Also, one can see that as $\mu_T$ increases, the decision contour becomes more uncertainty-taking because of the expected benefit of the potentially less uncertain information in the future. However, comparing to Figure 5.7, the larger $\sigma_{IM}$ is, the larger the difference in the decision contours. This is consistent with the intuition that one will only want to delay the decision if the current information is uncertain. Note that again, when $\mu_T$ is less than 2s, no decision contours are shown in the figure.

This is because the action is never taken due to the lack of benefit from an incomplete action. As mentioned in Section 5.3.2, the backup action is triggered when necessary.

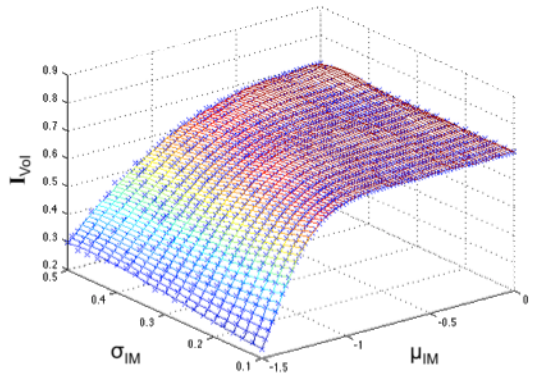


Figure 5.8: RVM surrogate model for $I_{VoI}$ as a function of $\mu_{IM}$ and $\sigma_{IM}$ ($T_1 = 2.5$, $P_0 = 0.3$ fixed).

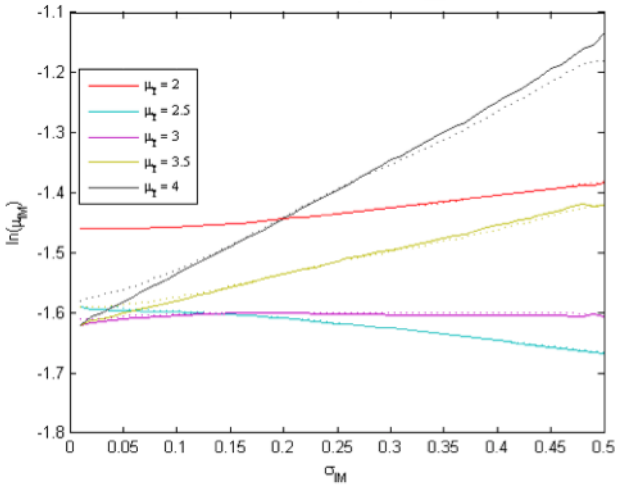


Figure 5.9: Decision contours with value-of-information model (Solid line: MCS, dotted line: RVM).

### 5.3.4 Example

A segment of the San Andreas Fault (from Palmdale to San Bernardino) is selected to demonstrate this proposed application to elevator control. A building with parameters $T_1 = 2.5s$ and $\alpha_0 = 3.125$ is chosen (same values as previously used in the analyses), that is located in downtown Los Angeles. The solid black line in Figure 5.10 shows the causative fault segment and the star indicates the building location.

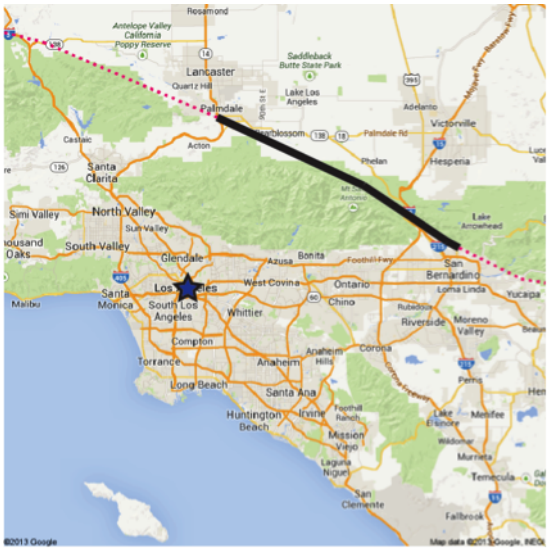


Figure 5.10: Location of a segment of San Andreas Fault (solid black line) and a chosen building in LA downtown (star).

Instead of parameterizing the PDF of $IM$ from EEW, $p(IM|D(t))$, into $\mu_{IM}$ and $\sigma_{IM}$, the PDF is found as a function of earthquake magnitude and hypocenter-to-site distance using the Ground Motion Prediction Equation developed by Boore and Atkinson (2008). Hence, instead of plotting the decision contours in a 2-D space of $\mu_{IM}$ and $\sigma_{IM}$, the contours are plotted in a 2-D space of earthquake magnitude and location along the chosen segment of the San Andreas Fault. Once again, the region above the decision contour represents taking action; the region below the decision contour represents taking no action. Change of decision contours is investigated based on two factors: (1) varying $\mu_T$ for a fixed $lnpfa_0$, (2) varying $lnpfa_0$ for a fixed $\mu_T$.

Figure 5.11 shows the result of this simulation. As one would expect, the location on the fault line that is the closest to the building has the lowest critical magnitude to trigger the action, and a decrease in $lnpfa_0$ lowers the whole decision contour in this plot. Note that no decision contour is shown in the plot for $lnpfa_0 = \ln(0.5)$ (the US standard) because the action is never taken within the tested range of magnitude on the chosen fault segment. This is not an intuitive result and the current standard may need to be changed if a robust decision framework is to be put in place. Also, $\mu_T = 2.5s$ leads to the lowest set of values of the critical magnitude along the fault segment because after including the lead time uncertainty, this is the mean lead time that has the least influence from both incomplete action model and the value of information model (there is just enough time to perform the action and both models penalize the benefit of taking action in some way).

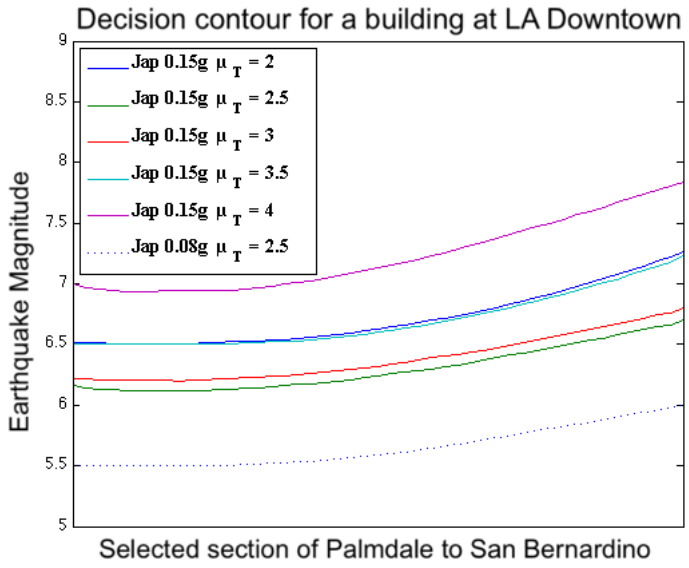


Figure 5.11: Decision contour of a dual system building ($T_1 = 2.5s$) at LA downtown for earthquake magnitude between M5 to M8 on a segment of San Andreas Fault between Palmdale and San Bernardino.

## 5.4 Conclusion

This chapter presents a decision framework for elevator control based on uncertain EEW information using the ePAD framework with a suggested structural model, decision model and lead time model. The analysis shows that instead of going through the complication of a complete cost-benefit analysis, a user may select the value of a related variable $P_0$ that can represent the users desired type of decision behavior. Also, the influence of lead time and EEW uncertainties on decisions can be easily understood through the use of decision contours, which represent different types of decision behaviors. A surrogate model using the machine learning algorithm RVM is created for the sake of fast computation of the value of information model. The steps to setup the algorithm for automated decisions of elevator control using uncertain EEW information are summarized by:

1. *Model parameters setup*: Choose $T_1$ and $\alpha_0$ based on a target building; choose $\Delta t$ and $lnpfa_0$ based on the EEW system operation and the elevator standard for the region where the building is located; choose $T_a$ and $r_0$ based on a specific elevator application.

2. *Evaluate decision contour*: Pick a $P_0$ value and generate decision contours as a function of ($\mu_T$, $\sigma_T$) and ($\mu_{IM}$, $\sigma_{IM}$) or (earthquake magnitude, fault line segments).

3. *Check decision behavior*: Iteratively increase or decrease $P_0$ to find a value that can best represent the user's desired decision behavior under uncertain EEW information.

Further refinement of the models employed in ePAD for elevator control could be explored. As explained in Chapter 4, more flexibility in the types of decision behavior can be obtained by adjusting $\Delta t$. Although the chosen structural model can be readily applied to various types of buildings, in order to obtain a better representation of a target building, a more sophisticated structural model can be used to replace the simpler model used in this paper. If necessary, the decision model and lead time model ($\beta_1$ and $\gamma_1$) can also be changed, at the possible expense of introducing extra complexity into the problem.

# Chapter 6

# Potential Advanced EEW Applications and Their Challenges

## 6.1 Potential advanced application 1: Multiple-action decisions

The examples shown in Chapter 4 and 5 are only considering a local application at a single site. Some other possible applications of EEW may involve a large area, for instance, emergency response planning of a city and transportation network control. There can be a large set of possible mitigation actions composed of various combinations of local mitigation action decisions. These local decisions may affect each other in a global sense that change the overall value of the combined final decision. For example, stopping a train in a railway network will have a cascading effect to the trains operating around it. Hence, the optimal timing to stop a train based on the EEW information cannot be decided individually. This adds a new layer of complexity to the decision problem of EEW applications. I call this the multiple-action decisions problem of EEW application. In this section, I investigate the possibility of applying the ePAD framework to multiple-action decisions through a hypothetical case study on a large bridge network.

### 6.1.1 Traffic control of bridge network

Let us consider a highway network with many bridges. Each entrance to the highway is equipped with traffic lights to control traffic flows in the network. The EEW information can be used to predict endangered sections of the network due to earthquake shaking, where the bridges have a high probability of significant damage or collapse. Then, a central system can stop traffic from going into those sections by switching the appropriate traffic lights to red.

For simplicity, I only consider two actions for each bridge in the network: closed or open. Here, closing a bridge means to turn all entrance traffic lights around the bridge to red. If there is $N_B$ bridges in the network, using the ePAD framework, the set of all possible actions $\Omega = \{a_0, a_1, ..., a_N\}$, where $N = 2^{N_B}$. Under the cost-benefit model in ePAD (Equation 4.4), $L_B$ is the expected lives saved and $L_C$ is the expected traffic delay induced by the chosen mitigation action. In fact, $L_C$ is only counting the expected traffic delay due to closing of some bridges between when the EEW is received and when either the strong shaking arrives or there is confirmation of a false warning. Given the complexity of a typical traffic flow analysis on a highway network, it is very hard to obtain an accurate estimate of the change of traffic flow within this short time frame. Instead of the cost-benefit-based decision criterion, I use the criterion based on the probability of a damage state $DM_S$ exceeding a predetermined threshold $P_{DM}$ (Equation 4.31). The damage state probability $P(DM|D(t))$ is calculated from a fragility model of the bridge and a ground motion prediction equation (GMPE) using EEW information, following the PBEEW methodology (Section 4.2.2).

### 6.1.2 Case study for 1989 Loma Prieta earthquake

Using a highway network located in Northern California, I set up a comparison study based on data from the 1989 Loma Prieta earthquake (Mitchell et al., 1991; Hanks and Brady, 1991). The network includes all bridges within latitude 36.8N to 38.8N and longitude 124W to 121W. A total of 1253 bridges are included in the network and 57 were recorded as severely damaged. Assuming the EEW system predicts the magnitude and hypocenter location of the Loma Prieta earthquake perfectly, i.e., M6.9 at 37.040N 121.877W, I compare the bridge closing decisions made by the ePAD framework with the actual damage data. The Boore and Atkinson (2008) GMPE model is chosen and the fragility functions of the bridges are based on the HAZUS model from Caltrans (Turner et al., 2009). Fragility curves of four damage states are assigned to each bridge: Slight damage, moderate damage, extensive damage and complete damage. $DM$ = extensive damage is chosen in my study.

Note that the total number of possible actions for 1253 bridges is around $10^{377}$, so it is impossible to perform any optimization. To solve this problem, I assumed spatial independence of ground motions between each bridge, which allows me to make the decision of opening or closing a bridge

individually. This simplifies the multiple-action decisions problem back to many single action decision problems. If a reasonable result is obtained from this method, this simplification can be used to approximate the multiple-action decisions problem.

For a given threshold value $P_{DM}$ on $P(DM|D(t))$, I can find the number of true positive (closed and damaged), true negative (open and undamaged), false positive (closed and undamaged) and false negative (open and damaged) by comparing the decision results from ePAD and the actual data. Based on the Receiver Operating Characteristic (ROC) method (Fawcett, 2006), I find the true positive rate and false positive rate for each $P_{DM}$ value between 0 and 1. Figure 6.1 shows the resulting ROC curve, where the diagonal line represents the random guess decision policy. The closer to curve is to the left upper corner, the better performance of the decision policy is. The resulting ROC curve from ePAD in this case is only slightly better than a random guess decision policy. This indicates that the proposed approach for a multiple-action decisions problem is not effective (next section explains the reasons).

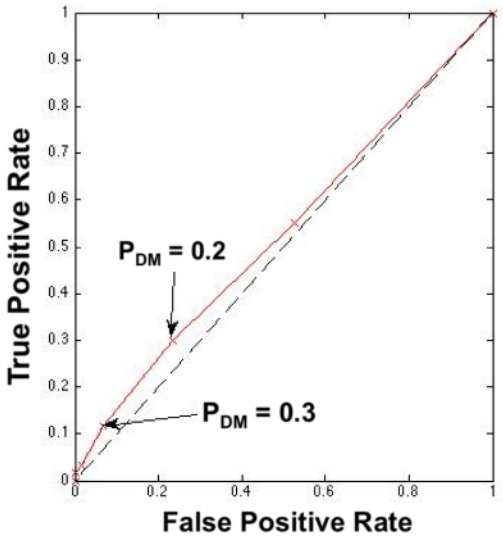


Figure 6.1: Receiver Operating Characteristic curve for bridge-closing decisions using the ePAD framework with the HAZUS fragility functions and Boore-Atkinson GMPE ($P_{DM}$ from 0 to 1).

### 6.1.3 Discussion

The major challenge of a multiple-action decisions problem is the combinatorial explosion. However, reducing the multiple-action decisions problem to many single action decision problems is often not

effective, as illustrated in my study above. One reason is that the proposed simplified approach suffers from the large uncertainty expressed the fragility functions and GMPE models. In fact, Porter et al. (2002) shows that the fragility model contributes to the second largest uncertainty (after ground motion uncertainty) in the PEER PBEE methodology. A possible solution is to use a cost-benefit model for decision criterion in order to improve the performance of decision-making under uncertainty in terms of practical concerns or user's preferences. Note that the presented ROC study does not take consequences into account, e.g., a false positive is often less important than a false negative in this case because drivers are likely to accept delay when they feel even a slight shaking. This can be reflected from a utility function in the cost-benefit analysis. There remains many challenges to estimate properties for a complex transportation network system, which are needed for a cost-benefit model. A recent study demonstrates a possible solution for estimating complex network reliability using Subset Simulation (Zuev et al., 2014).

Another reason for not able to effectively reduce the multiple-action decisions problem to many single action decision problems is that spatial correlation of the ground motions may play an important role in accurately predicting the local shaking intensity (Jayaram and Baker, 2009). Even though sometimes the ground motion is not strongly correlated, the cost-benefit model may involve a cascading effect from one site to the others (e.g., stopping a train, mentioned in Section 6.1).

Without a simplified approach, an efficient algorithm is needed to approximate the intractable optimization problem. This requires one to exploit the underlying structure of the problem, for example, the topology of a transportation network. Development of an efficient optimization algorithm for such decision problems remains as a challenging topic for future research.

## 6.2 Potential advanced application 2: Synergy with SHM

Theory and hardware development for structural health monitoring (SHM) has become one of the major subjects in structural engineering research in the past decade. Many of the existing SHM methodologies rely on detecting a change in a specific structural property, local loss of stiffness, to evaluate potential damage in the structure and its severity. These methods collect response data from a deployed sensor network, either periodically or before and after an event, and estimate stiffness change based on a linear structural model. A common approach is to use Bayesian updating,

or simply least-squares minimization, based on the difference between modal parameters calculated from a parameterized finite-element structural model and the corresponding modal frequency and mode shapes identified from a dynamic test (Vanik et al., 2000), usually performed with low-amplitude ambient vibrations. The investigation may be performed for damage assessment after a severe excitation, such as earthquake loading, or for long-term monitoring of deterioration due to fatigue and corrosion.

Acknowledging the development of earthquake early warning (EEW) systems in recent years, it would be valuable for a SHM system to be able to use EEW information to improve its robustness in damage detection and loss estimation. In a practical SHM network, the number of recorded response channels is usually much less than the degrees of freedom needed to accurately capture structural behavior. This condition of incomplete information motivates the use of a probabilistic approach in a SHM methodology. However, due to the level of complexity in this problem, such as modeling uncertainty, measurement noise, etc., a large resulting uncertainty is present. The synergy with EEW offers an opportunity to reduce uncertainty based on the extra information.

In this section, a framework for synergy between SHM and EEW is proposed for enhanced seismic protection of a target structure. The framework is divided into two parts: pre-event and post-event. For the pre-event case, the short lead time from EEW provides a quick damage prediction, which can be used by an automated decision system to decide whether to initiate an action to mitigate potential earthquake loss for the target structure (Chapter 4). Integrating with a SHM interface, the EEW information can also be exploited to assist the control of a structural sensor network immediately before an earthquake; for example, activate wireless sensors that are in "sleep" mode to reduce power consumption. Also, a graphical structural map of predicted structural damage or loss can be constructed for decision makers and continuously updated using the available information. For the post-event case, fast damage detection can be conducted using a probability-based SHM approach, which combines the sensor information with prior information provided by the EEW to obtain robust damage assessment. The EEW damage or loss structural map can be updated for post-event assessment. Because current applications of EEW is limited, there is a lack of actual SHM data suitable for an EEW synergy case study in practice. Instead, a method to evaluate the performance of such a synergistic system is presented.

### 6.2.1 Background on Bayesian SHM approach

The fundamental concept for model-based SHM is to update a structural model based on measured data to determine local loss of stiffness, which is taken to represent corresponding local structural damage in the actual structure. The simplest method is to minimize a measure of the difference between the identified modal parameters from response data and those calculated from a pre-determined structural model. This approach involves a modal identification procedure to estimate the current modal parameters. A generic objective function to be minimized is then a weighted sum of squares of the difference between the identified modal frequencies and mode shapes and those determined from a finite element model (Yuen et al., 2006a):

$$J = \sum_{i=1}^{m} \alpha_i (\omega_i - \hat{\omega}_i)^2 + \sum_{i=1}^{m} \beta_i \|\phi_i - \hat{\phi}_i\|^2 \tag{6.1}$$

where $m$ is the total number of modes included; $\alpha$ and $\beta$ are the chosen weighting factors; $\omega$ and $\phi$ are the natural frequencies and mode shapes from the structural model, respectively; and $\hat{\omega}$ and $\hat{\phi}$ are the natural frequencies and mode shapes identified from response data, respectively. A major challenge for this approach is so-called mode matching, which is to match the modes determined by the structural model with those determined from the response data. In practice, the limited amount of instrumentation that may not cover sufficient degrees of freedom to characterize the mode shapes, together with imperfect structural models, create a large uncertainty for mode matching. Furthermore, uncertainty about the predictive capability of any structural model, as well as the lack of sensitivity of the modal parameters to localized stiffness change, create additional challenges. Therefore, a single model is often not enough to provide reasonable results for SHM. Another difficulty is how to choose appropriate weights $\alpha$ and $\beta$ in Equation 6.1 since their values can have a significant effect on the optimal estimates of the model parameters.

In order to account for these large uncertainties, a Bayesian model updating approach provides a robust framework for SHM (Beck and Katafygiotis, 1998; Vanik et al., 2000). In this Bayesian framework, instead of a single plausible model, a set of models is considered with a derived posterior PDF over the set indicating their relative plausibility based on the data. Let $\theta$ be the vector of model parameters. First, the prior PDF of $\theta$ is established for a model class $M$, $p(\theta|M)$, based on engineering judgment and pre-damage structural analysis. Then, the prior PDF is updated to

the posterior PDF, $p(\theta|D, M)$, based on measured data $D$ and using Bayes' theorem (Equation 2.2). There are two major challenges in this Bayesian approach: 1) The evaluation of the likelihood function may be computationally intensive; 2) The evidence (a normalizing constant), which involves integrating the product of the likelihood and the prior with respect to $\theta$, may also be hard to evaluate. Many improvements in the Bayesian framework for SHM have been developed in the past decade: the idea of expanded mode shapes is developed to avoid mode matching (Beck et al., 2001; Ching and Beck, 2004); Gibbs MCMC sampling (Ching et al., 2006) of the posterior PDF was used to improve on the Laplace asymptotic method (Beck and Katafygiotis, 1998) employed in the original framework (Vanik et al., 2000); the eigenvalue equation was used in the prior to avoid any eigenvalue analysis of the structural model (Yuen et al., 2006a); a method directly using the dynamic time-domain data (Yuen et al., 2006b) was introduced to avoid the modal identification step; and data-based selection of the weighing factors $\alpha$ and $\beta$ was performed using Bayesian model class assessment (Goller et al., 2012).

### 6.2.2 Proposed synergistic framework

EEW provides valuable earthquake information in the early stage of an earthquake event. SHM provides structural response data for post-event damage detection and loss assessment. Both systems can be combined into a single framework to provide a continuous decision-support system. Figure 6.2 shows a timeline comparing the original SHM framework with the synergistic framework.

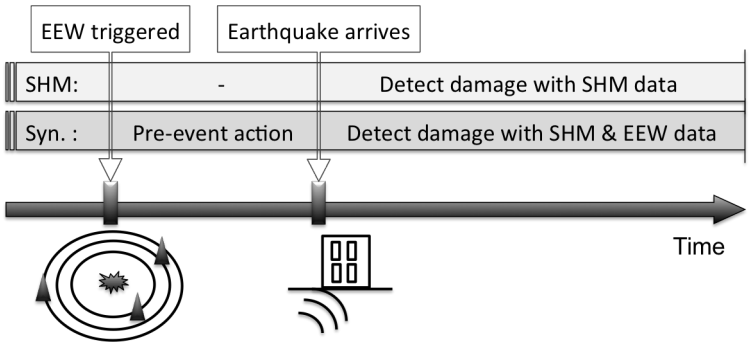


Figure 6.2: Timeline comparison between the SHM framework and the synergistic framework that combines information from EEW and SHM.

A decision support system for damage assessment that only relies on post-earthquake structural response data suffers from significant uncertainty. The synergistic framework aims to exploit the EEW information to potentially reduce the uncertainty of the SHM damage prediction, and to

allow loss mitigation with pre-event actions. This framework is composed of two stages. The first stage is the time between the EEW trigger and the earthquake arriving at a site. During this time, there are continual updates of the EEW prediction that will be fed into an automated decision system for taking pre-event actions in order to mitigate the potential earthquake loss (Chapter 4). The second stage starts after the earthquake arrives at the site of interest and structural response data becomes available from the SHM sensor network. By combining the information from EEW and SHM, more robust damage detection and assessment can be performed for a target structure.

Loss and safety assessments are performed before and after an earthquake with distinct purposes. Traditionally, pre-event assessments are used to evaluate the reliability of structures and to motivate retrofitting plans if needed. After the development of an EEW system, fast structural damage warning can be achieved by exploiting the short warning time available to the public. On the other hand, post-event assessments are used by decision makers or structure owners to evaluate aftershock risks and reduce further downtime loss. Near real-time loss assessment is feasible now due to improvements in seismic network and communication efficiency. An example of near real-time loss assessment is given in Porter et al. (2006) based on the PBEE methodology, which relies on real-time structural monitoring system and structural models. Mitrani-Reiser (2007) in her thesis proposed that these loss and safety assessments are integrated into a Virtual Inspector system based on the PBEE method.

Using the synergistic data from EEW and SHM, a complete decision-support system for rapid pre-event and post-event earthquake loss and safety assessment for civil structures based on a Virtual Inspector system is proposed to achieve the following (and summarized in Figure 6.3):

1. Before an earthquake occurs: for earthquake preparation, the seismic risk of a structure can be assessed based on seismic models developed using probabilistic seismic hazard analysis (PHSA). In some cases, an owner of a structure may be more concerned with some specific earthquake scenarios that may affect the structure. Then, multiple earthquake scenarios can be fed into the Virtual Inspector to provide pre-event safety assessments. Decisions for reducing the seismic risk of the structure, such as structural strengthening, can be made based on this information.

2. Before shaking arrives a site: the EEW information can be treated as a single earthquake scenario similar to case (1) above. It can then be fed into the Virtual Inspector to provide fast

structural damage warning, and to assist emergency response decisions, such as elevator control (Chapter 5). This may also allow the decision support for near real-time loss assessment mentioned in Porter et al. (2006) to be activated in an earlier stage.

3. After shaking arrives a site: information about the site intensity measure is often quickly known, either from an Internet-based shake map system or from a local sensor network. Updated earthquake and structural response data provided by a shake map or monitoring system can be fed into the Virtual Inspector immediately after an earthquake to provide rapid structural safety alerts; this information can subsequently be combined with near real-time loss assessment and used as decision support for structure owners and other stakeholders, as suggested in Porter et al. (2006).

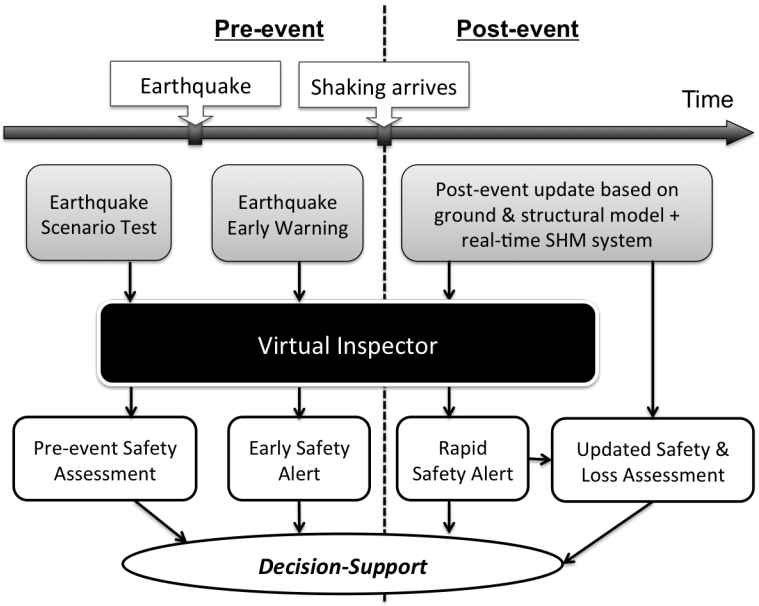


Figure 6.3: Outline of complete decision-support system based on a synergistic framework between EEW and SHM and centered around the Virtual Inspector.

### 6.2.3 Methodology for synergy of EEW and SHM data

The fundamental concept for synergy of EEW and SHM data is to take the EEW data as prior information to establish the prior PDF for the Bayesian SHM model. Since EEW provides extra information about the shaking expected at a site, and hence the expected damage of a structure compared to our original knowledge about it, the EEW-based prior can potentially reduce the

uncertainty in the SHM-based posterior PDF of damage in different substructures. A quantitative way of evaluating the benefits of the proposed synergy is introduced in the next section. A major challenge of this synergy method is the inconsistent metric for a local damage measure in existing EEW and SHM frameworks. One of the well-known earthquake loss assessment frameworks, known as the PEER PBEE methodology (Goulet et al., 2007; Porter, 2003), defines the damage state probability distributions for each damageable component using fragility curves, where the damage state variable, $DM$, is a set of discrete states. For example, $DM$ for a structural component would have possible values $\{DM_1, DM_2, , DM_n\}$ representing $n$ possible damage states of the component and the fragility function gives the probability that the component is in state $DM_i$ given the demand on the component (Goulet et al., 2007). On the other hand, as shown in Section 6.2.1, the Bayesian probabilistic approach for SHM usually defines a local damage measure in terms of continuous variables, $\theta$, which is typically a vector of fractional stiffness loss in all substructures in a building. Therefore, the synergy between EEW and SHM requires a probabilistic relationship for $DM_i$ in EEW in terms of $\theta$ in SHM or vice versa, in order to consistently evaluate potential damage or loss after an earthquake.

This motivates two ways of evaluating the posterior PDF of $DM$, $p(DM|D_S, D_E)$: 1) Updating from the prior PDF of $DM$, $p(DM|D_E)$ or 2) Updating from the prior PDF of $\theta$, $p(\theta|D_E)$, where the prior represents the damage state prediction, $DM$ or $\theta$, based on EEW data, $D_E$; while the posterior represents the damage state prediction updated with SHM data, $D_S$. In order to better illustrate the difference between the two proposed methods, we utilize the concept of Bayesian (Belief) Network (BN) to develop two models that represent the two methods, as shown in Figure 6.4.

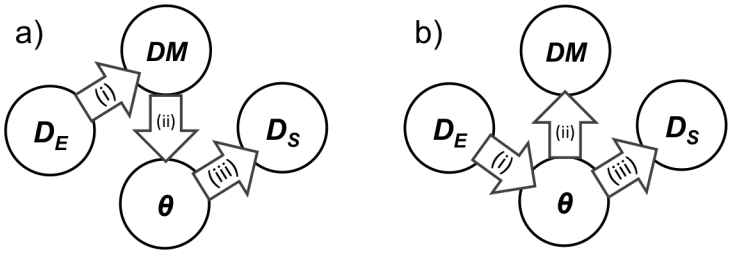


Figure 6.4: Bayesian network models. (a) In-series model; (b) $\theta$-centered model. (i) Prior PDF, $p(DM|D_E)$ or $p(\theta|D_E)$; (ii) Relationship between $DM$ and $\theta$, $p(DM|\theta)$ or $p(\theta|DM)$; (iii) Structural response model, $p(D_S|\theta)$.

#### 6.2.3.1 Method 1: In-series BN model (define $\theta$ in terms of $DM$)

By first using Bayes theorem, and then expanding the likelihood function, $p(D_S|DM, D_E)$, with the Total Probability Theorem, one can calculate the posterior by:

$$\begin{aligned} p(DM|D_S, D_E) &= \frac{p(D_S|DM, D_E)p(DM|D_E)}{p(D_S|D_E)} \\ \text{where } p(D_S|DM, D_E) &= \int p(D_S|\theta, DM, D_E)p(\theta|DM, D_E)\,\mathrm{d}\theta \end{aligned} \tag{6.2}$$

Since Equation 6.2 is still too complicated for practical use, for the In-series BN model, I simplify some of the PDFs. Under this model, as shown in Figure 6.4(a), $D_S$ is independent (in the information sense) of both $D_M$ and $D_E$ when $\theta$ is given, which means that $p(D_S|\theta, DM, D_E)$ equals $p(D_S|\theta)$. Also, $\theta$ is independent of $D_E$ when $DM$ is given, which means that $p(\theta|DM, D_E)$ equals $p(\theta|DM)$. Therefore, Equation 6.2 can be simplified to:

$$p(DM|D_S, D_E) = \frac{p(DM|D_E)\int p(D_S|\theta)p(\theta|DM)\,\mathrm{d}\theta}{p(D_S|D_E)} \tag{6.3}$$

$p(D_S|\theta)$ in Equation 6.3 corresponds to the likelihood function in Bayesian updating. The prior, $p(DM|D_E)$, is a known PDF calculated from the PBEEW framework based on EEW information and $p(D_S|D_E)$ is simply a normalizing constant for the posterior PDF. The only unknown PDF left is $p(\theta|DM)$. This could be developed by engineering judgment or by nonlinear deteriorating hysteretic structural analyses using a Gaussian model with a chosen mean and standard deviation that depend on DM. The advantage of this method is that there are no additional PDFs beyond those used in existing EEW and SHM frameworks except the required probabilistic relationship for $\theta$ in terms of $DM$. The disadvantage is that relating a set of continuous variables $\theta$ in terms of a set of discrete variables $DM$ may be relatively difficult, compared with the other way around.

#### 6.2.3.2 Method 2: $\theta$-centered BN model (define $DM$ in terms of $\theta$)

By first expanding the posterior of $DM$ with the Total Probability Theorem, and then applying Bayes theorem to the posterior of $\theta$, $p(\theta|D_S, D_E)$, one can calculate the posterior of $DM$ by:

$$\begin{aligned} p(DM|D_S, D_E) &= \int p(DM|\theta, D_S, D_E)p(\theta|D_S, D_E)\,\mathrm{d}\theta \\ \text{where } p(\theta|D_S, D_E) &= \frac{p(D_S|\theta, D_E)p(\theta|D_E)}{p(D_S|D_E)} \end{aligned} \tag{6.4}$$

Similar to Method 1, for the $\theta$-centered BN model, I simplify some of the PDFs in Equation 6.4. Under this model, as shown in Figure 6.4(b), $DM$ is independent of both $D_E$ and $D_S$ when $\theta$ is given, which means that $p(DM|\theta, D_S, D_E)$ equals $p(DM|\theta)$. Also, $D_S$ is independent of $D_E$ when $\theta$ is given, which means that $p(D_S|\theta, D_E)$ equals $p(D_S|\theta)$. Thus, Equation 6.4 can be simplified to:

$$p(DM|D_S, D_E) = \frac{\int p(DM|\theta)p(D_S|\theta)p(\theta|D_E)\,\mathrm{d}\theta}{p(D_S|D_E)} \tag{6.5}$$

Again, $p(D_S|\theta)$ is known from the SHM framework, $p(D_S|D_E)$ is a normalizing constant and $p(D_M|\theta)$ is a probabilistic relationship for $DM$ in terms of $\theta$ that must be established. The only other PDF to be established is the prior of $\theta$, $p(\theta|D_E)$, which can be calculated based on the first two steps of the four-step PBEE methodology:

$$p(\theta|D_E) = \int p(\theta|IM)p(IM|D_E)\,\mathrm{d}IM \tag{6.6}$$

In Equation 6.6, a surrogate model for the current substructure stiffness PDF $p(\theta|IM)$ can be established based on synthetic training data using a nonlinear deteriorating hysteretic structural model. Also, $p(IM|D_E)$ can be established from the EEW data and a ground motion prediction equation for shaking intensity measure $IM$. The advantage of Method 2 is that definition of a set of discrete variables in terms of a set of continuous variables is relatively straightforward. For example, one can define each damage state $DM_i$ as a range of $\theta$ (Vanik et al., 2000), which means $p(DM_i|\theta) = 1$ for $\theta$ in the corresponding fixed range. Furthermore, in this model, since $D_E$ is directly fed into the SHM system, the EEW-based decision-support system and the modified SHM system can be run in parallel and combined at the end stage. The disadvantage is that evaluation of $p(\theta|D_E)$ is not often included in common PBEE loss assessments. Therefore, extra structural

analyses are required before actual application.

Note that by comparing Equation 6.3 and 6.5, and using the probability product axiom:

$$p(DM, \theta|D_E) = p(DM|\theta)p(\theta|D_E) = p(\theta|DM)p(DM|D_E) \tag{6.7}$$

it can be shown mathematically that the two methods are equivalent, as long as the probability relations of $\theta$ and $DM$ in terms of each other are consistent. Therefore, one may choose either of the two methods depending on the situation.

### 6.2.4 Method to evaluate the benefits of the proposed synergy

A main benefit of the synergy framework based on Bayes theorem is to reduce the uncertainty of the posterior PDF by introducing extra information from EEW data. Thus, this imposes an important question of how large the benefit is, or in other words, how much extra information do we actually gain from EEW data $D_E$. This question can be answered quantitatively using information theory. A direct comparison can be done using relative entropy ($R.E.$) (Cover and Thomas, 2006), also known as Kullback-Leibler divergence, which is often used as a non-symmetric measure of the difference between two PDFs for the same variable, $X$, but it is also a measure of the information gain in bits about $X$ from information $I$:

$$R.E.(X|I) = \int p(X|I) \cdot \log_2 \frac{p(X|I)}{p(X)} \, \mathrm{d}X \tag{6.8}$$

It can be used as a measure of the information gain about $DM$ or $\theta$ from the EEW data $D_E$, by comparing the posterior with and without $D_E$. In Method 1, $D_E$ is used to predict $DM$. Hence, $R.E.(DM|D_E)$ is calculated by setting $p(X|I)$ equal to $p(DM|D_S, D_E)$ and $p(X)$ equal to $p(DM|D_S)$ and then after some manipulation based on the Bayes' theorem:

$$R.E.(DM|D_E) = \int p(DM|D_S, D_E) \cdot \log_2 \frac{p(DM|D_E)}{p(DM)} \, \mathrm{d}DM + \log_2 \frac{p(D_S)}{p(D_S|D_E)} \tag{6.9}$$

It is interesting to note that by adding a constant term that only depends on the data, $R.E.(DM|D_E)$ is influenced by the information difference between using the EEW prior and the original prior, which is exactly what needs to be measured.

In Method 2, since $D_E$ is used to predict $\theta$, $R.E.(\theta|D_E)$ is evaluated, instead of $R.E.(DM|D_E)$. Again, the expression can be manipulated to give:

$$R.E.(\theta|D_E) = \int p(\theta|D_S, D_E) \cdot \log_2 \frac{p(\theta|D_E)}{p(\theta)} \, \mathrm{d}\theta + \log_2 \frac{p(D_S)}{p(D_S|D_E)} \tag{6.10}$$

Note that in Equation 6.9, I assume $p(D_S|DM, D_E) = p(D_S|DM)$ and in Equation 6.9, I assume $p(D_S|\theta, D_E) = p(D_S|\theta)$ as implied by the BN models (a) and (b), respectively, in Figure 6.4.

### 6.2.5 Discussion

Ideally, the synergistic framework that utilizes information from both EEW and SHM systems provides more reliable loss estimation and safety alerts. EEW information can be used independently to provide pre-event loss estimation and decision support based on the PBEEW method and ePAD framework. The original probabilistic SHM system provides damage assessment, but usually suffers from high uncertainty in the final prediction. The EEW data used as a prior information can potentially reduce the prediction uncertainty in the SHM system. Also, the posterior information from the SHM system can be used as feedback information to update the EEW loss estimation and provide more reliable safety alerts after the earthquake is over. The decision-support system using the synergistic data from EEW and SHM is built based on the Virtual Inspector method. An evaluation method based on the theory of relative entropy can be used to assess the potential benefit of using the synergistic system versus the original systems.

Despite the completeness of the proposed synergistic framework, there still remain some major challenges in practice. A major challenge of this synergy method is the inconsistent metric for a local damage measure in existing EEW and SHM frameworks. I proposed two models to provide the missing link, but each has its own difficulty. In Method 1, relating a set of continuous variables $\theta$ in terms of a set of discrete variables $DM$ may be relatively difficult. On the other hand, in Method 2, evaluation of $p(\theta|D_E)$ is not often included in common PBEE loss assessments. Therefore, extra structural analyses are required before actual application. Furthermore, the value of EEW information as a prior for the Bayesian SHM analysis needs to be verified by quantitative results from a real case study. This is difficult because applications of EEW are still in an early development stage.

# Chapter 7

# Concluding Remarks

Large earthquakes that have happened in the past decade, such as the 2008 M7.9 Sichuan earthquake in China, the 2010 M8.8 Chile earthquake and the 2011 M9.0 Tohoku earthquake in Japan, have raised the world's attention to the importance of an earthquake early warning (EEW) system. Despite the rapid development of EEW research, there remains some challenges that limit its application in practice. Current EEW systems mainly rely on a point-sources model, which fails to provide accurate warning time and magnitude estimate for large earthquakes with a finite rupture length. Also, current systems often assume that only one event can happen in a short period of time, which causes false alarms due to the increased seismicity after a large earthquake. A perfect example is the significant increase of false alarms observed by the Japan Meteorological Agent (JMA) EEW system after the 2011 M9 Tohoku earthquake in Japan. EEW prediction is inherently embedded with large uncertainty because it uses incomplete waveform data to estimate earthquake parameters (e.g., hypocenter location, magnitude, origin time and local shaking intensity). The two mentioned model insufficiencies further increase the uncertainty of EEW. This becomes an obstacle to use EEW information for decision about the activation of any mitigation actions. Furthermore, the warning lead time of EEW is very short, usually around a few seconds to a minute or so. Human intervention in the decision process for activating a mitigation action will use up too much of the warning time, which becomes impractical for any EEW applications.

In this thesis, I exploited a Bayesian probability framework to make the following two contributions to the operation of EEW systems:

1. Develop a probability-based EEW algorithm to extend a deterministic EEW system in order to solve the problem of multiple concurrent earthquakes happening within a short period of time.

2. Develop an earthquake probability-based automated decision-making (ePAD) framework to provide automated decision for activating mitigation actions based on EEW information.

The improvement of EEW systems and their applications is a multi-disciplinary research problem. I applied decision theories from economics and machine learning techniques to make the contributions listed above.

In Chapter 3, I applied the Bayesian model class selection framework to solve for the number of concurrent events in the EEW multi-events problem. A simple numerical method, called the Rao-Blackwellized Importance Sampling, with a set of sequential proposal PDFs, is used to estimate the earthquake parameters of each event and necessary equations are derived for all the analytical parts of the solution. An algorithm is summarized based on the above concepts and some suggestions are given to improve the algorithm for practical use. A real example based on two months data (March 9 to April 30, 2011) of the 2011 M9 Tohoku earthquake is studied to verify the proposed algorithm. Significant improvement is shown by comparing with the existing JMA EEW system. The new algorithm is capable of accurately identifying concurrent earthquakes and providing a warning to the public.

In Chapter 4, I proposed the ePAD framework to provide automated decision for EEW applications. The ePAD framework makes fast and robust decisions about activating a mitigation action based on fundamental decision theory and a cost-benefit model that includes the influence of EEW uncertainty and warning lead time. I suggested using a surrogate model constructed by the relevance vector machine (RVM), a regression technique from machine learning, to greatly speed up the total computation time of ePAD. A highlighted novelty is the use of a value-of-information model to quantify the effect of delaying a decision in exchange for potentially more reliable EEW information in the future. Also, the concept of decision function and decision contour can be used to compare different methods of making decisions with various criteria. An example of finding the optimal time to broadcast an evacuation alert is studied to verify the ability of the ePAD framework to make rational decisions in a timely manner.

In Chapter 5, I studied a more sophisticated practical example using ePAD for elevator control based on EEW information. Cases of people being trapped in an elevator after a medium to large earthquake were observed in the past. This chapter used ePAD to find the optimal time to stop the elevators at the nearest floor and open the doors, based on EEW information. The results verified that ePAD can make rational decisions in all scenarios and it is flexible enough for users to pick their own desired decision behavior. Although simple models are used for the structural model, loss model and lead time model in this example, complicated models can be chosen at the expense of a more complex analysis for setting up an automated decision algorithm based on ePAD.

In Chapter 6, I presented two advanced applications of EEW and discuss their challenges: (1) Multiple-action decisions, and (2) Synergistic framework between EEW and structural health monitoring (SHM). In some large range EEW applications, for instance traffic control for a transportation network or a railway system, decision at a single site may have a cascading effect to the decisions at other sites. This creates a new layer of complexity when making multiple decisions at the same time. I showed that it is not practical to directly apply the current ePAD framework in this case. A new optimization scheme is needed to efficiently search for the optimal decision in this complex scenario. On the other hand, SHM systems provide information for decision support after a strong shaking arrives. This can be a good match with the EEW systems that provide information for automated decision/decision support before strong shaking arrives. I proposed a synergistic framework to utilize information from both systems under the Virtual Inspector model, a recently proposed method for risk assessment and decision support based on the PEER Performance-Based Earthquake Engineering method (Porter, 2003). However, development of new models is needed to bridge the inconsistent metric for a local damage measure in existing EEW and SHM frameworks. Real testing is needed to verify the value of using EEW as prior information for SHM analysis.

The Bayesian probability framework provides a platform to solve different aspects of the EEW problem using theories and methods from multiple disciplines. Appropriate techniques for uncertainty quantification and treatment lay a foundation for decision-making under uncertain information. Not only did a probabilistic approach improve different parts of the EEW problem individually, it can also become the central solution for the complete problem of EEW, starting from identifying earthquake events to making decisions for various applications. Future research for EEW may includes improvements of the existing EEW models to better predict different kinds of

earthquake events, new ways of using the EEW information to mitigate loss, reducing uncertainty in the whole process of EEW, etc. However, I believe that a long term goal is to develop a full probabilistic approach that links every component in the EEW problem. This will allow an appropriate treatment of uncertainties propagating from the seismic network to the final application decisions, which optimize the use of information in this extremely time sensitive problem.

# Appendix A

# Earthquake lists for JMA EEW

Table of the details of 71 earthquakes that the JMA EEW system released warning on between March 11 and April 30, 2011. Results of the seismic intensity estimates from the catalogue, JMA EEW system (JMA), an algorithm proposed by Tamaribuchi et al. (2014) (TK) and the proposed algorithm in this paper (RBIS) are listed.

| | | | | | Catalog | JMA | | TK | | RBIS | |
|---|---|---|---|---|---|---|---|---|---|---|---|
| No. | Date | Time | Location | Magnitude | SI | SI | Accurate? | SI | Accurate? | SI | Accurate? |
| 1 | 2011-03-11 | 14:46 | Off Miyagi Pref. | 9 | 7 | 6- | Yes | 7 | Yes | 6- | Yes |
| 2 | | 17:40 | Fukushima Pref. | 6 | 5+ | 5+ | Yes | 5- | Yes | 5- | No[2] |
| 3 | | 19:35 | Off Fukushima Pref. | 5.1 | 4 | 5+ | No | 4 | Yes | 3 | Yes |
| 4 | 2011-03-12 | 3:11 | Off Fukushima Pref. | 6 | 3 | 5- | No | 5- | No | 4 | Yes |
| 5 | | 3:59 | Niigata Pref. | 6.7 | 6+ | 6- | Yes | 6+ | Yes | 6+ | Yes |
| 6 | | 4:08 | Off Ibaraki Pref. | 5.2 | 4 | 5- | Yes | 5- | Yes | 4 | Yes |
| 7 | | 4:16 | Off Fukushima Pref. | 4 | 3 | 5+ | No | 4 | Yes | 0 | Yes[1] |
| 8 | | 4:31 | Niigata Pref. | 5.9 | 6- | 5+ | Yes | 6- | Yes | 5+ | Yes |
| 9 | | 5:11 | Off Miyagi Pref. | 6.4 | 3 | 5+ | No | 4 | Yes | 3 | Yes |
| 10 | | 5:42 | Niigata Pref. | 5.3 | 6- | 5- | Yes | 4 | No | 5- | Yes |
| 11 | | 6:19 | Nagano Pref. | 3.7 | 3 | 6- | No | 4 | Yes | 3 | Yes |
| 12 | | 6:34 | Off Fukushima Pref. | 4.8 | 3 | 6+ | No | 4 | Yes | 0 | Yes[1] |
| 13 | | 6:48 | E off Chiba Pref. | 4.6 | 3 | 5- | No | 4 | Yes | 0 | Yes[1] |
| 14 | | 22:15 | Off Fukushima Pref. | 6.2 | 5- | 5- | Yes | 5+ | Yes | 4 | Yes |
| 15 | | 22:24 | Off Iwate Pref. | 5 | 3 | 5- | No | 0 | Yes[1] | 3 | Yes |
| 16 | | 22:26 | Off Iwate Pref. | 5.4 | 2 | 5- | No | 4 | Yes | 0 | Yes[1] |
| 17 | | 23:34 | Niigata Pref. | 3.7 | 5- | 6+ | No | 4 | Yes | 3 | Yes |
| 18 | | 23:43 | Off Iwate Pref. | 5.9 | 4 | 5- | Yes | 5- | Yes | 4 | Yes |
| 19 | 2011-03-13 | 8:25 | Off Miyagi Pref. | 6.2 | 5- | 5- | Yes | 5- | Yes | 4 | Yes |
| 20 | | 10:26 | Off Ibaraki Pref. | 6.6 | 4 | 5- | Yes | 5- | Yes | 5- | Yes |
| 21 | 2011-03-14 | 10:02 | Off Ibaraki Pref. | 6.2 | 5- | 5- | Yes | 5+ | Yes | 5- | Yes |
| 22 | | 15:12 | Off Fukushima Pref. | 5.2 | 4 | 6- | No | 4 | Yes | 4 | Yes |
| 23 | | 16:25 | Off Ibaraki Pref. | 5 | 3 | 6- | No | 3 | Yes | 3 | Yes |
| 24 | 2011-03-15 | 1:36 | Tokyo Bay | 3.3 | 2 | 5- | No | 3 | Yes | 0 | Yes[1] |
| 25 | | 5:33 | E off Chiba Pref. | 3.6 | 1 | 5+ | No | 3 | Yes | 0 | Yes[1] |

| | | | | | Catalog | JMA | | TK | | RBIS | |
|---|---|---|---|---|---|---|---|---|---|---|---|
| No. | Date | Time | Location | Magnitude | SI | SI | Accurate? | SI | Accurate? | SI | Accurate? |
| 26 | 2011-03-15 | 7:29 | Fukushima Pref. | 4.3 | 3 | 6+ | No | 4 | Yes | 3 | Yes |
| 27 | | 22:31 | Yamanashi Pref. | 6.4 | 6+ | 5- | No | 6- | Yes | 5+ | Yes |
| 28 | 2011-03-16 | 2:40 | Chiba Pref. | 4 | 2 | 5+ | No | 4 | Yes | 0 | Yes[1] |
| 29 | | 12:23 | Off Fukushima Pref. | 4.7 | 2 | 5- | No | 3 | Yes | 0 | Yes[1] |
| 30 | | 12:52 | E off Chiba Pref. | 6.1 | 5- | 6- | Yes | 6- | Yes | 5+ | Yes |
| 31 | 2011-03-17 | 21:32 | E off Chiba Pref. | 5.7 | 4 | 5- | Yes | 5- | Yes | 5- | Yes |
| 32 | 2011-03-19 | 6:18 | Off Ibaraki Pref. | 4.8 | 2 | 5- | No | 3 | Yes | 0 | Yes[1] |
| 33 | | 8:32 | Off Iwate Pref. | 5.7 | 4 | 5- | Yes | 4 | Yes | 3 | Yes |
| 34 | | 18:56 | Ibaraki Pref. | 4 | 4 | 5+ | No | 6- | No | 5+ | No[3] |
| 35 | | 18:57 | Ibaraki Pref. | 6.1 | 5+ | 5- | Yes | 6- | Yes | 5+ | Yes |
| 36 | | 18:57 | Ibaraki Pref. | 6.1 | 5+ | 5+ | No[5] | 6- | Yes | 5+ | Yes |
| 37 | 2011-03-20 | 14:19 | Fukushima Pref. | 4.7 | 3 | 6- | No | 4 | Yes | 4 | Yes |
| 38 | 2011-03-22 | 12:38 | E off Chiba Pref. | 5.9 | 4 | 6+ | No | 4 | Yes | 4 | Yes |
| 39 | 2011-03-23 | 1:12 | Off Ibaraki Pref. | 5.4 | 3 | 6+ | No | 3 | Yes | 3 | Yes |
| 40 | | 7:12 | Fukushima Pref. | 6 | 5+ | 5+ | Yes | 6- | Yes | 5+ | Yes |
| 41 | | 7:36 | Fukushima Pref. | 5.8 | 5+ | 5+ | Yes | 5+ | Yes | 5+ | Yes |
| 42 | | 8:46 | E off Chiba Pref. | 5 | 2 | 5- | No | 3 | Yes | 2 | Yes |
| 43 | 2011-03-25 | 20:36 | Off Miyagi Pref. | 6.3 | 4 | 6- | No | 5- | Yes | 4 | Yes |
| 44 | 2011-03-27 | 19:23 | E off Chiba Pref. | 5 | 2 | 5+ | No | 3 | Yes | 3 | Yes |
| 45 | 2011-03-28 | 7:23 | Off Miyagi Pref. | 6.5 | 5- | 6- | Yes | 5- | Yes | 4 | Yes |
| 46 | 2011-04-01 | 19:49 | Akita Pref. | 5 | 5+ | 5- | Yes | 5- | Yes | 4 | No[4] |
| 47 | 2011-04-03 | 16:38 | Off Fukushima Pref. | 5.4 | 4 | 5+ | No | 4 | Yes | 4 | Yes |
| 48 | 2011-04-04 | 18:29 | Off Fukushima Pref. | 4 | 2 | 5+ | No | 3 | Yes | 0 | Yes[1] |
| 49 | 2011-04-07 | 23:33 | Off Miyagi Pref. | 7.2 | 6+ | 6- | Yes | 6- | Yes | 6- | Yes |
| 50 | 2011-04-11 | 17:16 | Fukushima Pref. | 7 | 6- | 6+ | Yes | 7 | Yes | 6- | Yes |
| 51 | 2011-04-11 | 17:26 | Fukushima Pref. | 5.4 | 5- | 5- | Yes | 5+ | Yes | 4 | Yes |
| 52 | | 18:05 | Fukushima Pref. | 5.1 | 4 | 5- | Yes | 5- | Yes | 4 | Yes |
| 53 | | 20:42 | Off Fukushima Pref. | 5.9 | 5- | 6- | Yes | 4 | Yes | 5- | Yes |
| 54 | 2011-04-12 | 8:08 | E off Chiba Pref. | 6.4 | 5- | 7 | No | 5- | Yes | 5- | Yes |
| 55 | | 8:08 | E off Chiba Pref. | 6.4 | 5- | 5- | Yes | 5- | Yes | 5- | Yes |
| 56 | | 10:23 | Chiba Pref. | 4.2 | 2 | 5+ | No | 2 | Yes | 0 | Yes[1] |
| 57 | | 12:20 | E off Chiba Pref. | 3.8 | 2 | 5- | No | 0 | Yes[1] | 0 | Yes[1] |
| 58 | | 14:07 | Fukushima Pref. | 6.4 | 6- | 6- | Yes | 6+ | Yes | 5+ | Yes |
| 59 | | 16:14 | Nagano Pref. | 3.1 | 2 | 6- | No | 4 | Yes | 3 | Yes |
| 60 | 2011-04-13 | 10:07 | Fukushima Pref. | 5.7 | 5- | 6+ | No | 5- | Yes | 4 | Yes |
| 61 | 2011-04-14 | 6:43 | Fukushima Pref. | 4.1 | 3 | 6- | No | 3 | Yes | 2 | Yes |
| 62 | | 12:08 | Fukushima Pref. | 5.4 | 4 | 5- | Yes | 4 | Yes | 5- | Yes |
| 63 | | 20:24 | Fukushima Pref. | 4.4 | 3 | 6- | No | 5- | No | 3 | Yes |
| 64 | | 21:24 | Fukushima Pref. | 3.9 | 3 | 5- | No | 4 | Yes | 3 | Yes |
| 65 | 2011-04-15 | 23:34 | Off Iwate Pref. | 5 | 3 | 6+ | No | 3 | Yes | 0 | Yes[1] |
| 66 | 2011-04-16 | 11:19 | Ibaraki Pref. | 5.9 | 5+ | 5- | Yes | 6+ | Yes | 5- | Yes |
| 67 | 2011-04-19 | 4:14 | Akita Pref. | 4.9 | 5- | 5- | Yes | 6- | Yes | 5- | Yes |
| 68 | | 6:33 | Ibaraki Pref. | 4.8 | 3 | 5- | No | 3 | Yes | 0 | Yes[1] |
| 69 | 2011-04-21 | 22:37 | Chiba Pref. | 6 | 5- | 5- | Yes | 5- | Yes | 4 | Yes |
| 70 | 2011-04-24 | 20:50 | Fukushima Pref. | 3.1 | 3 | 6- | No | 4 | Yes | 2 | Yes |
| 71 | 2011-04-30 | 2:04 | E off Chiba Pref. | 4.7 | 3 | 6+ | No | 4 | Yes | 3 | Yes |

1: Events with small seismic intensity that did not triggers a new event
2: Correctly identified earthquake, but later cancelled
3: Two overlapping concurrent events
4: Accurate hypocenter location, origin time and magnitude estimate with bad seismic intensity estimate
5: JMA EEW system created an extra fake event (other two systems did not)

# Bibliography

R.M. Allen and H. Kanamori. The potential for earthquake early warning in Southern California. *Science*, 300(5620):786–789, 2003.

R.M. Allen, H.M. Brown, M. Hellweg, O. Khainovski, P. Lombard, and D. Neuhauser. Real-time earthquake detection and hazard assessment by ElarmS across California. *Geophysical Research Letters*, 36(L00B08), March 2009a.

R.M. Allen, P. Gasparini, O. Kamigaichi, and M. Böse. The status of Earthquake Early Warning around the world: An introductory overview. *Seismological Research Letters*, 80(5):682–693, 2009b.

R.V. Allen. Automatic earthquake recognition and timing from single traces. *Bulletin of the Seismological Society of America*, 68(5):1521–1532, 1978.

M.S. Arulampalam, S. Maskell, N. Gordon, and T. Clapp. A tutorial on particle filters for online nonlinear/non-Gaussian Bayesian tracking. *IEEE Transactions on Signal Processing*, 50(2):174–188, February 2002.

S.K. Au and J.L. Beck. Estimation of small failure probabilities in high dimensions by subset simulation. *Probabilistic Engineering Mechanics*, 16(4):263–277, October 2001.

J.L. Beck. Bayesian system identification based on probability logic. *Structural Control and Health Monitoring*, 17(7):825–847, 2010.

J.L. Beck and S.K. Au. Bayesian updating of structural models and reliability using Markov Chain Monte Carlo simulation. *Journal of Engineering Mechanics–ASCE*, 128(4):380–391, April 2002.

J.L. Beck and L.S. Katafygiotis. Updating models and their uncertainties. I: Bayesian statistical framework. *Journal of Engineering Mechanics–ASCE*, 124(4):455–461, April 1998.

J.L. Beck and K.M. Zuev. Asymptotically Independent Markov Sampling: a new MCMC scheme for Bayesian inference. *International Journal for Uncertainty Quantification*, 3(2):445–474, 2013.

J.L. Beck, S.K. Au, and M.V. Vanik. Monitoring structural health using a probabilistic measure. *Computer-aided Civil and Infrastructure Engineering*, 16(1):1–11, January 2001.

D.M. Boore and G.M. Atkinson. Ground-motion prediction equations for the average horizontal component of PGA, PGV, and 5%-damped PSA at spectral periods between 0.01 s and 10.0 s. *Earthquake Spectra*, 24(1):99–138, February 2008.

M. Böse, E. Hauksson, K. Solanki, H. Kanamori, and T.H. Heaton. Real-time testing of the on-site warning algorithm in Southern California and its performance during the July 29 2008 Mw5.4 Chino Hills earthquake. *Geophysical Research Letters*, 36(L00B03), February 2009a.

M. Böse, E. Hauksson, K. Solanki, H. Kanamori, Y.M. Wu, and T.H. Heaton. A new trigger criterion for improved real-time performance of Onsite Earthquake Early Warning in Southern California. *Bulletin of the Seismological Society of America*, 99(2A):897–905, April 2009b.

M. Böse, T.H. Heaton, and E. Hauksson. Real-time finite fault rupture detector (FinDer) for large earthquakes. *Geophysical Journal International*, 191(2):803–812, 2012.

M. Böse, R.M. Allen, H. Brown, G. Cua, E. Hauksson, T.H. Heaton, M. Hellweg, M. Liukis, D. Neuhauser, P. Maechling, and CISN EEW Group. CISN ShakeAlert—an earthquake early warning demonstration system for California. In F. Wenzel and J. Zschau, editors, *Early Warning for Geological Disasters—Scientific methods and current practice*, chapter 3, pages 49–69. Springer-Verlag Berlin Heidelberg New York, 2014.

K.W. Campbell and Y. Bozorgnia. NGA ground motion model for the geometric mean horizontal component of PGA, PGV, PGD and 5% damped linear elastic response spectra for periods ranging from 0.01 to 10 s. *Earthquake Spectra*, 24(1):139–171, February 2008.

M.H. Cheng, S. Wu, T.H. Heaton, and J.L. Beck. Earthquake Early Warning application to buildings. *Engineering Structures*, 60:155–164, 2014.

J. Ching and J.L. Beck. Bayesian analysis of the Phase II IASC–ASCE structural health monitoring

experimental benchmark data. *Journal of Engineering Mechanics–ASCE*, 130(10):1233–1244, October 2004.

J.Y. Ching and Y.C. Chen. Transitional Markov Chain Monte Carlo method for Bayesian model updating, model class selection, and model averaging. *Journal of Engineering Mechanics–ASCE*, 133(7):816–832, July 2007.

J.Y. Ching, M. Muto, and J.L. Beck. Structural model updating and health monitoring with incomplete modal data using Gibbs Sampler. *Computer-aided Civil and Infrastructure Engineering*, 21 (4):242–257, May 2006.

C. Cortes and V. Vapnik. Support-vector networks. *Machine Learning*, 20(3):273–297, 1995.

T.M. Cover and J.A. Thomas. *Elements of Information Theory*. Wiley-Interscience, 2006.

G. Cua and T.H. Heaton. The Virtual Seismologist (VS) method: a Bayesian approach to Earthquake Early Warning. In P. Gasparini, G. Manfredi, and J. Zschau, editors, *Earthquake Early Warning Systems*, pages 97–132, Naples, Italy, 2007. Springer-Verlag Berlin Heidelberg.

G. Cua, M. Fischer, T.H. Heaton, and S. Wiemer. Real-time performance of the Virtual Seismologist earthquake early warning algorithm in Southern California. *Seismological Research Letters*, 80 (5):740–747, 2009.

Division of Occupational Safety and Health (Cal/OSHA). Title 8 regulations. Sub-chapter 6, elevator safety orders. Group 3, new elevator installations. Article 37, seismic requirements for elevators, escalators and moving walks. Section 3137. `http://www.dir.ca.gov/Title8/3137.html`, 2012. [Accessed 27 April, 2014].

K. Doi. Earthquake early warning system in Japan. In *Proceedings of Early Warning Systems for Natural Disaster Reduction*, pages 447–452, Berlin, Germany, 2000. Springer-Verlag Berlin.

M. Faulkner, M. Olsona nd R. Chandy, J. Krause, K.M. Chandy, and A. Krause. The next big one: detecting earthquakes and other rare events from community-based sensors. In *Proceedings of the 10th ACM/IEEE International Conference on Information Processing in Sensor Networks*, pages 13–24, Chicago, IL, USA, April 12–14 2011.

T. Fawcett. An introduction to ROC analysis. *Pattern Recognition Letters*, 27:861–874, 2006.

S. Fujita, K. Minagawa, G. Tanaka, and H. Shimosaka. Intelligent seismic isolation system using air bearings and earthquake early warning. *Soil Dynamics and Earthquake Engineering*, 31(2): 223–230, February 2011.

P. Gasparini, G. Manfredi, and J. Zschau, editors. *Earthquake Early Warning Systems*. Springer-Verlag Berlin Heidelberg, 2007.

B. Goller, J.L. Beck, and G.I. Schueller. Evidence-based identification of weighting factors in Bayesian model updating using modal data. *Journal of Engineering Mechanics–ASCE*, 138(5): 430–440, 2012.

C.A. Goulet, C.B. Haselton, J. Mitrani-Reiser, J.L. Beck, G.G. Deierlein, K.A. Porter, and J.P. Stewart. Evaluation of the seismic performance of a code-conforming reinforced-concrete frame building-from seismic hazard to collapse safety and economic losses. *Earthquake Engineering and Structural Dynamics*, 36(13):1973–1997, 2007.

V.F. Grasso. *Seismic Early Warning Systems: Procedure for Automated Decision Making*. PhD thesis, Università degli Studi di Napoli Federico II, 2005.

V.F. Grasso, J.L. Beck, and G. Manfredi. Automated decision procedure for earthquake early warning. *Engineering Structures*, 29(12):3455–3463, December 2007.

T.C. Hanks and A.G. Brady. The Loma-Prieta earthquake, ground motion, and damage in Oakland, Treasure-Island, and San-Francisco. *Bulletin of the Seismological Society of America*, 81(5):2019–2047, 1991.

C.B. Haselton, C.A. Goulet, J. Mitrani-Reiser, J.L. Beck, G.G. Deierlein, K.A. Porter, J.P. Stewart, and E. Taciroglu. An assessment to benchmark the seismic performance of a code-conforming reinforced concrete moment-frame building. Technical Report 12, Pacific Earthquake Engineering Research Center, 2007.

T.H. Heaton. A model for a seismic computerized alert network. *Science*, 228(4702):987–990, 1985.

D. Hilbring, T. Titzschkau, A. Buchmann, G. Bonn, F. Wenzel, and E. Hohnecker. Earthquake Early Warning for transport lines. *Natural Hazards*, pages 1–31, September 2010.

M. Hoshiba. Real-time prediction of ground motion by Kirchhoff-Fresnel boundary integral equation method: Extended front detection method for Earthquake Early Warning. *Journal of Geophysical Research: Solid Earth*, 118:1038–1050, 2013.

M. Hoshiba, O. Kamigaichi, M. Saito, S. Tsukada, and N. Hamada. Earthquake early warning starts nationwide in Japan. *EOS Trans. AGU*, 89:73–74, 2008.

M. Hoshiba, K. Iwakiri, N. Hayashimoto, and T. Shimoyama. Outline of the 2011 off the Pacific coast of Tohoku earthquake (Mw 9.0)—earthquake early warning and observed seismic intensity. *Earth Planets and Space*, 63(7):547–551, 2011.

R.A. Howard. Information value theory. *IEEE Transactions on Systems Science and Cybernetics*, 2(1):22–26, 1966.

Y. Huang, J.L. Beck, S. Wu, and H. Li. Robust Bayesian compressive sensing for signals in structural health monitoring. *Computer-Aided Civil and Infrastructure Engineering*, 29(3):160–179, March 2014.

I. Iervolino. Performance-based earthquake early warning. *Soil Dynamics and Earthquake Engineering*, 31(2):209–222, February 2011.

I. Iervolino, M. Giorgio, and G. Manfredi. Expected loss-based alarm threshold set for earthquake early warning systems. *Earthquake Engineering and Structural Dynamics*, 36(9):1151–1168, July 2007.

Japan Meteorological Agency (JMA). 2nd earthquake early warning meeting (technical). `http://www.seisvol.kishou.go.jp/eq/EEW/Meeting_HYOUKA/t02/index.html`, 2010. [Accessed 17 September, 2013].

Japan Meteorological Agency (JMA). 4th earthquake early warning meeting (technical). `http://www.seisvol.kishou.go.jp/eq/EEW/Meeting_HYOUKA/t04/index.html`, 2012. [Accessed 17 September, 2013].

Japan Meteorological Agency (JMA). 4th earthquake early warning meeting. `http://www.seisvol.kishou.go.jp/eq/EEW/Meeting_HYOUKA/04/index.html`, 2013a. [Accessed 30 August, 2013].

Japan Meteorological Agency (JMA). Earthquake early warning report. `http://www.seisvol.kishou.go.jp/eq/EEW/kaisetsu/joho/joho.html`, 2013b. [Accessed 16 October, 2013].

N. Jayaram and J.W. Baker. Correlation model for spatially-distributed ground-motion intensities. *Earthquake Engineering and Structural Dynamics*, 38(15):1687–1708, 2009.

E.T. Jaynes. Probability theory as logic. In *9th Annual Workshop on Maximum Entropy and Bayesian Methods*, volume 39, pages 1–16, 1990.

E.T. Jaynes. *Probability Theory: The Logic of Science*. Cambridge University Press, June 2003.

O. Kamigaichi. JMA Earthquake Early Warning. *Journal of Japan Association for Earthquake Engineering*, 4:134–137, 2004.

H. Kanamori. Real-time seismology and earthquake damage mitigation. *Annual Review of Earth and Planetary Sciences*, 33:195–214, 2005.

G. Karakus and T.H. Heaton. Simple linear inverse for complex sources in early warning. In *Abstract S53B-2500 Presented at AGU Fall Meeting*, San Francisco, CA, December 3–7 2012.

L. Kasai, W.C. Pu, and A. Wada. Responses of tall buildings in Tokyo during the 2011 Great East Japan Earthquake. In *Proceedings of Behavior of Steel Structures in Seismic Area (STESSA)*, pages 25–35, Santiago, Chile, January 9–11 2012.

A.I. Khuri and S. Mukhopadhyay. Response surface methodology. *Wiley Interdisciplinary Reviews: Computational Statistics*, 2(2):128–149, 2010.

T. Kubo, Y. Hisada, M. Murakami, F. Kosuge, and K. Hamano. Applications of an Earthquake Early Warning system and a real-time strong motion monitoring system in emergency response in a high-rise building. *Soil Dynamics and Earthquake Engineering*, 31(2):231–239, February 2011.

A. Liu and M. Yamada. Bayesian approach for identification of multiple events in an early warning system. *Bulletin of the Seismological Society of America*, 104(3), 2014. [Accepted].

J.S. Liu. *Monte Carlo Strategies in Scientific Computing*. Berlin: Springer-Verlag, 2002.

D.J.C. Mackay. Bayesian methods for backpropagation networks. In J.L. van Nemmen and K. Schulten, editors, *Models of Neural Networks III*, chapter 6, pages 211–254. Springer, 1994.

D.J.C. Mackay. Introduction to Gaussian Processes. In *NATO Asi Series, Series F, Computer and Systems Sciences*. Kluwer Academic Press, 1998.

G. Maddaloni, N. Caterino, and A. Occhiuzzi. Semi-active control of the benchmark highway bridge based on seismic early warning systems. *Bulletin of Earthquake Engineering*, 9(5):1703–1715, October 2011.

E. Miranda and C.J. Reyes. Approximate lateral drift demands in multi-story buildings with nonuniform stiffness. *Journal of Structural Engineering (ASCE)*, 128(7):840–849, 2002.

E. Miranda and S. Taghavi-Ardakan. Approximate floor acceleration demands in multistory buildings. I. forumulation. *Journal of Structural Engineering (ASCE)*, 131(2):203–211, 2005.

D. Mitchell, R. Tinawi, and R.G. Sexsmith. Performance of bridges in the 1989 Loma-Prieta earthquake—lessons for Canadian designers. *Canadian Journal of Civil Engineering*, 18(4):711–734, 1991.

J. Mitrani-Reiser. *An Ounce of Prevention: Probabilistic Loss Estimation for Performance-based Earthquake Engineering*. PhD thesis, California Institute of Technology, January 2007.

Y. Nakamura and J. Saita. UrEDAS, the Earthquake Warning System: Today and tomorrow. In P. Gasparini, G. Manfredi, and J. Zschau, editors, *Earthquake Early Warning Systems*, number 13, pages 249–281. Springer-Verlag Berlin Heidelberg, 2007.

Y. Nakamura, J. Saita, and T. Sato. On an Earthquake Early Warning System (EEW) and its applications. *Soil Dynamics and Earthquake Engineering*, 31(2):127–136, February 2011.

National Research Institute for Earth Science and Disaster Prevention (NIED). JMA earthquake catalogue. `http://www.hinet.bosai.go.jp/`, 2014. [Accessed 10 April, 2014].

R.M. Neal. Probabilistic inference using Markov Chain Monte Carlo methods. Technical Report CRG-TR-93-1, Department of Computer Science, University of Toronto, September 1993.

N.J. Newton. Variance reduction for simulated diffusions. *SIAM Journal on Applied Mathematics*, 54(6):1780–1805, 1994.

K. Porter, J. Mitrani-Reiser, and J.L. Beck. Near-real-time loss estimation for instrumented buildings. *Structural Design of Tall and Special Buildings*, 15(1):3–20, March 2006.

K.A. Porter. An overview of PEER's Performance-Based Earthquake Engineering methodology. In A. Der Kiureghian, S. Madanat, and J.M. Pestana, editors, *Proceedings of the International Conference on Applications of Statistics and Probability in Civil Engineering*, volume 1–2, pages 973–980, CALTECH, Dept Civil Engn, Pasadena, CA 91125 USA, July 2003. Millpress Science Publishers.

K.A. Porter, J.L. Beck, and R.V. Shaikhutdinov. Sensitivity of building loss estimates to major uncertain variables. *Earthquake Spectra*, 18:719–743, 2002.

H. Raiffa and R. Schlaifer. *Applied Statistical Decision Theory.* M.I.T. Press, Cambridge, MA, 1961.

C. Satriano, Y.M. Wu, A. Zollo, and H. Kanamori. Earthquake Early Warning: Concepts, methods and physical grounds. *Soil Dynamics and Earthquake Engineering*, 31(2):106–118, February 2011.

S. Taghavi-Ardakan. *Probabilistic seismic assessment of floor acceleration demands in multi-story buildings.* PhD thesis, Stanford University, June 2006.

K. Tamaribuchi, M. Yamada, and S. Wu. A new approach to identify multiple concurrent events for improvement of Earthquake Early Warning. *Zisin2*, 2014. [Accepted].

M.E. Tipping. Sparse Bayesian learning and the Relevance Vector Machine. *Journal of Machine Learning Research*, 1(3):211–244, 2001.

M.E. Tipping. Bayesian inference: An introduction to principles and practice in machine learning. In *Advanced Lectures on Machine Learning*, volume 3176, pages 41–62. Springer, 2004.

M.E. Tipping and A.C. Faul. Fast marginal likelihood maximization for sparse Bayesian models. In C.M. Bishop and B.J. Frey, editors, *Proceedings of the Ninth International Workshop on Artificial Intelligence and Statistics*, Key West, FL, January 2003.

S.T. Tokdar and R.E. Kass. Importance sampling: a review. *Wiley Interdisciplinary Reviews: Computational Statistics*, 2(1):54–60, 2010.

L.L. Turner, D. Wald, and K.W. Lin. ShakeCast—developing a tool for rapid post-earthquake response. Technical report, State of California Department of Transportation, 2009.

M.W. Vanik, J.L. Beck, and S.K. Au. Bayesian probabilistic approach to structural health monitoring. *Journal of Engineering Mechanics–ASCE*, 126(7):738–745, July 2000.

J. Von Neumann and O. Morgenstern. *Theory of Games and Economic Behavior*. Princeton University Press, Princeton, NJ, 1944.

Wikipedia. Earthquake Early Warning (Japan). `http://en.wikipedia.org/wiki/Earthquake_Early_Warning_(Japan)`, 2014. [Accessed 27 April, 2014].

S. Wu and J.L. Beck. Synergistic combination of systems for structural health monitoring and earthquake early warning for structural health prognosis and diagnosis. In *Proceedings of SPIE*, number 8348:83481Z, 2012.

S. Wu, J.L. Beck, and T.H. Heaton. Decision criteria for earthquake early warning applications. In *Proceedings of the 15th World Conference on Earthquake Engineering*, number 0973, Lisbon, Portugal, 2012.

S. Wu, J.L. Beck, and T.H. Heaton. ePAD: Earthquake probability-based automated decision-making framework for earthquake early warning. *Computer-aided Civil and Infrastructure Engineering*, 28:737–752, October 2013.

G. Wurman, R.M. Allen, and P. Lombard. Toward earthquake early warning in Northern California. *Journal of Geophysical Research*, 112(B08311), 2007.

Yahoo News. Strong earthquake rattles Taiwan, no reports of casualties. `http://news.yahoo.com/earthquake-6-7-magnitude-strikes-taiwan-usgs-122240396.html`, 2013. [Accessed 9 April, 2014].

M. Yamada and T.H. Heaton. Real-time estimation of fault rupture extent using envelopes of acceleration. *Bulletin of the Seismological Society of America*, 98(2):607–619, 2008.

M. Yamada, T.H. Heaton, and J.L. Beck. Real-time estimation of fault rupture extent using near-source versus far-source classification. *Bulletin of the Seismological Society of America*, 97(6): 1890–1910, December 2007.

M. Yamada, A. Liu, and J. Mori. Classification of simultaneous multiple earthquakes for the Earthquake Early Warning system. In *JpGU Annual Meeting*, May 2012. [Abstract].

M. Yamada, K. Tamaribuchi, and S. Wu. Faster and more accurate Earthquake Early Warning system—combination of velocity and acceleration-type seismometers. *Journal of Japan Association for Earthquake Engineering*, 2014. [Accepted].

F. Yamazaki, K. Meguro, and S. Noda. Developments of early earthquake damage assessment systems in Japan. In N. Shiraishi, M. Shinozuka, and Y.K. Wen, editors, *Structural Safety and Reliability*, volume 1–3, pages 1573–1580, Univ Tokyo, Inst Ind Sci, Tokyo, Japan, 1998. A.A. Balkema Publishers.

K.V. Yuen, J.L. Beck, and L.S. Katafygiotis. Efficient model updating and health monitoring methodology using incomplete modal data without mode matching. *Structural Control and Health Monitoring*, 13(1):91–107, 2006a.

K.V. Yuen, J.L. Beck, and L.S. Katafygiotis. Unified probabilistic approach for model updating and damage detection. *Journal of Applied Mechanics–Transactions of the ASME*, 73(4):555–564, 2006b.

K.M. Zuev, S. Wu, and J.L. Beck. General network reliability problem and its efficient solution by subset simulation. *SIAM/ASA Journal on Uncertainty Quantification*, 2014. [Submitted].